EXPLOITING COST-PERFORMANCE TRADEOFFS FOR MODERN CLOUD SYSTEMS

BY

MUNTASIR RAIHAN RAHMAN

DISSERTATION

Submitted in partial fulfillment of the requirements
for the degree of Doctor of Philosophy in Computer Science
in the Graduate College of the
University of Illinois at Urbana-Champaign, 2016

Urbana, Illinois

ABSTRACT

The trade-off between cost and performance is a fundamental challenge for modern cloud systems. This thesis explores cost-performance tradeoffs for three types of systems that permeate today's clouds, namely (1) storage, (2) virtualization, and (3) computation. A distributed key-value storage system must choose between the cost of keeping replicas synchronized (consistency) and performance (latency) or read/write operations. A cloud-based disaster recovery system can reduce the cost of managing a group of VMs as a single unit for recovery by implementing this abstraction in software (instead of hardware) at the risk of impacting application availability performance. As another example, run-time performance of graph analytics jobs sharing a multi-tenant cluster can be made better by trading of the cost of replication of the input graph dataset stored in the associated distributed file system.

Today cloud system providers have to *manually* tune the system to meet desired trade-offs. This can be challenging since the optimal trade-off between cost and performance may vary depending on network and workload conditions. Thus our hypothesis is that *it is feasible to imbue a wide variety of cloud systems with adaptive and opportunistic mechanisms to efficiently navigate the cost-performance tradeoff space to meet desired tradeoffs.* The types of cloud systems considered in this thesis include key-value stores, cloud-based disaster recovery systems, and multi-tenant graph computation engines.

Our first contribution, PCAP is an adaptive distributed storage system. The foundation of the PCAP system is a probabilistic variation of the classical CAP theorem, which quantifies the (un-)achievable envelope of probabilistic consistency and latency under different network conditions characterized by a probabilistic partition model. Our PCAP system proposes adaptive mechanisms for tuning control knobs to meet desired consistency-latency tradeoffs expressed in terms in service-level agreements.

Our second system, GeoPCAP is a geo-distributed extension of PCAP. In GeoPCAP, we propose generalized probabilistic composition rules for composing consistency-latency tradeoffs across geodistributed instances of distributed key-value stores, each running on separate datacenters. GeoPCAP also includes a geo-distributed adaptive control system that adapts new controls knobs to meet SLAs across geo-distributed data-centers.

Our third system, GCVM proposes a light-weight hypervisor-managed mechanism for taking crash consistent snapshots across VMs distributed over servers. This mechanism enables us to move the consistency group abstraction from hardware to software, and thus lowers reconfiguration cost while incurring modest VM pause times which impact application availability.

Finally, our fourth contribution is a new opportunistic graph processing system called OPTiC for efficiently scheduling multiple graph analytics jobs sharing a multi-tenant cluster. By opportunistically creating at most 1 additional replica in the distributed file system (thus incurring cost), we show up to 50% reduction in median job completion time for graph processing jobs under realistic network and workload conditions. Thus with a modest increase in storage and bandwidth cost in disk, we can reduce job completion time (improve performance).

For the first two systems (PCAP, and GeoPCAP), we exploit the cost-performance tradeoff space through efficient navigation of the tradeoff space to meet SLAs and perform close to the optimal tradeoff. For the third (GCVM) and fourth (OPTiC) systems, we move from one solution point to another solution point in the tradeoff space. For the last two systems, explicitly mapping out the tradeoff space allows us to consider new design tradeoffs for these systems.

I dedicate this thesis to my family.

ACKNOWLEDGMENTS

First and foremost, I would like to express my deep gratitude to my advisor, Indranil Gupta (Indy), for giving me the opportunity to work under his guidance, for pushing me forward and inspiring me when things got tough in the middle of my PhD program, for all the valuable discussions, un-solicited advice, and encouragement, and above all for being a great mentor, and a true friend. I could not have completed this difficult journey without Indy believing in me. Thank you Indy!

I would like to sincerely thank the rest of my thesis committee members, Nitin Vaidya, Aditya Parameswaran, and Rean Griffith for their valuable feedback, insightful comments, and hard questions that helped shape this thesis in its current form. Nitin introduced me to the beautiful and elegant world of distributed algorithms in his course. Learning about distributed algorithms from him has immensely helped me to think about distributed systems research problems in a principled manner. Rean Griffith was also my mentor at VMware, and since then he has been a constant source of valuable advice about systems research, industry, and just about anything else.

I would like to thank my current and former colleagues in the Distributed Protocols Research Group, with whom I spent several wonderful graduate years. In particular, I am grateful to Imranul Hoque, Brian Cho, Mainak Ghosh, Wenting Wang, Le Xu, Luke Leslie, Shegufta Ahsan, Tej Chajed, Yosub Shin, Hilfi Alkaff, Ala' Alkhadi, Simon Krueger, Mayank Pundir, Son Nguyen, Rajath Subramanyam. Imranul has been like a big brother to me, and whenever I had a question, or I just wanted to chat or complain, he was always there for me. He has always been a great mentor and idol to me. I am thankful to Mainak for countless intellectual discussions and fun chats we had throughout the years. Le always managed to cheer me up with a fun conversation. I am indebted to Son Nguyen, Akash Kapoor, and Haozhen

Ding for assisting me with software implementation during my PhD.

I started my PhD journey along with many other fellow graduate students. Among them, I am particularly grateful to Anupam Das, Shen Li, and Lewis Tseng. Anupam and I come from the same country, and we formed our own two person support group. Shen Li helped me alot with advice and giving me valuable feedback during my qualifying exam and job talk preparations. Lewis collaborated with me on one of my research projects, and was my go to guy for any theory question that was beyond me. I thank them all sincerely.

I had the great privilege of doing four wonderful research internships at Xerox, HP Labs, Microsoft Research, and VMware during my PhD program. I am grateful to Nathan Gnanasambandam, Wojciech Golab, Sergey Bykov, and Ilya Languev for hosting me during these internships.

The current and former members of Bangaldeshi community here at UIUC have been a source of great joy, encouragement, and mental support for me. I am especially grateful to Ahmed Khurshid, Mehedi Bakht, Shakil Bin Kashem, Gourab Kundu, Anupam Das, Roman Khan, Mazhar Islam, Md. Abul Hassan Samee, Piyas Bal, Hasib Uddin, Mohammad Sharif Ullah, Reaz Mohiuddin, Tanvir Amin, Shama Farabi, Shameem Ahmed, Moushumi Sharmin, Sharnali Islam, Fariba Khan, Sonia Jahid, Wasim Akram, Ahsan Arefin, Maifi Khan, Farhana Ashraf, Munawar Hafiz, Rezwana Silvi, Md Yusuf Sarwar Uddin, Md Ashiqur Rahman, Abdullah Al Nayeem, and Tawhid Ezaz. Ahmed Khurshid, Mehedi Bakht, and Mohammad Sharif Ullah were truly like my elder brothers in Urbana-Champaign. I am indebted to them for self-less support, and guidance.

I want to thank Kathy Runck, Mary Beth Kelley, and Donna Coleman for shielding me from various administrative stuff involved in the PhD program. VMware supported one year of my PhD program through a generous PhD fellowship. I am grateful to VMware for this support during my PhD program.

Finally I could not completed this difficult journey without the unconditional love and support of my family. My father Md. Mujibur Rahman, and my mother Mariam Rahman had to endure the pain of being separated from me for several years. I wanted to make them proud, and I believe that is what helped me go through this program. My sister Samia Nawar Rahman is the most wonderful sister one can ask for. Sometimes I feel like even though she is younger than me, she is actually my elder sister looking after me. I would like to express my gratitude to my beautiful and caring wife Farhana Afzal. She had to endure several years of my graduate years that was mixed with joy, despair, and finally hope. She kept me motivated when things were not going well, she took care of me when I fell sick or got upset, and she cherished and celebrated all my successes during my PhD program, however small they were. Last, but in no way least, I am grateful to my daughter Inaaya Rayya Rahman. She was born near the end of my PhD program. Her birth was the best thing that ever happened to me. Every morning her smiling face gave me the extra boost to get through my PhD. I dedicate this thesis to them.

TABLE OF CONTENTS

Chapter 1

Introduction

1.1 Motivation

The trade-off between cost and performance is a fundamental challenge for modern cloud systems. This thesis explores cost-performance tradeoffs for three types of systems that permeate today's clouds, namely: (1) storage, (2) virtualization, and (3) computation. A distributed key-value storage system must choose between the cost of keeping replicas synchronized (consistency) and performance (latency) or read/write operations. A cloud based disaster recovery system faces tradeoffs between managing consistency groups (a group of VMs snapshotted and replicated as a unit) in software vs hardware. Hardware consistency groups require manual reconfiguration which increases the cost of reconfiguration, but can minimize application unavailability. On the other hand, software consistency groups lower the cost of reconfiguring groups at the hypervisor level, but impacts application availability performance by incurring VM pause overheads. As another example, the run-time performance of multiple graph analytics jobs sharing a multi-tenant cluster can be improved by trading the storage and bandwidth cost of at-most one additional replica of the graph input stored in the associated distributed file system.

Today cloud system providers have to *manually* tune the system to meet desired trade-offs. This can be challenging since the optimal trade-off between cost and performance may vary depending on network and workload conditions. This leads us to the central hypothesis of our thesis:

We claim that *it is feasible to imbue a wide variety of cloud systems with adaptive and opportunistic mechanisms to efficiently navigate the cost-performance tradeoff space to meet desired tradeoffs.*

The various systems considered in this proposal are summarized in Table 1.1.

System	Cost	Performance	Mechanism
PCAP	Consistency	Latency	Read Delay
GeoPCAP	Consistency	Latency	Geo-read Delay
GCVM	Reconfiguration	Availability	Consistency Groups
OPTiC	Replication	Job Run-time	Replica Placement

Table 1.1: Systems considered in this thesis.

1.2 Contributions

The main contributions of this thesis are briefly mentioned below.

1.2.1 Probabilistic CAP System (PCAP)

Leveraging a generalized version of the CAP theorem [122], we present a new adaptive middleware system called PCAP, which allows applications to specify either an availability SLA or a consistency SLA. The PCAP system automatically adapts in real-time and under changing network conditions, to meet the SLA while optimizing the other metric. We built and deployed our adaptive middleware on top of two popular distributed key-value stores.

1.2.2 Geo-distributed PCAP (GeoPCAP)

We develop a theoretical framework for probabilistically composing consistency and latency models of multiple distributed storage systems running across geo-distributed datacenters. Using this framework, we also design and implement a geo-distributed adaptive system to meet consistency-latency (PCAP) SLAs.

1.2.3 Software-defined Group Consistent Snapshots for VMs (GCVM)

For a hardware storage array, a *consistency group* is defined as a group of devices that can be checkpointed and replicated as a group [12]. We propose to move consistency group abstractions from hardware to software. This allows increased flexibility for defining consistency groups for checkpointing and replication. It also reduces the cost of reconfiguring consistency groups, which can now be done at the hypervisor level. However this approach incurs the cost of pausing the VM pause leading to increased application unavailability. Our implemented mechanism correctly takes crash-consistent snapshots of a group of VMs, while keeping the VM pause overhead bounded by 50 msec. With some constraints on application write ordering, we demonstrate that this approach can be used to recover real applications without complicated distributed snapshot algorithms or coordination.

1.2.4 Opportunistic Graph Processing in Multi-tenant Clusters (OPTiC)

We investigate for the first time how multiple graph analytics jobs sharing a cluster can improve overall job performance by trading the additional storage and bandwidth cost of one more replica of the input graph data. The placement of the additional replica is opportunistically selected based on novel progress metrics for current running graph analytics jobs. We incorporated our system on top of Apache Giraph running on Apache YARN in conjunction with HDFS. Our deployment experiments under realistic network and workload conditions show around 40% performance improvement in average job completion time, at the cost of increased data replication.

1.3 Cost-Performance Tradeoffs as First Class Citizens for Cloud Systems

A central tenet of this thesis is that we should consider cost-performance tradeoffs as first class citizens when designing cloud systems. Today many cloud systems are designed with only an explicit goal of either optimizing performance or minimizing cost, but not both. Explicitly mapping out the cost performance tradeoff space for cloud systems allows us to better design and reason about cloud systems in the following ways:

1. It allows us to characterize the optimal tradeoff (PCAP, Chapter 2), or conjecture what the optimal tradeoff can look like (OPTiC, Chapter 5).

2. It allows us to think of future designs of the same system with new tradeoffs in the tradeoff space, and predict cost and performance for such designs (GCVM, Chapter 4).

These points are discussed in further detail at the end of this thesis in Chapter 6.

1.4 Thesis Organization

The rest of the thesis is organized as follows. Chapter 2 presents the design, implementation, and evaluation of PCAP, an adaptive distributed storage system for meeting novel probabilistic consistency/latency SLAs for applications running inside a data-center under realistic network conditions. Chapter 3 presents GeoPCAP, which is a geo-distributed extension of PCAP (Chapter 2). Chapter 4 presents the design and evaluation of GCVM, which is a hypervisor-managed system for implementing consistency group abstractions for a group of virtual machines. Chapter 5 discusses the design, implementation and evaluation of OPTiC, a system to opportunistically schedule graph processing jobs in a shared multi-tenant cluster. Finally we summarize and discuss future directions in Chapter 6.

Chapter 2

PCAP: Characterizing and Adapting the Consistency-Latency Tradeoff for Distributed Key-Value Stores

In this chapter we present our system PCAP. PCAP is based on a new probabilistic characterization of the consistency-latency tradeoffs for a distributed key-value store [123]. PCAP leverages adaptive techniques to meet novel consistency-latency SLAs under varying network conditions in a data-center network. We have incorporated our PCAP system design on top of two popular open-source key-value stores: Apache Cassandra and Basho Riak. Deployment experiments confirm that PCAP can meet probabilistic consistency and latency SLAs under network variations within a single data-center environment.

2.1 Introduction

Storage systems form the foundational platform for modern Internet services such as Web search, analytics, and social networking. Ever increasing user bases and massive data sets have forced users and applications to forgo conventional relational databases, and move towards a new class of scalable storage systems known as NoSQL key-value stores. Many of these distributed key-value stores (e.g., Cassandra [8], Riak [7], Dynamo [71], Voldemort [24]) support a simple GET/PUT interface for accessing and updating data items. The data items are replicated at multiple servers for fault tolerance. In addition, they offer a very weak notion of consistency known as eventual consistency [139, 48], which roughly speaking, says that if no further updates are sent to a given data item, all replicas will eventually hold the same value.

These key-value stores are preferred by applications for whom eventual consistency suffices, but where high availability and low latency (i.e., fast reads and writes [40]) are paramount. Latency is a critical metric for such cloud services because latency is correlated to user satisfaction – for instance, a 500 ms increase in latency for operations at Google.com can cause a 20% drop in revenue [1]. At Amazon, this translates to a $6M yearly loss per added millisecond of latency [2]. This correlation between delay and lost retention is fundamentally human. Humans suffer from a phenomenon called *user cognitive drift*, wherein if more than a second (or so) elapses between clicking on something and receiving a response, the user's mind is already elsewhere.

At the same time, clients in such applications expect freshness, i.e., data returned by a read to a key should come from the latest writes done to that key by any client. For instance, Netflix uses Cassandra to track positions in each video [66], and freshness of data translates to accurate tracking and user satisfaction. This implies that clients care about a *time-based* notion of data freshness. Thus, this chapter focuses on consistency based on the notion of data freshness (as defined later).

The CAP theorem was proposed by Brewer et al. [57, 56], and later formally proved by [78, 108]. It essentially states that a system can choose at most two of three desirable properties: Consistency (C), Availability (A), and Partition tolerance (P). Recently, [40] proposed to study the consistency-latency tradeoff, and unified the tradeoff with the CAP theorem. The unified result is called PACELC. It states that when a network partition occurs, one needs to choose between Availability and Consistency, otherwise the choice is between Latency and Consistency. We focus on the latter tradeoff as it is the common case. These prior results provided qualitative characterization of the tradeoff between consistency and availability/latency, while we provide a *quantitative* characterization of the tradeoff.

Concretely, traditional CAP literature tends to focus on situations where "hard" network partitions occur and the designer has to choose between C or A, e.g., in geo-distributed data-centers. However, individual data-centers themselves suffer far more frequently from "soft" partitions [70], arising from periods of elevated message delays or loss rates (i.e., the "otherwise" part of PACELC) within a data-center. Neither the original CAP theorem nor the existing work on consistency in key-value stores [50, 71, 80, 88, 102, 105, 106, 130, 135, 139] address such soft partitions for a single data-center.

In this chapter we state and prove two CAP-like impossibility theorems. To state these theorems, we present probabilistic[1] models to characterize the three important elements: soft partition, latency requirements, and consistency requirements. All our models take timeliness into account. Our latency model specifies soft bounds on operation latencies, as might be provided by the application in an SLA (Service Level Agreement). Our consistency model captures the notion of data freshness returned by read operations. Our partition model describes propagation delays in the underlying network. The resulting theorems show the un-achievable envelope, i.e., which combinations of the parameters in these three models (partition, latency, consistency) make them impossible to achieve together. Note that the focus of the chapter is neither defining a new consistency model nor comparing different types of consistency models. Instead, we are interested in the un-achievable envelope of the three important elements and measuring how close a system can

[1]By probabilistic, we mean the behavior is statistical over a long time period.

perform to this envelop.

Next, we describe the design of a class of systems called PCAP (short for Probabilistic CAP) that perform close to the envelope described by our theorems. In addition, these systems allow applications running inside a single data-center to specify either a probabilistic latency SLA or a probabilistic consistency SLA. Given a probabilistic latency SLA, PCAP's adaptive techniques meet the specified operational latency requirement, while optimizing the consistency achieved. Similarly, given a probabilistic consistency SLA, PCAP meets the consistency requirement while optimizing operational latency. PCAP does so under real and continuously changing network conditions. There are known use cases that would benefit from an latency SLA – these include the Netflix video tracking application [66], online advertising [26], and shopping cart applications [135] – each of these needs fast response times but is willing to tolerate some staleness. A known use case for consistency SLA is a Web search application [135], which desires search results with bounded staleness but would like to minimize the response time. While the PCAP system can be used with a variety of consistency and latency models (like PBS [50]), we use our PCAP models for concreteness.

We have integrated our PCAP system into two key-value stores – Apache Cassandra [8] and Riak [7]. Our experiments with these two deployments, using YCSB [67] benchmarks, reveal that PCAP systems satisfactorily meets a latency SLA (or consistency SLA), optimize the consistency metric (respectively latency metric), perform reasonably close to the envelope described by our theorems, and scale well.

2.2 Consistency-Latency Tradeoff

We consider a key-value store system which provides a read/write API over an asynchronous distributed message-passing network. The system consists of clients and servers, in which, servers are responsible for replicating the data (or read/write object) and ensuring the specified consistency requirements, and clients can invoke a write (or read) operation that stores (or retrieves) some value of the specified key by contacting server(s). We assume each client has a corresponding client proxy at the set of servers, which submits read and write operations on behalf of clients [105, 129]. Specifically, in the system, data can be propagated from a writer client to multiple servers by a replication mechanism or background mechanism such as read repair [71], and the data stored at servers can later be read by clients. There may be multiple versions of the data corresponding to the same key, and the exact value to be read by reader clients depends on how the system ensures the consistency requirements. Note that as addressed earlier, we define consistency based on freshness of the value returned by read operations (defined below). We first present our probabilistic models for soft partition, latency and consistency. Then we present our impossibility results. These results only hold for a single data-center. Later in Section 3 we deal with the multiple data-center case.

2.2.1 Models

To capture consistency, we defined a new notion called *t-freshness*, which is a form of eventual consistency. Consider a single key (or read/write object) being read and written concurrently by multiple clients. An operation O (read or write) has a start time $\tau_{start}(O)$ when the client issues O, and a finish time $\tau_{finish}(O)$ when the client receives an answer (for a read) or an acknowledgment (for a write). The write operation ends when the client receives an acknowledgment from the server. The value of a write operation can be reflected on the server side (i.e., visible to other clients) any time after the write starts. For clarity of our presentation, we assume that all write operations end, which is reasonable given client retries. Note that the written value can still propagate to other servers after the write ends by the background mechanism.We assume that at time 0 (initial time), the key has a default value.

Definition 1 ***t*-freshness and *t*-staleness:** *A read operation R is said to be* <u>*t-fresh*</u> *if and only if R returns a value written by any write operation that starts at or after time $\tau_{fresh}(R,t)$, which is defined below:*

1. *If there is at least one write starting in the interval $[\tau_{start}(R)-t, \tau_{start}(R)]$: then $\tau_{fresh}(R,t) = \tau_{start}(R) - t$.*
2. *If there is no write starting in the interval $[\tau_{start}(R)-t, \tau_{start}(R)]$, then there are two cases:*
   - *(a) No write starts before R starts: then $\tau_{fresh}(R,t) = 0$.*
   - *(b) Some write starts before R starts: then $\tau_{fresh}(R,t)$ is the start time of the last write operation that starts before $\tau_{start}(R) - t$.*

A read that is not t-fresh is said to be <u>*t-stale*</u>*.*

Note that the above characterization of $t_{fresh}(R,t)$ only depends on *start times* of operations.

Fig. 2.1 shows three examples for t-freshness. The figure shows the times at which several read and write operations are issued (the time when operations complete are not shown in the figure). $W(x)$ in the figure denotes a write

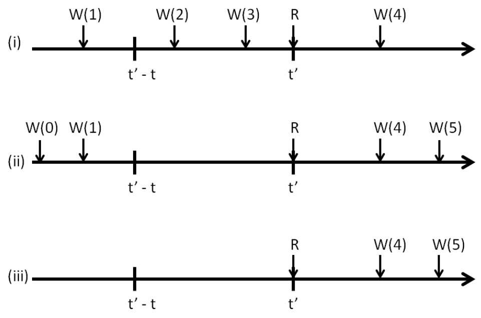

Figure 2.1: Examples illustrating Definition 1. Only start times of each operation are shown.

operation with a value x. Note that our definition of *t-freshness* allows a read to return a value that is written by a write issued after the read is issued. In Fig. 2.1(i), $\tau_{fresh}(R,t) = \tau_{start}(R) - t = t' - t$; therefore, R is t-fresh if it returns $2, 3$ or 4. In Fig. 2.1(ii), $\tau_{fresh}(R,t) = \tau_{start}(W(1))$; therefore, R is t-fresh if it returns $1, 4$ or 5. In Fig. 2.1(iii), $\tau_{fresh}(R,t) = 0$; therefore, R is t-fresh if it returns $4, 5$ or the default.

Definition 2 Probabilistic Consistency: *A key-value store satisfies* (t_c, p_{ic})-*consistency*[2] *if in* <u>*any execution*</u> *of the system, the fraction of read operations satisfying* t_c*-freshness is at least* $(1 - p_{ic})$.

Intuitively, p_{ic} is the *likelihood of returning stale data*, given the time-based freshness requirement t_c.

Two similar definitions have been proposed previously: (1) t-visibility from the Probabilistically Bounded Staleness (PBS) work [50], and (2) Δ-atomicity [81]. These two metrics do not require a read to return the latest write, but provide a time bound on the staleness of the data returned by the read. The main difference between t-freshness and these is that we consider the

[2]The subscripts c and ic stand for consistency and inconsistency, respectively.

start time of write operations rather than the end time. This allows us to characterize consistency-latency tradeoff more precisely. While we prefer t-freshness, our PCAP system (Section 2.3) is modular and could use instead t-visibility or Δ-atomicity for estimating data freshness.

As noted earlier, our focus is not comparing different consistency models, nor achieving linearizability. We are interested in the un-achievable envelope of soft partition, latency requirements, and consistency requirements. Traditional consistency models like linearizability can be achieved by delaying the effect of a write. On the contrary, the achievability of t-freshness closely ties to the latency of read operations and underlying network behavior as discussed later. In other words, t-freshness by itself is not a complete definition.

2.2.2 Use Case for $t - freshness$

Consider a bidding application (e.g., eBay), where everyone can post a bid, and we want every other participant to see posted bids as fast as possible. Assume that User 1 submits a bid, which is implemented as a write request (Figure 2.2). User 2 requests to read the bid before the bid write process finishes. The same User 2 then waits a finite amount of time after the bid write completes and submits another read request. Both of these read operations must reflect User 1's bid, whereas t-visibility only reflects the write in User 2's second read (with suitable choice of t). The bid write request duration can include time to send back an acknowledgment to the client, even after the bid has committed (on the servers). A client may not want to wait that long to see a submitted bid. This is especially true when the auction is near the end.

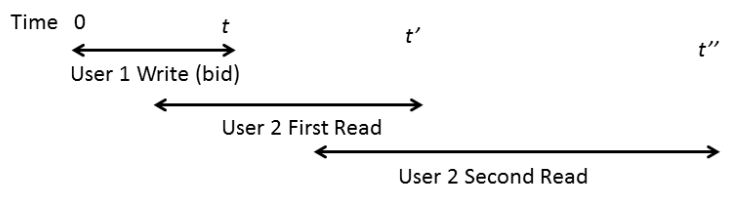

Figure 2.2: Example motivating use of Definition 2.

We define our probabilistic notion of latency as follows:

Definition 3 ***t*-latency:** *A read operation R is said to satisfy $\underline{t\text{-latency}}$ if and only if it completes within t time units of its start time.*

Definition 4 Probabilistic Latency: *A key-value store satisfies (t_a, p_{ua})-latency[3] if in $\underline{\text{any execution}}$ of the system, the fraction of t_a-latency read operations is at least $(1 - p_{ua})$.*

Intuitively, given response time requirement t_a, p_{ua} is the *likelihood of a read violating the* t_a.

Finally, we capture the concept of a *soft partition* of the network by defining a probabilistic partition model. In this section, we assume that the partition model for the network does not change over time. (Later, our implementation and experiments in Section 2.5 will measure the effect of time-varying partition models.)

In a key-value store, data can propagate from one client to another via the other servers using different approaches. For instance, in Apache Cassandra [8], a write might go from a writer client to a coordinator server to a replica server, or from a replica server to another replica server in the form of read repair [71]. Our partition model captures the delay of all such

[3]The subscripts a and ua stand for availability and unavailability, respectively.

propagation approaches. Please note that the partition model applies not to the network directly, but to the paths taken by the read or write operation queries themselves. This means that the network as a whole may be good (or bad), but if the paths taken by the queries are bad (or good), only the latter matters.

Definition 5 Probabilistic Partition:

An execution is said to suffer (t_p, α)-partition if the fraction f of paths from one client to another client, via a server, which have latency higher than t_p, is such that $f \geq \alpha$.

Our delay model loosely describes the message delay caused by any underlying network behavior without relying on the assumptions on the implementation of the key-value store. We do not assume eventual delivery of messages. We neither define propagation delay for each message nor specify the propagation paths (or alternatively, the replication mechanisms). This is because we want to have general lower bounds that apply to all systems that satisfy our models.

2.2.3 Impossibility Results

We now present two theorems that characterize the consistency-latency tradeoff in terms of our probabilistic models.[4]

First, we consider the case when the client has tight expectations, i.e., the client expects all data to be fresh within a time bound, and all reads need to be answered within a time bound.

[4]These impossibility results are not a contribution of this thesis. They were discovered independently by Lewis Tseng and Indranil Gupta. Since they form the foundation of our PCAP system (which is a contribution of this thesis), we include the results here only as background material.)

Theorem 1 *If* $t_c + t_a < t_p$*, then it is impossible to implement a read/write data object under a* $(t_p, 0)$*-partition while achieving* $(t_c, 0)$-consistency*, and* $(t_a, 0)$-latency*, i.e., there exists an execution such that these three properties cannot be satisfied simultaneously.*

Proof: The proof is by contradiction. In a system that satisfies all three properties in all executions, consider an execution with only two clients, a writer client and a reader client. There are two operations: (i) the writer client issues a write W, and (ii) the reader client issues a read R at time $\tau_{start}(R) = \tau_{start}(W) + t_c$. Due to $(t_c, 0)$-consistency, the read R must return the value from W.

Let the delay of the write request W be exactly t_p units of time (this obeys $(t_p, 0)$-partition). Thus, the earliest time that W's value can arrive at the reader client is $(\tau_{start}(W) + t_p)$. However, to satisfy $(t_a, 0)$-latency, the reader client must receive an answer by time $\tau_{start}(R) + t_a = \tau_{start}(W) + t_c + t_a$. However, this time is earlier than $(\tau_{start}(W) + t_p)$ because $t_c + t_a < t_p$. Hence, the value returned by W cannot satisfy $(t_c, 0)$-consistency. This is a contradiction. □

Essentially, the above theorem relates the clients' expectations of freshness (t_c) and latency (t_a) to the propagation delays (t_p). If client expectations are too stringent when the maximum propagation delay is large, then it may not be possible to guarantee both consistency and latency expectations.

However, if we allow a fraction of the reads to return late (i.e., after t_a), or return t_c-stale values (i.e., when either p_{ic} or p_{ua} is non-zero), then it may be possible to satisfy the three properties together even if $t_c + t_a < t_p$. Hence, we consider non-zero p_{ic}, p_{ua} and α in our second theorem.

Theorem 2 *If* $t_c + t_a < t_p$, *and* $p_{ua} + p_{ic} < \alpha$, *then it is impossible to implement a read/write data object under a* (t_p, α)*-partition while achieving* (t_c, p_{ic})-consistency*, and* (t_a, p_{ua})-latency*, i.e., there exists an execution such that these three properties cannot be satisfied simultaneously.*

Proof: The proof is by contradiction. In a system that satisfies all three properties in all executions, consider an execution with only two clients, a writer client and a reader client. The execution contains alternating pairs of write and read operations $W_1, R_1, W_2, R_2, \ldots, W_n, R_n$, such that:

- Write W_i starts at time $(t_c + t_a) \cdot (i - 1)$,
- Read R_i starts at time $(t_c + t_a) \cdot (i - 1) + t_c$, and
- Each write W_i writes a distinct value v_i.

By our definition of (t_p, α)-partition, there are at least $n \cdot \alpha$ written values v_j's that have propagation delay $> t_p$. By a similar argument as in the proof of Theorem 1, each of their corresponding reads R_j are such that R_j cannot both satisfy t_c-freshness and also return within t_a. That is, R_j is either t_c-stale or returns later than t_a after its start time. There are $n \cdot \alpha$ such reads R_j; let us call these "bad" reads.

By definition, the set of reads S that are t_c-stale, and the set of reads A that return after t_a are such that $|S| \leq n \cdot p_{ic}$ and $|A| \leq n \cdot p_{ua}$. Put together, these imply:

$n \cdot \alpha \leq |S \cup A| \leq |S| + |A| \leq n \cdot p_{ic} + n \cdot p_{ua}$.

The first inequality arises because all the "bad" reads are in $S \cup A$. But this inequality implies that $\alpha \leq p_{ua} + p_{ic}$, which violates our assumptions. $\Box$

The intuition behind the theorem is as follows. As network conditions worsen, the values for (α, t_p) go up. On the other hand a client can get better freshness (latency) for reads by lowering the values of (p_{ic}, t_c) $((p_{ua}, t_a))$. Thus high values for (α, t_p) prevent the values for (p_{ic}, t_c), and (p_{ua}, t_a) to be arbitrarily small. The inequalities thus represent the best freshness (p_{ic}, t_c) and latency (p_{ua}, t_a) combinations for a given network characterized by (α, t_p).

2.3 PCAP Key-value Stores

Having formally specified the (un)achievable envelope of consistency-latency (Theorem 2), we now move our attention to designing systems that achieve performance close to this theoretical envelope. We also convert our probabilistic models for consistency and latency from Section 2.2 into SLAs, and show how to design adaptive key-value stores that satisfy such probabilistic SLAs inside a single data-center. We call such systems PCAP systems. So PCAP systems (1) can achieve performance close to the theoretical consistency-latency tradeoff envelope, and (2) can adapt to meet probabilistic consistency and latency SLAs inside a single data-center. Our PCAP systems can also alternatively be used with SLAs from PBS [50] or Pileus [45, 135].

Assumptions about underlying Key-value Store PCAP systems can be built on top of existing key-value stores. We make a few assumptions about such key-value stores. First, we assume that each key is replicated on multiple servers. Second, we assume the existence of a "coordinator" server that acts as a client proxy in the system, finds the replica locations for a key (e.g., using consistent hashing [134]), forwards client queries to replicas, and finally relays replica responses to clients. Most key-value stores feature such a coordinator [7, 8]. Third, we assume the existence of a background mechanism such as read repair [71] for reconciling divergent replicas. Finally, we assume that the clocks on each server in the system are synchronized using a protocol like NTP so that we can use global timestamps to detect stale data (most key-value stores running within a datacenter already require this assumption, e.g., to decide which updates are fresher). It should be noted that our impossibility results in Section 2.2 do not depend on the accuracy of the clock synchronization protocol. However the sensitivity of the protocol affects the ability of PCAP systems to adapt to network delays. For example, if the servers are synchronized to within 1 ms using NTP, then the PCAP system cannot react to network delays lower than 1 ms.

SLAs We consider two scenarios, where the SLA specifies either: i) a probabilistic latency requirement, or ii) a probabilistic consistency requirement. In the former case, our adaptive system optimizes the probabilistic consistency while meeting the SLA requirement, whereas in the latter it optimizes probabilistic latency while meeting the SLA. These SLAs are probabilistic, in the sense that they give statistical guarantees to operations over a long duration.

A latency SLA (i) looks as follows:

Given: Latency $SLA =< p_{ua}^{sla}, t_a^{sla}, t_c^{sla} >$;

Ensure that: The fraction p_{ua} of reads, whose finish and start times differ by more than t_a^{sla}, is such that: p_{ua} stays below p_{ua}^{sla} ;

Minimize: The fraction p_{ic} of reads which do not satisfy t_c^{sla}-freshness.

This SLA is similar to latency SLAs used in industry today. As an example, consider a shopping cart application [135] where the client requires that at most 10% of the operations take longer than 300 ms, but wishes to minimize staleness. Such an application prefers latency over consistency. In our system, this requirement can be specified as the following PCAP latency

SLA:

$< p_{ua}^{sla}, t_a^{sla}, t_c^{sla} >=< 0.1, 300\ ms, 0\ ms >$.

A consistency SLA looks as follows:

Given: Consistency $SLA =< p_{ic}^{sla}, t_a^{sla}, t_c^{sla} >$;

Ensure that: The fraction p_{ic} of reads that do not satisfy t_c^{sla}-freshness is such that: p_{ic} stays below p_{ic}^{sla} ;

Minimize: The fraction p_{ua} of reads whose finish and start times differ by more than t_a^{sla}.

Note that as mentioned earlier, consistency is defined based on freshness of the value returned by read operations. As an example, consider a web search application that wants to ensure no more than 10% of search results return data that is over 500 ms old, but wishes to minimize the fraction of operations taking longer than 100 ms [135]. Such an application prefers consistency over latency. This requirement can be specified as the following PCAP consistency SLA:

$< p_{ic}^{sla}, t_a^{sla}, t_c^{sla} >=< 0.10, 100\ ms, 500\ ms >$.

Our PCAP system can leverage three control knobs to meet these SLAs: 1) *read delay*, 2) *read repair rate*, and 3) *consistency level.* The last two of these are present in most key-value stores. The first (read delay) has been discussed in previous literature [10, 50, 75, 83, 145].

2.3.1 Control Knobs

Table 2.1 shows the effect of our three control knobs on latency and consistency. We discuss each of these knobs and explain the entries in the table.

The knobs of Table 2.1 are all directly or indirectly applicable to the read

Increased Knob	Latency	Consistency
Read Delay	Degrades	Improves
Read Repair Rate	Unaffected	Improves
Consistency Level	Degrades	Improves

Table 2.1: Effect of Various Control Knobs.

path in the key-value store. As an example, the knobs pertaining to the Cassandra query path are shown in Fig. 2.3, which shows the four major steps involved in answering a read query from a front-end to the key-value store cluster: (1) Client sends a read query for a key to a coordinator server in the key-value store cluster; (2) Coordinator forwards the query to one or more replicas holding the key; (3) Response is sent from replica(s) to coordinator; (4) Coordinator forwards response with highest timestamp to client; (5) Coordinator does *read repair* by updating replicas, which had returned older values, by sending them the freshest timestamp value for the key. Step (5) is usually performed in the background.

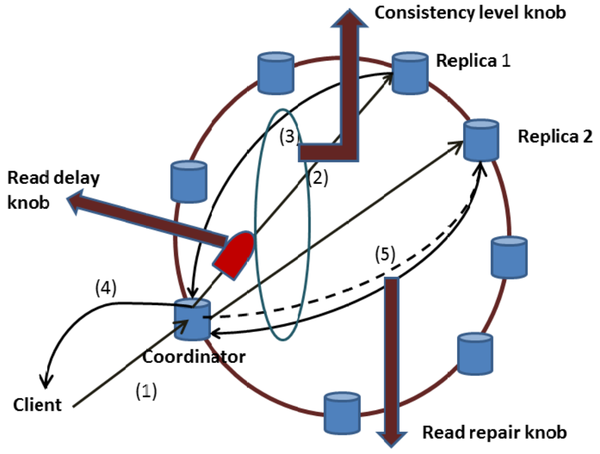

Figure 2.3: Cassandra Read Path and PCAP Control Knobs.

A *read delay* involves the coordinator artificially delaying the read query for a specified duration of time before forwarding it to the replicas. i.e., between step (1) and step (2). This gives the system some time to converge after previous writes. Increasing the value of read delay improves consistency (lowers p_{ic}) and degrades latency (increases p_{ua}). Decreasing read delay achieves the reverse. Read delay is an attractive knob because: 1) it does not interfere with client specified parameters (e.g., consistency level in Cassandra), and 2) it can take any non-negative continuous value instead of only discrete values allowed by consistency levels. Our PCAP system inserts read delays only when it is needed to satisfy the specified SLA.

However, read delay cannot be negative, as one cannot speed up a query and send it back in time. This brings us to our second knob: read repair rate. Read repair was depicted as distinct step (5) in our outline of Fig. 2.3, and is typically performed in the background. The coordinator maintains a buffer of recent reads where some of the replicas returned older values along with the associated freshest value. It periodically picks an element from this buffer and updates the appropriate replicas. In key-value stores like Apache Cassandra and Riak, read repair rate is an accessible configuration parameter per column family.

Our read repair rate knob is the probability with which a given read that returned stale replica values will be added to the read repair buffer. Thus, a read repair rate of 0 implies no read repair, and replicas will be updated only by subsequent writes. Read repair rate = 0.1 means the coordinator performs read repair for 10% of the read requests.

Increasing (respectively, decreasing) the read repair rate can improve (respectively degrade) consistency. Since the read repair rate does not directly affect the read path (Step (5) described earlier, is performed in the background), it does not affect latency. Table 2.1 summarizes this behavior.[5]

[5]Although read repair rate does not affect latency directly, it introduces some background traffic and can impact propagation delay. While our model ignores such small impacts, our experiments reflect the net effect of the background traffic.

The third potential control knob is consistency level. Some key-value stores allow the client to specify, along with each read or write operation, how many replicas the coordinator should wait for (in step (3) of Fig. 2.3) before it sends the reply back in step (4). For instance, Cassandra offers consistency levels: `ONE`, `TWO`, `QUORUM`, `ALL`. As one increases consistency level from `ONE` to `ALL`, reads are delayed longer (latency decreases) while the possibility of returning the latest write rises (consistency increases).

Our PCAP system relies primarily on read delay and repair rate as the control knobs. Consistency level can be used as a control knob only for applications in which user expectations will not be violated, e.g., when reads do not specify a specific discrete consistency level. That is, if a read specifies a higher consistency level, it would be prohibitive for the PCAP system to degrade the consistency level as this may violate client expectations. Techniques like continuous partial quorums (CPQ) [113], and adaptive hybrid quorums [69] fall in this category, and thus interfere with application/client expectations. Further, read delay and repair rate are *non-blocking* control knobs under replica failure, whereas consistency level is *blocking*. For example, if a Cassandra client sets consistency level to `QUORUM` with replication factor 3, then the coordinator will be blocked if two of the key's replicas are on failed nodes. On the other hand, under replica failures read repair rate does not affect operation latency, while read delay only delays reads by a maximum amount.

2.3.2 Selecting A Control Knob

As the primary control knob, the PCAP system prefers read delay over read repair rate. This is because the former allows tuning both consistency and latency, while the latter affects only consistency. The only exception occurs when during the PCAP system adaptation process, a state is reached where consistency needs to be degraded (e.g., increase p_{ic} to be closer to the SLA) but the read delay value is already zero. Since read delay cannot be lowered further, in this instance the PCAP system switches to using the secondary knob of read repair rate, and starts decreasing this instead.

Another reason why read repair rate is not a good choice for the primary knob is that it takes longer to estimate p_{ic} than for read delay. Because read repair rate is a probability, the system needs a larger number of samples (from the operation log) to accurately estimate the actual p_{ic} resulting from a given read repair rate. For example, in our experiments, we observe that the system needs to inject $k \geq 3000$ operations to obtain an accurate estimate of p_{ic}, whereas only $k = 100$ suffices for the read delay knob.

2.3.3 PCAP Control Loop

The PCAP control loop adaptively tunes control knobs to always meet the SLA under continuously changing network conditions. The control loop for consistency SLA is depicted in Fig. 2.4. The control loop for a latency SLA is analogous and is not shown.

This control loop runs at a standalone server called the PCAP Coordinator.[6] This server runs an infinite loop. In each iteration, the coordinator: i) injects k operations into the store (line 6), ii) collects the log $\mathcal{L}$ for the k recent operations in the system (line 8), iii) calculates p_{ua}, p_{ic} (Section 2.3.4) from $\mathcal{L}$ (line 10), and iv) uses these to change the knob (lines 12-22).

The behavior of the control loop in Fig. 2.4 is such that the system will

[6]The PCAP Coordinator is a special server, and is different from Cassandra's use of a coordinator for clients to send reads and writes.

```
procedure CONTROL($\mathcal{SLA} =< p_{ic}^{sla}, t_c^{sla}, t_a^{sla} >, \epsilon$)
    $p_{ic}^{sla'} := p_{ic}^{sla} - \epsilon$;
    Select control_knob; // (Sections 2.3.1, 2.3.2)
    $inc := 1$;
    $dir = +1$;
    while (true) do
        Inject $k$ new operations (reads and writes)
          into store;
        Collect log $\mathcal{L}$ of recent completed reads
            and writes (values, start and finish times);
        Use $\mathcal{L}$ to calculate
            $p_{ic}$ and $p_{ua}$; // (Section 2.3.4)
        $new\_dir := (p_{ic} > p_{ic}^{sla'})? + 1 : -1$;
        if $new\_dir = dir$ then
            $inc := inc * 2$; // Multiplicative increase
            if $inc > MAX\_INC$ then
                $inc := MAX\_INC$:
            end if
        else
            $inc := 1$; // Reset to unit step
            $dir := new\_dir$; // Change direction
        end if
        $control\_knob := control\_knob + inc * dir$;
    end while
end procedure
```

Figure 2.4: Adaptive Control Loop for Consistency SLA.

converge to "around" the specified SLA. Because our original latency (consistency) SLAs require p_{ua} (p_{ic}) to stay below the SLA, we introduce a *laxity* parameter ϵ, subtract ϵ from the target SLA, and treat this as the target SLA in the control loop. Concretely, given a target consistency SLA $< p_{ic}^{sla}, t_a^{sla}, t_c^{sla} >$, where the goal is to control the fraction of stale reads to be under p_{ic}^{sla}, we control the system such that p_{ic} quickly converges around $p_{ic}^{sla'} = p_{ic}^{sla} - \epsilon$, and thus stay below p_{ic}^{sla}. Small values of ϵ suffice to guarantee convergence (for instance, our experiments use $\epsilon \leq 0.05$).

We found that the naive approach of changing the control knob by the smallest unit increment (e.g., always 1 ms changes in read delay) resulted in a long convergence time. Thus, we opted for a *multiplicative* approach (Fig. 2.4, lines 12-22) to ensure quick convergence.

We explain the control loop via an example. For concreteness, suppose only the read delay knob (Section 2.3.1) is active in the system, and that the system has a consistency SLA. Suppose p_{ic} is higher than $p_{ic}^{sla'}$. The multiplicative-change strategy starts incrementing the read delay, initially starting with a unit step size (line 3). This step size is exponentially *increased* from one iteration to the next, thus multiplicatively increasing read delay (line 14). This continues until the measured p_{ic} goes just under $p_{ic}^{sla'}$. At this point, the *new_dir* variable changes sign (line 12), so the strategy reverses direction, and the step is reset to unit size (lines 19-20). In subsequent iterations, the read delay starts *decreasing* by the step size. Again, the step size is increased exponentially until p_{ic} just goes above $p_{ic}^{sla'}$. Then its direction is reversed again, and this process continues similarly thereafter. Notice that (lines 12-14) from one iteration to the next, as long as p_{ic} continues to remain above (or below) $p_{ic}^{sla'}$, we have that: i) the direction of movement does not change, and ii) exponential increase continues. At steady state, the control loop keeps changing direction with a unit step size (bounded oscillation), and the metric stays converged under the SLA. Although advanced techniques such as *time dampening* can further reduce oscillations, we decided to avoid them to minimize control loop tuning overheads. Later in Chapter 3, we utilized control theoretic techniques for the control loop in geo-distributed settings to reduce excessive oscillations.

In order to prevent large step sizes, we cap the maximum step size (line 15-17). For our experiments, we do not allow read delay to exceed 10 ms, and the unit step size is set to 1 ms.

We preferred active measurement (whereby the PCAP Coordinator injects queries rather than passive due to two reasons: i) the active approach gives the PCAP Coordinator better control on convergence, thus convergence rate is more uniform over time, and ii) in the passive approach if the client operation rate were to become low, then either the PCAP Coordinator would need to inject more queries, or convergence would slow down. Nevertheless, in Section 2.5.3, we show results using a passive measurement approach. Exploration of hybrid active-passive approaches based on an operation rate threshold could be an interesting direction.

Overall our PCAP controller satisfies SASO (Stability, Accuracy, low Settling time, small Overshoot) control objectives [87].

2.3.4 Complexity of Computing p_{ua} and p_{ic}

We show that the computation of p_{ua} and p_{ic} (line 10, Fig. 2.4) is efficient. Suppose there are r reads and w writes in the log, thus log size $k = r + w$. Calculating p_{ua} makes a linear pass over the read operations, and compares the difference of their finish and start times with t_a. This takes $O(r) = O(k)$.

p_{ic} is calculated as follows. We first extract and sort all the writes according to start timestamp, inserting each write into a hash table under key <object value, write key, write timestamp>. In a second pass over the read operations, we extract its matching write by using the hash table key (the third entry of the hash key is the same as the read's returned value timestamp). We also extract neighboring writes of this matching write in constant time (due to the sorting), and thus calculate t_c-freshness for each read. The first pass takes time $O(r+w+w\log w)$, while the second pass takes $O(r+w)$. The total time complexity to calculate p_{ic} is thus $O(r+w+w\log w) = O(k\log k)$.

2.4 Implementation Details

In this section, we discuss how support for our consistency and latency SLAs can be easily incorporated into the Cassandra and Riak key-value stores (in a single data-center) via minimal changes.

2.4.1 PCAP Coordinator

From Section 2.3.3, recall that the PCAP Coordinator runs an infinite loop that continuously injects operations, collects logs ($k = 100$ operations by default), calculates metrics, and changes the control knob. We implemented a modular PCAP Coordinator using Python (around 100 LOC), which can be connected to any key-value store.

We integrated PCAP into two popular NoSQL stores: Apache Cassandra [8] and Riak [7] – each of these required changes to about 50 lines of original store code.[7]

2.4.2 Apache Cassandra

First, we modified the Cassandra v1.2.4 to add read delay and read repair rate as control knobs. We changed the Cassandra Thrift interface so that it accepts read delay as an additional parameter. Incorporating the read delay into the read path required around 50 lines of Java code.

Read repair rate is specified as a column family configuration parameter, and thus did not require any code changes. We used YCSB's Cassandra connector as the client, modified appropriately to talk with the clients and

[7]The implementation of PCAP on top of Riak is not a contribution of this thesis. This implementation was done by Son Nguyen under the guidance of the author of this thesis. The design of PCAP Riak closely follows the design of PCAP Cassandra which is a contribution of this thesis.

the PCAP Coordinator.

2.4.3 Riak

We modified Riak v1.4.2 to add read delay and read repair as control knobs. Due to the unavailability of a YCSB Riak connector, we wrote a separate YCSB client for Riak from scratch (250 lines of Java code). We decided to use YCSB instead of existing Riak clients, since YCSB offers flexible workload choices that model real world key-value store workloads.

We introduced a new system-wide parameter for read delay, which was passed via the Riak http interface to the Riak coordinator which in turn applied it to all queries that it receives from clients. This required about 50 lines of Erlang code in Riak. Like Cassandra, Riak also has built-in support for controlling read repair rate.

2.5 Experiments

Our experiments are in two stages: microbenchmarks for a single data-center (Section 2.5.2) and deployment experiments for a single data-center (Section 2.5.3).

2.5.1 Experiment Setup

Our single data-center PCAP Cassandra system and our PCAP Riak system were each run with their default settings. We used YCSB v 0.1.4 [36] to send operations to the store. YCSB generates synthetic workloads for key-value stores and models real-world workload scenarios (e.g., Facebook photo storage workload). It has been used to benchmark many open-source and commercial key-value stores, and is the de facto benchmark for key-value stores [67].

Each YCSB experiment consisted of a load phase, followed by a work phase. Unless otherwise specified, we used the following YCSB parameters: 16 threads per YCSB instance, 2048 B values, and a read-heavy distribution (80% reads). We had as many YCSB instances as the cluster size, one co-located at each server. The default key size was 10 B for Cassandra, and Riak. Both YCSB-Cassandra and YCSB-Riak connectors were used with the weakest quorum settings and 3 replicas per key. The default throughput was 1000 ops/s. All operations use a consistency level of `ONE`.

Both PCAP systems were run in a cluster of 9 d710 Emulab servers [140], each with 4 core Xeon processors, 12 GB RAM, and 500 GB disks. The default network topology was a LAN (star topology), with 100 Mbps bandwidth and inter-server round-trip delay of 20 ms, dynamically controlled using traffic shaping.

We used NTP to synchronize clocks within 1 ms. This is reasonable since we are limited to a single data-center. This clock skew can be made tighter by using atomic or GPS clocks [68]. This synchronization is needed by the PCAP coordinator to compute the SLA metrics.

2.5.2 Microbenchmark Experiments (Single Data-center)

Impact of Control Knobs on Consistency

We study the impact of two control knobs on consistency: read delay and read repair rate.

Fig. 2.5 shows the inconsistency metric p_{ic} against t_c for different read delays. This shows that when applications desire fresher data (left half of

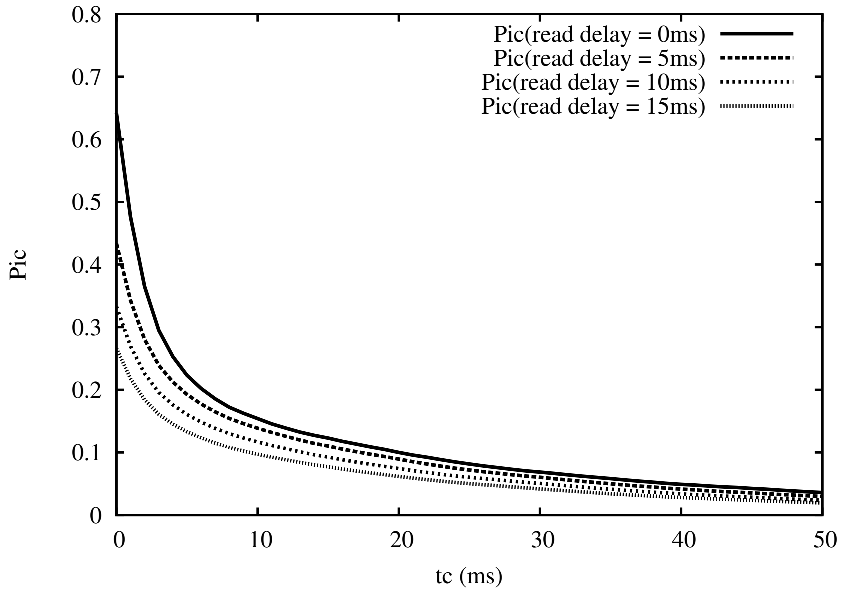

Figure 2.5: Effectiveness of Read Delay knob in PCAP Cassandra. Read repair rate fixed at 0.1.

the plot), read delay is flexible knob to control inconsistency p_{ic}. When the freshness requirements are lax (right half of plot), the knob is less useful. However, p_{ic} is already low in this region.

On the other hand, read repair rate has a relatively smaller effect. We found that a change in read repair rate from 0.1 to 1 altered p_{ic} by only 15%, whereas Fig. 2.5 showed that a 15 ms increase in read delay (at $t_c = 0\ ms$) lowered inconsistency by over 50%. As mentioned earlier, using read repair rate requires calculating p_{ic} over logs of at least $k = 3000$ operations, whereas read delay worked well with $k = 100$. Henceforth, by default we use read delay as our sole control knob.

PCAP vs. PBS

To show that our system can work with PBS [50], we integrated t-visibility into PCAP. Fig. 2.6 compares, for a 50%-write workload, the probability of inconsistency against t for both existing work PBS (t-visibility) [50] and

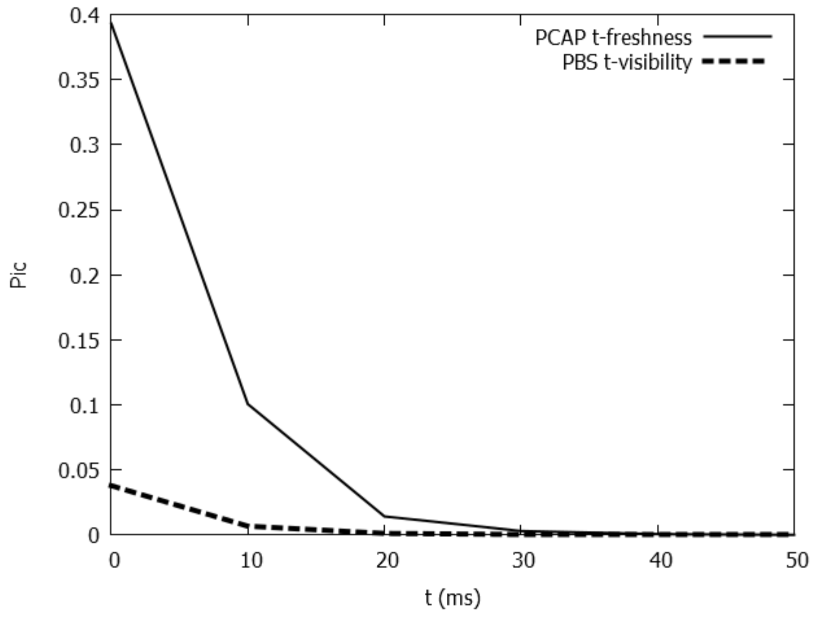

Figure 2.6: p_{ic} PCAP vs. PBS consistency metrics. Read repair rate set to 0.1, 50% writes.

PCAP (t-freshness) described in Section 2.2.1 We observe that PBS's reported inconsistency is lower compared to PCAP. This is because, PBS considers a read that returns the value of an in-flight write (overlapping read and write) to be always fresh, by default. However the comparison between PBS and PCAP metrics is not completely fair, since the PBS metric is defined in terms of write operation end times, whereas our PCAP metric is based on write start times. It should be noted that the purpose of this experiment is not to show which metric captures client-centric consistency better. Rather, our goal is to demonstrate that our PCAP system can be made to run by using PBS t-visibility metric instead of PCAP t-freshness.

PCAP Metric Computation Time

Fig. 2.7 shows the total time for the PCAP Coordinator to calculate p_{ic} and p_{ua} metrics for values of k from 100 to 10K, and using multiple threads.

We observe low computation times of around 1.5 s, except when there are 64 threads and a 10K-sized log: under this situation, the system starts to degrade as too many threads contend for relatively few memory resources. Henceforth, the PCAP Coordinator by default uses a log size of $k = 100$ operations and 16 threads.

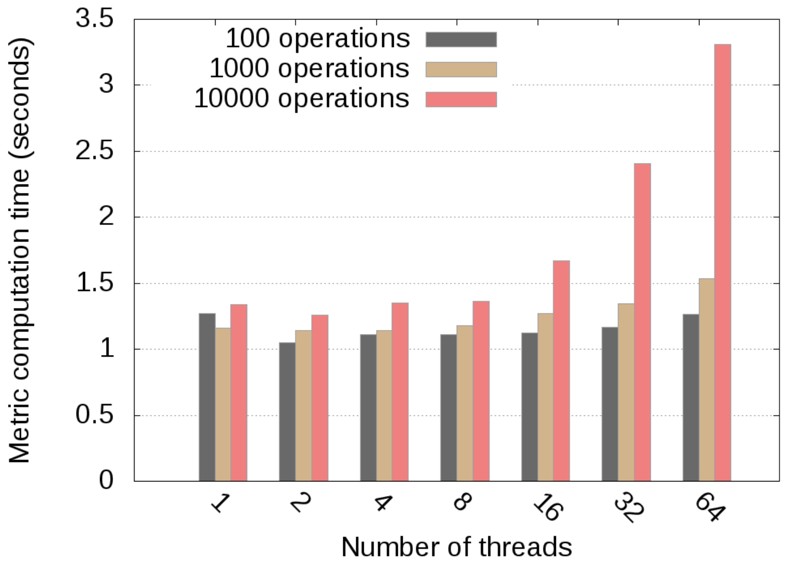

Figure 2.7: PCAP Coordinator time taken to both collect logs and compute p_{ic} and p_{ua} in PCAP Cassandra.

2.5.3 Deployment Experiments

We now subject our two PCAP systems to network delay variations and YCSB query workloads. In particular, we present two types of experiments: 1) *sharp network jump* experiments, where the network delay at some of the servers changes suddenly, and 2) *lognormal* experiments, which inject continuously-changing and realistic delays into the network. Our experiments use $\epsilon \leq 0.05$ (Section 2.3.3).

Table 2.2 summarizes the various of SLA parameters and network conditions used in our experiments.

System	SLA	Parameters	Delay Model	Plot
Riak	Latency	$p_{ua} = 0.2375$, $t_a = 150\ ms$, $t_c = 0\ ms$	Sharp delay jump	Fig. 2.11
Riak	Consistency	$p_{ic} = 0.17$, $t_c = 0\ ms$, $t_a = 150\ ms$	Lognormal	Fig. 2.15
Cassandra	Latency	$p_{ua} = 0.2375$, $t_a = 150\ ms$, $t_c = 0\ ms$	Sharp delay jump	Figs. 2.8, 2.9, 2.10
Cassandra	Consistency	$p_{ic} = 0.15$, $t_c = 0\ ms$, $t_a = 150\ ms$	Sharp delay jump	Fig. 2.12
Cassandra	Consistency	$p_{ic} = 0.135$, $t_c = 0\ ms$, $t_a = 200\ ms$	Lognormal	Figs. 2.13, 2.14, 2.19, 2.20
Cassandra	Consistency	$p_{ic} = 0.2$, $t_c = 0\ ms$, $t_a = 200\ ms$	Lognormal	Fig. 2.21
Cassandra	Consistency	$p_{ic} = 0.125$, $t_c = 0\ ms$, $t_a = 25\ ms$	Lognormal	Figs. 2.16, 2.17
Cassandra	Consistency	$p_{ic} = 0.12$, $t_c = 3\ ms$, $t_a = 200\ ms$	Lognormal	Figs. 2.22, 2.23
Cassandra	Consistency	$p_{ic} = 0.12$, $t_c = 3\ ms$, $t_a = 200\ ms$	Lognormal	Figs. 2.24, 2.25

Table 2.2: Deployment Experiments: Summary of Settings and Parameters.

Latency SLA under Sharp Network Jump

Fig. 2.8 shows the timeline of a scenario for PCAP Cassandra using the following latency SLA: $p_{ua}^{sla} = 0.2375$, $t_c = 0$ ms, $t_a = 150$ ms.

In the initial segment of this run ($t = 0$ s to $t = 800$ s) the network delays are small; the one-way server-to-LAN switch delay is 10 ms (this is half the machine to machine delay, where a machine can be either a client or a server). After the warm up phase, by $t = 400$ s, Fig. 2.8 shows that p_{ua} has converged to the target SLA. Inconsistency p_{ic} stays close to zero.

We wish to measure how close the PCAP system is to the optimal-achievable envelope (Section 2.2). The envelope captures the lowest possible values for consistency (p_{ic}, t_c), and latency (p_{ua}, t_a), allowed by the network partition model (α, t_p) (Theorem 2). We do this by first calculating α for our specific network, then calculating the optimal achievable non-SLA metric, and finally seeing how close our non-SLA metric is to this optimal.

First, from Theorem 1 we know that the achievability region requires $t_c + t_a \geq t_p$; hence, we set $t_p = t_c + t_a$. Based on this, and the probability distribution of delays in the network, we calculate analytically the exact value of α as the fraction of client pairs whose propagation delay exceeds t_p (see Definition 5).

Given this value of α at time t, we can calculate the optimal value of p_{ic} as $p_{ic}(opt) = \max(0, \alpha - p_{ua})$. Fig. 2.8 shows that in the initial part of the plot (until $t = 800$ s), the value of α is close to 0, and the p_{ic} achieved by PCAP Cassandra is close to optimal.

At time $t = 800$ s in Fig. 2.8, we sharply increase the one-way server-to-LAN delay for 5 out of 9 servers from 10 ms to 26 ms. This sharp network jump results in a lossier network, as shown by the value of α going up from

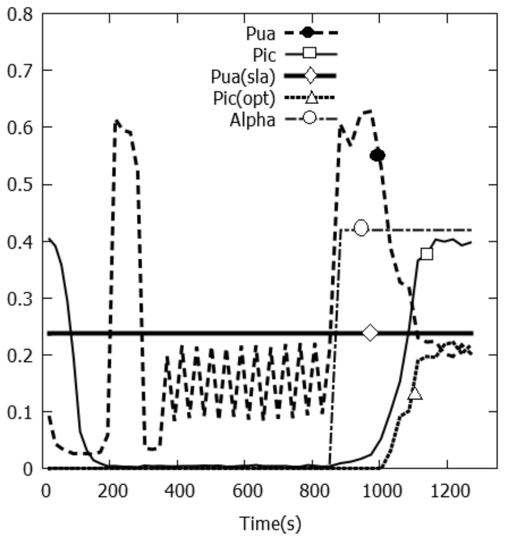

Figure 2.8: Latency SLA with PCAP Cassandra under Sharp Network Jump at 800 s: Timeline.

0 to 0.42. As a result, the value of p_{ua} initially spikes – however, the PCAP system adapts, and by time $t = 1200$ s the value of p_{ua} has converged back to under the SLA.

However, the high value of $\alpha (= 0.42)$ implies that the optimal-achievable $p_{ic}(opt)$ is also higher after $t = 800\ s$. Once again we notice that p_{ic} converges in the second segment of Fig. 2.8 by $t = 1200$ s.

To visualize how close the PCAP system is to the optimal-achievable envelope, Fig. 2.9 shows the two achievable envelopes as piecewise linear segments (named "before jump" and "after jump") and the (p_{ua}, p_{ic}) data points from our run in Fig. 2.8. The figure annotates the clusters of data points by their time interval. We observe that in the stable states both before the jump (dark circles) and after the jump (empty triangles) are close to their optimal-achievable envelopes.

Fig. 2.10 shows the CDF plot for p_{ua} and p_{ic} in the steady state time interval [400 s, 800 s] of Fig. 2.8, corresponding to the bottom left cluster from Fig. 2.9. We observe that p_{ua} is always below the SLA.

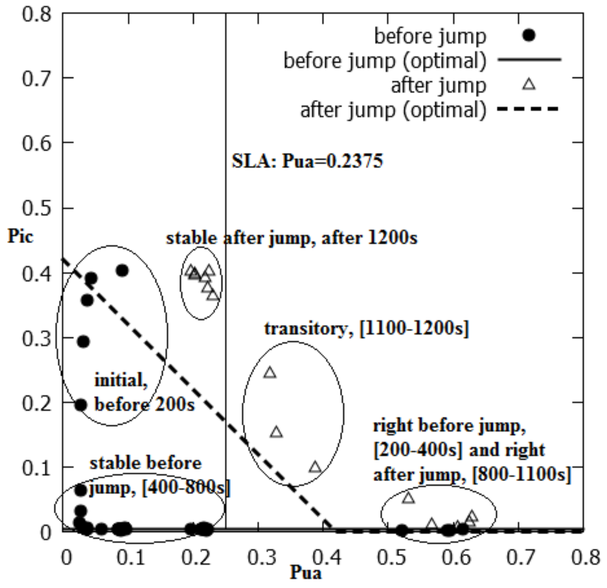

Figure 2.9: Latency SLA with PCAP Cassandra under Sharp Network Jump: Consistency-Latency Scatter plot.

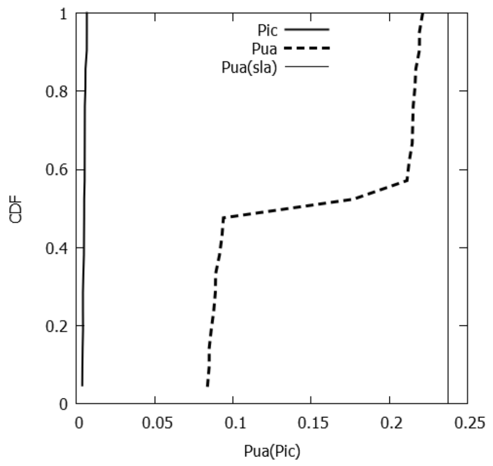

Figure 2.10: Latency SLA with PCAP Cassandra under Sharp Network Jump: Steady State CDF [400 s, 800 s].

Fig. 2.11 shows a scatter plot for our PCAP Riak system under a latency SLA ($p_{ua}^{sla} = 0.2375$, $t_a = 150\ ms$, $t_c = 0\ ms$). The sharp network jump occurs at time $t = 4300$ s when we increase the one-way server-to-LAN delay for 4 out of the 9 Riak nodes from 10 ms to 26 ms. It takes about 1200 s for p_{ua} to converge to the SLA (at around $t = 1400$ s in the warm up segment and $t = 5500$ s in the second segment).

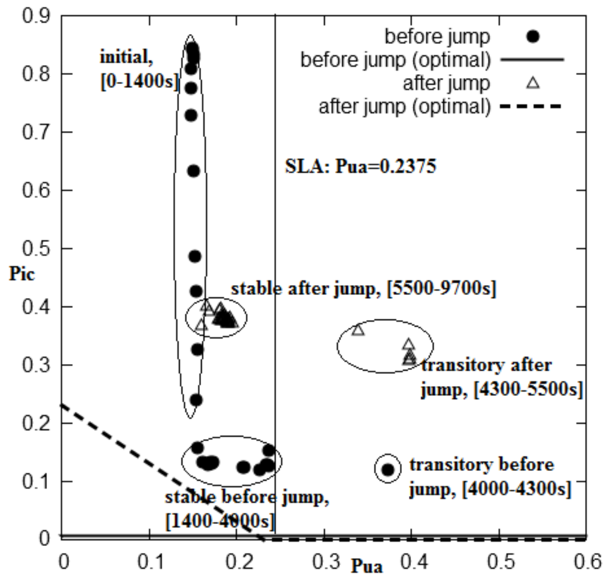

Figure 2.11: Latency SLA with PCAP Riak under Sharp Network Jump: Consistency-Latency Scatter plot.

Consistency SLA under Sharp Network Jump

We present consistency SLA results for PCAP Cassandra (PCAP Riak results are similar and are omitted). We use $p_{ic}^{sla} = 0.15$, $t_c = 0\ ms$, $t_a = 150\ ms$. The initial one-way server-to-LAN delay is 10 ms. At time 750 s, we increase the one-way server-to-LAN delay for 5 out of 9 nodes to 14 ms. This changes α from 0 to 0.42.

Fig. 2.12 shows the scatter plot. First, observe that the PCAP system meets the consistency SLA requirements, both before and after the jump.

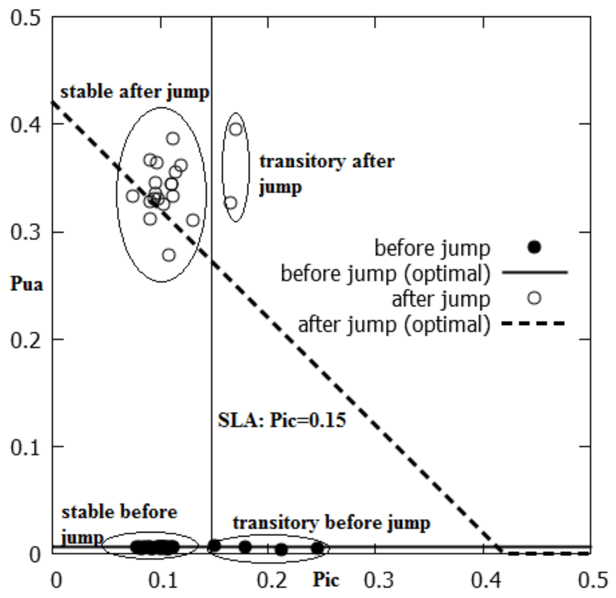

Figure 2.12: Consistency SLA with PCAP Cassandra under Sharp Network Jump: Consistency-Latency Scatter plot.

Second, as network conditions worsen, the optimal-achievable envelope moves significantly. Yet the PCAP system remains close to the optimal-achievable envelope. The convergence time is about 100 s, both before and after the jump.

Experiments with Realistic Delay Distributions

This section evaluates the behavior of PCAP Cassandra and PCAP Riak under continuously-changing network conditions and a consistency SLA (latency SLA experiments yielded similar results and are omitted).

Based on studies for enterprise data-centers [52] we use a lognormal distribution for injecting packet delays into the network. We modified the Linux traffic shaper to add lognormally distributed delays to each packet. Fig. 2.13 shows a timeline where initially ($t = 0$ to 800 s) the delays are lognormally distributed, with the underlying normal distributions of $\mu = 3$ ms and $\sigma = 0.3$ ms. At $t = 800$ s we increase μ and σ to 4 ms and 0.4 ms

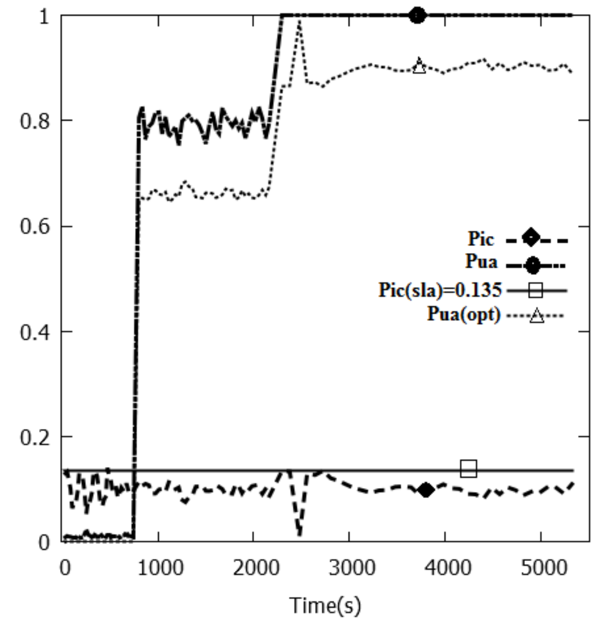

Figure 2.13: Consistency SLA with PCAP Cassandra under Lognormal delay distribution: Timeline.

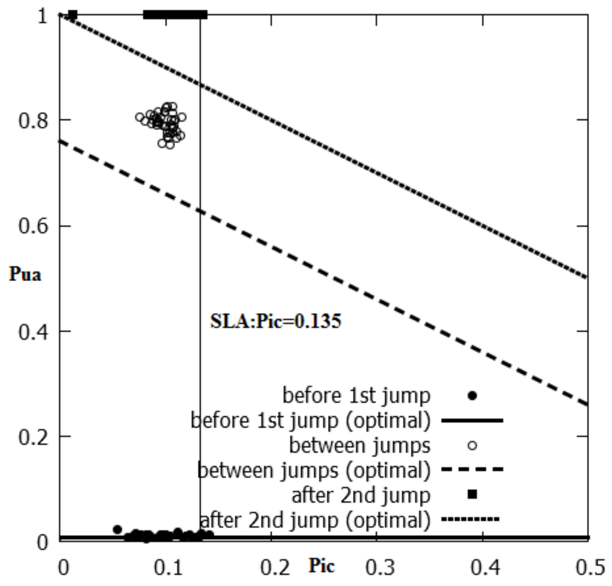

Figure 2.14: Consistency SLA with PCAP Cassandra under Lognormal delay distribution: Consistency-Latency Scatter plot.

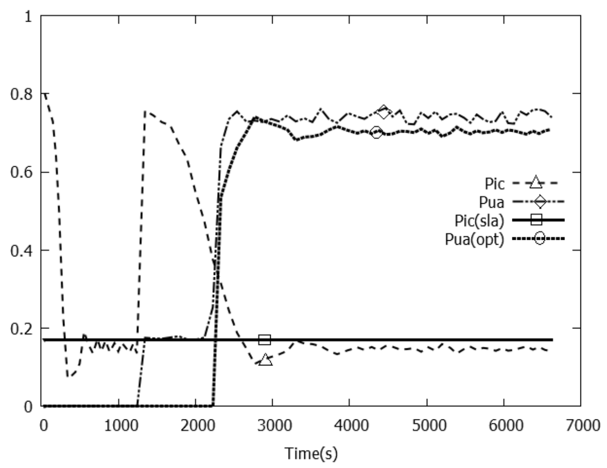

Figure 2.15: Consistency SLA with PCAP Riak under Lognormal delay distribution: Timeline.

respectively. Finally at around 2100 s, μ and σ become 5 ms and 0.5 ms respectively. Fig. 2.14 shows the corresponding scatter plot. We observe that in all three time segments, the inconsistency metric p_{ic}: i) stays below the SLA, and ii) upon a sudden network change converges back to the SLA. Additionally, we observe that p_{ua} converges close to its optimal achievable value.

Fig. 2.15 shows the effect of worsening network conditions on PCAP Riak. At around $t = 1300$ s we increase μ from 1 ms to 4 ms, and σ from 0.1 ms to 0.5 ms. The plot shows that it takes PCAP Riak an additional 1300 s to have inconsistency p_{ic} converge to the SLA. Further the non-SLA metric p_{ua} converges close to the optimal.

So far all of our experiments were conducted using lax timeliness requirements ($t_a = 150\ ms, 200\ ms$), and were run on top of relatively high delay networks. Next we perform a stringent consistency SLA experiment ($t_c = 0\ ms, p_{ic} = .125$) with a very tight latency timeliness requirement ($t_a = 25\ ms$). Packet delays are still lognormally distributed, but with lower values. Fig. 2.16 shows a timeline where initially the delays are lognormally distributed with $\mu = 1\ ms$, $\sigma = 0.1\ ms$. At time $t = 160\ s$ we increase μ and σ to 1.5 ms and 0.15 ms respectively. Then at time $t = 320\ s$, we decrease μ and σ to return to the initial network conditions. We observe that in all three time segments, p_{ic} stays below the SLA, and quickly converges back to the SLA after a network change. Since the network delays are very low throughout the experiment, α is always 0. Thus the optimal p_{ua} is also 0. We observe that p_{ua} converges very close to optimal before the first jump and after the second jump ($\mu = 1\ ms, \sigma = 0.1\ ms$). In the middle time segment ($t = 160$ to $320\ s$), p_{ua} degrades in order to meet the consistency SLA under slightly higher packet delays. Fig. 2.17 shows the corresponding scatter plot. We observe that the system is close to the optimal envelope in the first and last time segments, and the SLA is always met. We note that we are far from optimal in the middle time segment, when the network delays are slightly higher. This shows that when the network conditions are relatively good, the PCAP system is close to the optimal envelope, but when situations worsen we move away. The gap between the system performance and the envelope indicates that the bound (Theorem 2) could be improved further. We leave this as an open question.

Effect of Read Repair Rate Knob

All of our deployment experiments use read delay as the only control knob. Fig. 2.18 shows a portion of a run when only read repair rate was used by our PCAP Cassandra system. This was because read delay was already zero, and we needed to push p_{ic} up to p_{ic}^{sla}. First we notice that p_{ua} does not change with read repair rate, as expected (Table 2.1). Second, we notice that the convergence of p_{ic} is very slow – it changes from 0.25 to 0.3 over a long period

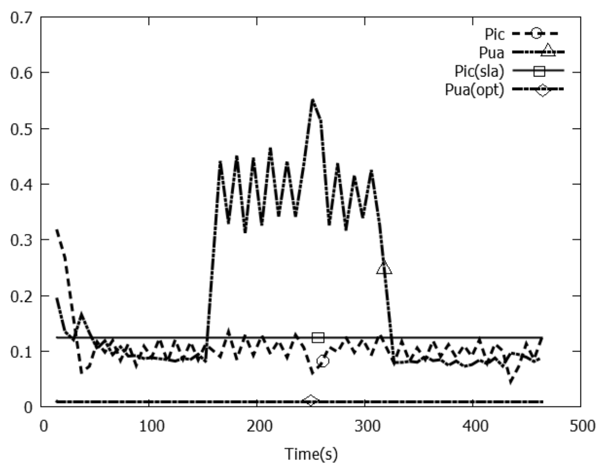

Figure 2.16: Consistency SLA ($t_c = 0\ ms, p_{ic} = 0.125, t_a = 25\ ms$) with PCAP Cassandra under Lognormal delay (low) distribution: Timeline.

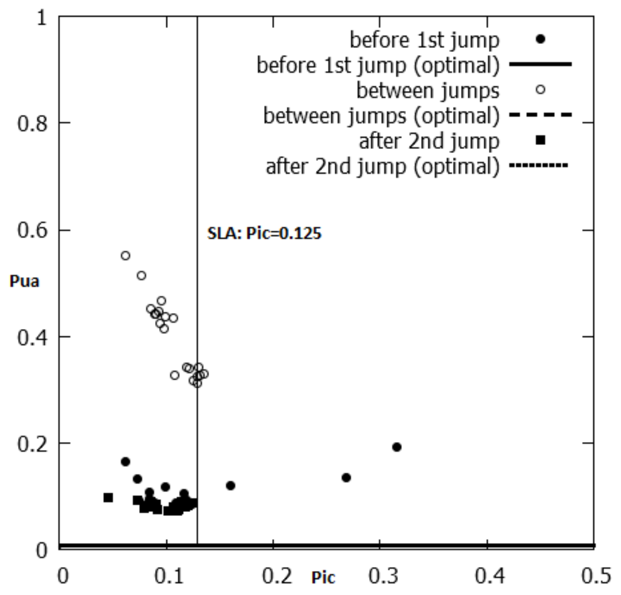

Figure 2.17: Consistency SLA ($t_c = 0\ ms, p_{ic} = 0.125, t_a = 25\ ms$) with PCAP Cassandra under Lognormal delay (low) distribution: Scatter Plot.

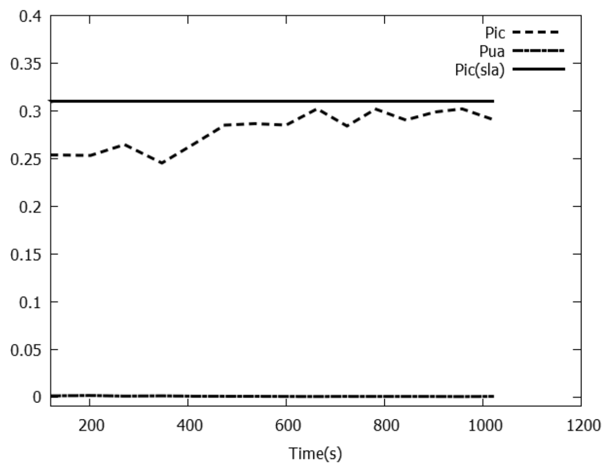

Figure 2.18: Effect of Read Repair Rate on PCAP Cassandra. $p_{ic} = 0.31$, $t_c = 0\ ms$, $t_a = 100\ ms$.

of 1000 s.

Due to this slow convergence, we conclude that read repair rate is useful only when network delays remain relatively stable. Under continuously changing network conditions (e.g., a lognormal distribution) convergence may be slower and thus read delay should be used as the only control knob.

Scalability

We measure scalability via an increased workload on PCAP Cassandra. Compared to Fig. 2.14, in this new run we increased the number of servers from 9 to 32, and throughput to 16000 ops/s, and ensured that each server stores at least some keys. All other settings are unchanged compared to Fig. 2.14. The result is shown Fig. 2.19. Compared with Fig. 2.14, we observe an improvement with scale – in particular, increasing the number of servers brings the system closer to optimal. As the number of servers in the system increase, the chance of finding a replica server close to a client proxy also increases. This in turn lowers read latency, thus bringing the system closer to the optimal envelope.

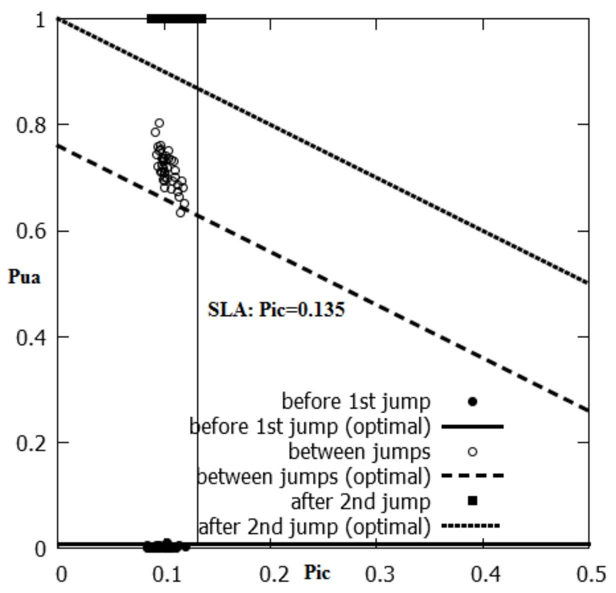

Figure 2.19: Scatter plot for same settings as Fig. 2.14, but with 32 servers and 16K ops/s.

Effect of Timeliness Requirement

The timeliness requirements in an SLA directly affect how close the PCAP system is to the optimal-achievable envelope. Fig. 2.20 shows the effect of varying the timeliness parameter t_a in a consistency SLA ($t_c = 0\ ms$, $p_{ic} = 0.135$) experiment for PCAP Cassandra with 10 ms node to LAN delays. For each t_a, we consider the cluster of the (p_{ua}, p_{ic}) points achieved by the PCAP system in its stable state, calculate its centroid, and measure (and plot on vertical axis) the distance d from this centroid to the optimal-achievable consistency-latency envelope. Note that the optimal envelope calculation also involves t_a, since α depends on it (Section 2.5.3).

Fig. 2.20 shows that when t_a is too stringent (< 100 ms), the PCAP system may be far from the optimal envelope even when it satisfies the SLA. In the case of Fig. 2.20, this is because in our network, the average time to cross four hops (client to coordinator to replica, and the reverse) is $20 \times 4 = 80$ ms.[8] As

[8]Round-trip time for each hop is $2 \times 10 = 20$ ms.

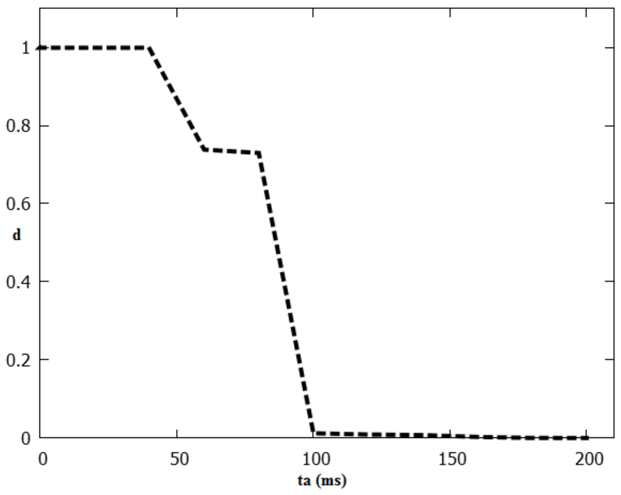

Figure 2.20: Effect of Timeliness Requirement (t_a) on PCAP Cassandra. Consistency SLA with $p_{ic} = 0.135$, $t_c = 0\ ms$.

t_a starts to go beyond this (e.g., $t_a \geq 100$ ms), the timeliness requirements are less stringent,and PCAP is essentially optimal (very close to the achievable envelope).

Passive Measurement Approach

So far all our experiments have used the active measurement approach. In this section, we repeat a PCAP Cassandra consistency SLA experiment ($p_{ic} = 0.2$, $t_c = 0\ ms$) using a passive measurement approach.

In Figure 2.21, instead of actively injecting operations, we sample ongoing client operations. We estimate p_{ic} and p_{ua} from the 100 latest operations from 5 servers selected randomly.

At the beginning, the delay is lognormally distributed with $\mu = 1\ ms$, $\sigma = 0.1\ ms$. The passive approach initially converges to the SLA. We change the delay ($\mu = 2\ ms$, $\sigma = 0.2\ ms$) at $t = 325\ s$. We observe that, compared to the active approach, 1) consistency (SLA metric) oscillates more, and 2) the availability (non-SLA metric) is farther from optimal and takes longer

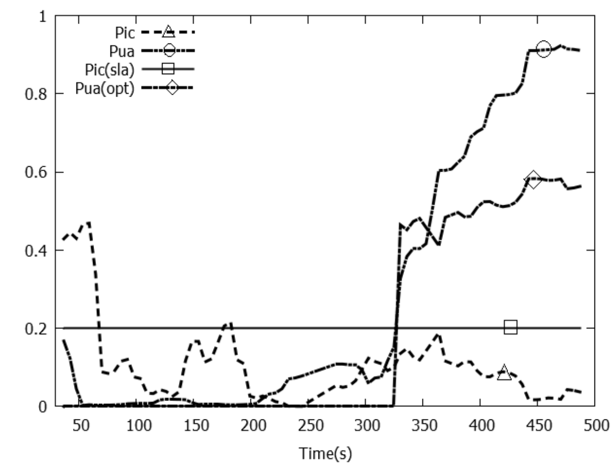

Figure 2.21: Consistency SLA with PCAP Cassandra under Lognormal delay distribution: Timeline (Passive).

to converge. For the passive approach, SLA convergence and non-SLA optimization depends heavily on the sampling of operations used to estimate the metrics. Thus we conclude that it is harder to satisfy SLA and optimize the non-SLA metric with the passive approach.

YCSB Benchmark Experiments

So far we have used YCSB client workloads for all our experiments. Specifically, we used a read-heavy (80% reads) workload. However a 80% read-heavy workload is not one of the standard YCSB benchmark workloads [37]. Thus to facilitate benchmark comparisons of PCAP with other systems with similar capabilities in the future, we show experimental results for PCAP using two standard YCSB benchmark workloads: (1) Workload A (Update heavy) which has 50/50 reads and writes, and (2) Workload D (Read latest with 95% reads) where most recently inserted records are the most popular.

Read Latest Workload In this section, we show the results of a PCAP Cassandra consistency SLA experiment ($p_{ic} = 0.12$, $t_c = 3\ ms$, $t_a = 200\ ms$)

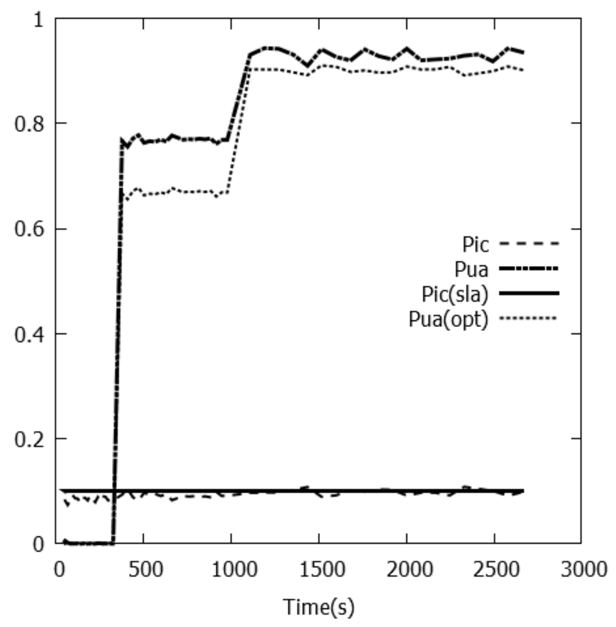

Figure 2.22: Consistency SLA ($t_c = 3\ ms, p_{ic} = 0.12, t_a = 200\ ms$) with PCAP Cassandra under Lognormal delay (latest) distribution: Timeline.

using a read latest workload (YCSB workload d). The timeline plot is shown in Figure 2.22. Initially ($t = 0$ to 380 s) the network delays are lognormally distributed, with the underlying normal distributions of $\mu = 3$ ms and $\sigma = 0.3$ ms. At $t = 380$ s we increase μ and σ to 4 ms and 0.4 ms respectively. Finally at around 1100 s, μ and σ become 5 ms and 0.5 ms respectively. The timeline plots shows that for read-latest workload (with 95% reads), PCAP Cassandra meets the SLA, and also latency p_{ua} converges close to the optimal. This is also evident from the corresponding scatter plot in Figure 2.23. The trends for read-latest do not exhibit marked differences from our previous experiments with read-heavy workloads (80% reads).

Update Heavy Workload Next we present results of a PCAP Cassandra consistency SLA experiment ($p_{ic} = 0.12$, $t_c = 3\ ms$, $t_a = 200\ ms$) using an update heavy workload (YCSB workload a, 50% writes). For this experiment, we increase the average network delay from 3 ms to 4 ms at time

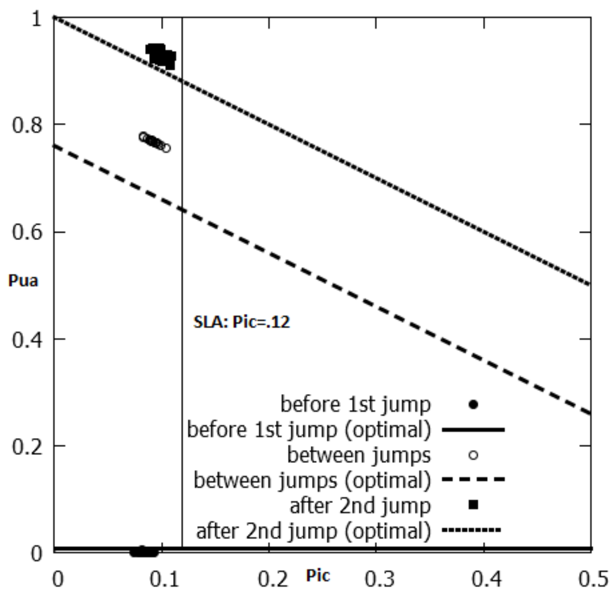

Figure 2.23: Consistency SLA ($t_c = 3\ ms, p_{ic} = 0.12, t_a = 200\ ms$) with PCAP Cassandra under Lognormal delay (latest) distribution: Scatter Plot.

540 s, and from 4 ms to 5 ms at time 1630 s. The timeline plot in Figure 2.24 indicates poor convergence behavior compared to read-heavy and read-latest distributions. Especially after the second jump, it takes about 1000 s to converge back to SLA. This is because our target key-value stores (Cassandra, Riak) rely heavily on read-repair mechanisms to sycnhronize replicas in the background. With an update-heavy workload, read-repair synchronization mechanisms lose their effectiveness, which makes it harder to guarantee consistency SLA convergence. The scatter plot in Figure 2.25 however shows that PCAP Cassandra performs close to the optimal envelope, except for some outliers which are transient states before convergence. It should be noted that an update-heavy workload is not a realistic workload for many key-value stores, and we have only presented results with such workloads for future comparison with other systems using standard benchmarks like YCSB.

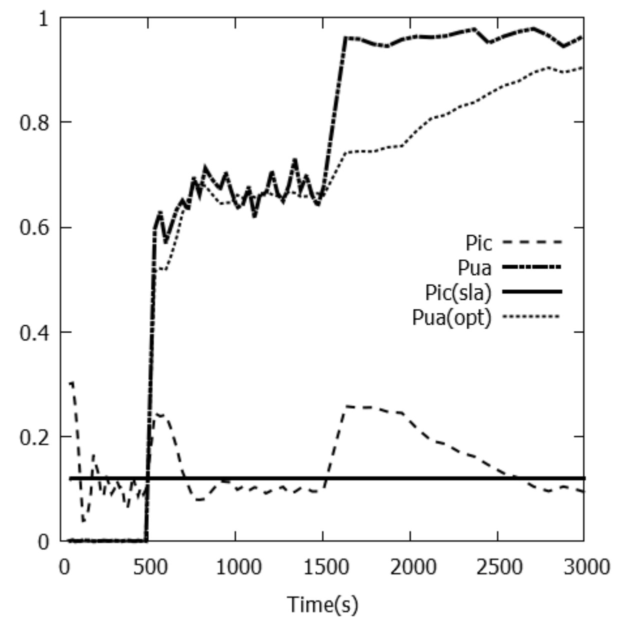

Figure 2.24: Consistency SLA ($t_c = 3\ ms, p_{ic} = 0.12, t_a = 200\ ms$) with PCAP Cassandra under Lognormal delay (update-heavy) distribution: Timeline.

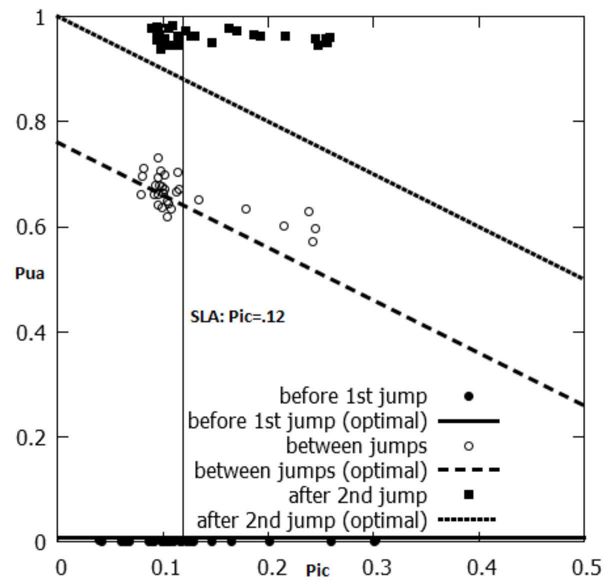

Figure 2.25: Consistency SLA ($t_c = 3\ ms, p_{ic} = 0.12, t_a = 200\ ms$) with PCAP Cassandra under Lognormal delay (update-heavy) distribution: Scatter Plot.

2.6 Related Work

In this section we discuss related work for our PCAP system.

2.6.1 Consistency-Latency Tradeoffs

In addition to the Weak CAP Principle [76] and PACELC [40] discussed in Section 2.1, there has been work on theoretically characterizing the tradeoff between latency and strong consistency models. Attiya and Welch [47] studied the tradeoff between latency and linearizability and sequential consistency. Subsequent work has explored linearizablity under different delay models [72, 112]. All these papers are concerned with strong consistency models whereas we consider t-freshness, which models data freshness in eventually consistent systems. Moreover, their delay models are different from our partition model. There has been theoretical work on probabilistic quorum systems [41, 101, 111]. Their consistency models are different from ours; moreover, they did not consider the tradeoff between consistency and availability.

There are two classes of systems that are closest to our work. The first class of systems are concerned with metrics for measuring data freshness or staleness. We do not compare our work against this class of systems in this chapter, as it is not our goal to propose yet another consistency model or metric. [49, 50] propose a probabilistic consistency model (PBS) for quorum-based stores, but did not consider latency, soft partitions or the CAP theorem. [81] propose a time-based staleness metric called Δ-atomicity. Δ-atomicity is considered the gold standard for measuring atomicity violations (staleness) across multiple read and write operations. The Γ metric [82] is inspired by the Δ metric and improves upon it on multiple fronts. For example, the Γ metric makes fewer technical assumptions than the Δ metric and produces less noisy results. It is also more robust against clock skew. All these related data freshness metrics cannot be directly compared to our t-freshness metric. The reason is that unlike our metric which considers write start times, these existing metrics consider end time of write operations when calculating data freshness.

The second class of systems deal with adaptive mechanisms for meeting consistency-latency SLAs for key-value stores. The Pileus system [135] considers families of consistency/latency SLAs, and requires the application to specify a utility value with each SLA. In comparison, PCAP considers probabilistic metrics of p_{ic}, p_{ua}. Tuba [45] extends the predefined and static Pileus mechanisms with dynamic replica reconfiguration mechanisms to maximize Pileus style utility functions without impacting client read and write operations. [83] propose consistency amplification, which is a framework for supporting consistency SLAs by injecting delays at servers or clients. In comparison, in our PCAP system, we only add delays at servers. [113] propose continuous partial quorums (CPQ), which is a technique to randomly choose between multiple discrete consistency levels for fine-grained consistency-latency tuning, and compare CPQ against consistency amplification. Compared to all these systems where the goal is to meet SLAs, in our work, we also (1) quantitatively characterize the (un)achievable consistency-latency tradeoff envelope, and (2) show how to design systems that perform close to this envelope, in addition to (3) meeting SLAs. The PCAP system can be setup to work with any of these SLAs listed above; but we don't do this in the chapter since our main goal is to measure how close the PCAP system is to the optimal consistency-latency envelope.

Recently, there has been work on declarative ways to specify application consistency and latency requirements – PCAP proposes mechanisms to satisfy such specifications [133].

2.6.2 Adaptive Systems

There are a few existing systems that controls consistency in storage systems. FRACS [146] controls consistency by allowing replicas to buffer updates up to a given staleness. AQuA [98] continuously moves replicas between "strong" and "weak" consistency groups to implement different consistency levels. [76] show how to trade consistency (harvest) for availability (yield) in the context of the Inktomi search engine. While harvest and yield capture continuously changing consistency and availability conditions, we characterize the consistency-availability (latency) tradeoff in a quantitative manner. TACT [142] controls staleness by limiting the number of outstanding writes at replicas (order error) and bounding write propagation delay (staleness). All the mentioned systems provide *best-effort* behavior for consistency, within the latency bounds. In comparison, the PCAP system explicitly allows applications to specify SLAs. Consistency levels have been adaptively changed to deal with node failures and network changes in [69], however this may be intrusive for applications that explicitly set consistency levels for operations. Artificially delaying read operations at servers (similar to our read delay knob) has been used to eliminate staleness spikes (improve consistency) which are correlated with garbage collection in a specific key-value store (Apache Cassandra) [75]. Similar techniques have been used to guarantee causal consistency for client-side applications [145]. Simba [121] proposes new consistency abstractions for mobile application data synchronization services, and allows applications to choose among various consistency models.

For stream processing, [77] propose a control algorithm to compute the optimal resource requirements to meet throughput requirements. There has been work on adaptive elasticity control for storage [104], and adaptively tuning Hadoop clusters to meet SLAs [89]. Compared to the controllers present in these systems, our PCAP controller achieves control objectives [87] using a different set of techniques to meet SLAs for key-value stores.

2.7 Summary

In this chapter, we have first formulated and proved a probabilistic variation of the CAP theorem which took into account probabilistic models for consistency, latency, and soft partitions within a data-center. Our theorems show the un-achievable envelope, i.e., which combinations of these three models make them impossible to achieve together. We then show how to design systems (called PCAP) that (1) perform close to this optimal envelope, and (2) can meet consistency and latency SLAs derived from the corresponding models. We then incorporated these SLAs into Apache Cassandra and Riak running in a single data-center. Our experiments with YCSB workloads and realistic traffic demonstrated that our PCAP system meets the SLAs, that its performance is close to the optimal-achievable consistency-availability envelope, and that it scales well.

Chapter 3

GeoPCAP: Probabilistic Composition and Adaptive Control for Geo-distributed Key-Value Stores

In this chapter, we extend our PCAP system presented in Chapter 2 from a single data-center to multiple geo-distributed data-centers. We call this system GeoPCAP. The key contribution of GeoPCAP is a set of rules for composing probabilistic consistency/latency models from across multiple data-centers in order to derive the global consistency-latency tradeoff behavior. Realistic simulations demonstrate that GeoPCAP can satisfactorily meet consistency/latency SLAs for applications interacting with multiple data-centers, while optimizing the other metric.

3.1 Introduction

Distributed key-value stores (e.g., Cassandra [8], Riak [7], Dynamo [71], Voldemort [24]) are preferred by applications for whom eventual consistency suffices, but where high availability (i.e., fast reads and writes [40]) is paramount. Availability is a critical metric for such cloud services because latency is correlated to user satisfaction – for instance, a 500 ms increase in latency for operations at Google.com can cause a 20% drop in revenue [1]. At Amazon, this translates to a $6M yearly loss per added millisecond of latency [2]. At the same time, clients in such applications expect freshness, i.e., data returned by a read to a key should come from the latest writes done to that key by any client. For instance, Netflix uses Cassandra to track positions in each video [66], and freshness of data translates to accurate tracking and user satisfaction. This implies a *time-based* notion of consistency.

Internet Web applications built out of key value stores are facing an ever worsening scalability challenge due to multiple reasons. First, the number of users is growing across an increasing number of geographic regions (Facebook had over 1.39 billion active users as of Dec 2014 [14]). Second, the storage needs per user is also growing as more information is stored online. As users accumulate more data, the systems also store more information per user for generating targeted ads and user recommendations. Finally, replication of data for fault-tolerance also rapidly increases storage space. As a result many of these applications need to be geo-distributed, hence the need for geo-distributed deployment for key-value stores.

Geo-distributed key-value stores use geo-replication, meaning the same key is replicated at different data-centers. So these systems offer high availability by replicating data across datacenters, and low latency by placing data close to clients. From a client perspective, there should be no difference between interacting with a single datacenter vs interacting with multiple geo-distributed datacenters transparently. Hence if we compose a geo-distributed key-value service by composing multiple instances of a key-value service (one in each data-center), then the customer should be transparent to this geo-distribution.

For example, assume an Internet service has three storage systems at three regional data-centers; one in America, one in Europe, and one in Asia. Depending on user requirements, the data for a particular user can be stored/replicated from one to all three locations. Also the storage systems within each region can replicate the data multiple times. Based on storage configurations, each data-center storage system instance offers different tradeoffs between data consistency and latency/availability. Thus when the service provider offers a read API to a client, it should transparently compose the service offered from one or more per data-center instances in order to satisfy the client read request with a given consistency or latency requirement. This requires a principled way to compose consistency-latency guarantees from different geo-distributed storage services.

In this chapter we develop a formal probabilistic framework for composing consistency-latency models of different storage services geo-distributed across multiple data-centers. A service provider can thus use these rules to compose services of different storage instances to meet desired consistency-latency tradeoffs. We offer two types of composition rules. First the `QUICKEST` composition rule ensures that at-least one data-center instance provides the desired service level. The other rule is `ALL` composition, which guarantees all data-centers meet the desired per data-center consistency-latency requirement. Our rules are generic and hold for an arbitrary number of data-center instances.

Next we present the design and implementation of a system called GeoPCAP, which is a geo-distributed extension of the PCAP system presented in Chapter 2. GeoPCAP uses the probabilistic composition rules and an adaptive control loop based on PID control theory to continuously meet SLAs for a geo-distributed key-value storage system under WAN network delay variations. Realistic simulation results indicate that GeoPCAP can satisfactorily meet SLAs in the presence of WAN delay variations.

3.2 System Model

Assume there are n data-centers. Each data-center stores multiple replicas for each data-item. When a client application submits a query, the query is first forwarded to the data-center closest to the client. We call this data-center the *local* data-center for the client. If the local data-center stores a replica of the queried data item, that replica might not have the latest value, since write operations at other data-centers could have updated the data item. Thus in our system model, the local data-center contacts one or more of other remote data-centers, to retrieve (possibly) fresher values for the data item.

3.3 Probabilistic Composition Rules

Each data-center is running our PCAP-enabled key-value store. Each such PCAP instance defines per data-center probabilistic latency and consistency models (Section 2.2). To obtain the global behavior, we need to compose these probabilistic consistency and latency/availability models across different data-centers. This is done by our composition rules.

The composition rules for merging independent latency/consistency models from data-centers check whether the SLAs are met by the composed system. Since single data-center PCAP systems define probabilistic latency and consistency models, our composition rules are also probabilistic in nature. However in reality, our composition rules do not require all data-centers to run PCAP-enabled key-value stores systems. As long as we can measure consistency and latency at each data-center, we can estimate the probabilistic models of consistency/latency at each data-center and use our composition rules to merge them.

We consider two types of composition rules: (1) `QUICKEST` (Q), where at-least one data-center (e.g., the local or closest remote data-center) satisfies client specified latency or freshness (consistency) guarantees; and (2) `ALL` (A), where all the data-centers must satisfy latency or freshness guarantees. These two are, respectively, generalizations of Apache Cassandra multi-data-center deployment [38] consistency levels (CL): `LOCAL_QUORUM` and `EACH_QUORUM`.

Compared to Section 2.2, which analyzed the fraction of executions that satisfy a predicate (the proportional approach), in this section we use a simpler probabilistic approach. This is because although the proportional approach is more accurate, it is more intractable than the probabilistic model in the geo-distributed case.

Our probabilistic composition rules fall into three categories: (1) composing consistency models; (2) composing latency models; and (3) composing a wide-area-network (WAN) partition model with a data-center (consistency or latency) model. The rules are summarized in Table 3.1, and we discuss them next.

3.3.1 Composing Latency Models

Assume there are n data-centers storing the replica of a key with latency models $(t_a^1, p_{ua}^1), (t_a^2, p_{ua}^2), \ldots, (t_a^n, p_{ua}^n)$. Let $\mathcal{C}^A$ denote the composed system. Let (p_{ua}^c, t_a^c) denote the latency model of the composed system $\mathcal{C}^A$. This indicates that the fraction of reads in $\mathcal{C}^A$ that complete within t_a^c time units is at least $(1 - p_{ua}^c)$. This is the latency SLA expected by clients. Let $p_{ua}^c(t)$ denote the probability of missing deadline by t time units in the composed model. Let X_j denote the random variable measuring read latency in data center j. Let $E_j(t)$ denote the event that $X_j > t$. By definition we have that,

Consistency/Latency/WAN	Composition	$\forall j$, is $t_a^j = t$?	Rule
Latency	`QUICKEST`	Y	$p_{ua}^c(t) = \Pi_j \ p_{ua}^j, \forall j, \ t_a^j = t$
Latency	`QUICKEST`	N	$p_{ua}^c(min_j \ t_a^j) \geq \Pi_j \ p_{ua}^j \geq p_{ua}^c(max_j \ t_a^j)$, $min_j \ t_a^j \leq t_a^c \leq max_j \ t_a^j$
Latency	`ALL`	Y	$p_{ua}^c(t) = 1 - \Pi_j \ (1 - p_{ua}^j), \forall j, \ t_a^j = t$
Latency	`ALL`	N	$p_{ua}^c(min_j \ t_a^j) \geq 1 - \Pi_j \ (1 - p_{ua}^j) \geq p_{ua}^c(max_j \ t_a^j)$, $min_j \ t_a^j \leq t_a^c \leq max_j \ t_a^j$
Consistency	`QUICKEST`	Y	$p_{ic}^c(t) = \Pi_j \ p_{ic}^j, \forall j, \ t_c^j = t$
Consistency	`QUICKEST`	N	$p_{ic}^c(min_j \ t_c^j) \geq \Pi_j \ p_{ic}^j \geq p_{ic}^c(max_j \ t_c^j)$, $min_j \ t_c^j \leq t_c^c \leq max_j \ t_c^j$
Consistency	`ALL`	Y	$p_{ic}^c(t) = 1 - \Pi_j \ (1 - p_{ic}^j), \forall j, \ t_c^j = t$
Consistency	`ALL`	N	$p_{ic}^c(min_j \ t_c^j) \geq 1 - \Pi_j \ (1 - p_{ic}^j) \geq p_{ic}^c(max_j \ t_c^j)$, $min_j \ t_c^j \leq t_c^c \leq max_j \ t_c^j$
Consistency-WAN	N. A.	N. A.	$Pr[X + Y \geq t_c + t_p^G] \geq p_{ic} \cdot \alpha^G$
Latency-WAN	N. A.	N. A.	$Pr[X + Y \geq t_a + t_p^G] \geq p_{ua} \cdot \alpha^G$

Table 3.1: GeoPCAP Composition Rules.

$Pr[E_j(t_a^j)] = p_{ua}^j$, and $Pr[\bar{E}_j(t_a^j)] = 1 - p_{ua}^j$. Let $f_j(t)$ denote the cumulative distribution function (CDF) for X_j. So by definition, $f_j(t_a^j) = Pr[X_j \leq t_a^j] = 1 - Pr[X_j > t_a^j]$. The following theorem articulates the probabilistic latency composition rules:

Theorem 3 *Let n data-centers store the replica for a key with latency models* $(t_a^1, p_{ua}^1), (t_a^2, p_{ua}^2), \ldots, (t_a^n, p_{ua}^n)$*. Let* $\mathcal{C}^A$ *denote the composed system with latency model* (p_{ua}^c, t_a^c)*. Then for composition rule* `QUICKEST` *we have:*

$$\begin{aligned} p_{ua}^c(min_j\ t_a^j) \geq \Pi_j\ p_{ua}^j \geq p_{ua}^c(max_j\ t_a^j), \\ and\ \ min_j\ t_a^j \leq t_a^c \leq max_j\ t_a^j, \\ where j \in \{1, \cdots, n\}. \end{aligned} \tag{3.1}$$

For composition rule `ALL`*,*

$$\begin{aligned} p_{ua}^c(min_j\ t_a^j) \geq 1 - \Pi_j\ (1 - p_{ua}^j) \geq p_{ua}^c(max_j\ t_a^j), \\ and\ \ min_j\ t_a^j \leq t_a^c \leq max_j\ t_a^j, \\ where j \in \{1, \cdots, n\}. \end{aligned} \tag{3.2}$$

Proof: We outline the proof for composition rule `QUICKEST`. In `QUICKEST`, a latency deadline t is violated in the composed model when all data-centers miss the t deadline. This happens with probability $p_{ua}^c(t)$ (by definition). We first prove a simpler Case 1, then the general version in Case 2.

Case 1: Consider the simple case where all t_a^j values are identical, i.e., $\forall j, t_a^j = t_a$: $p_{ua}^c(t_a) = Pr[\cap_i E_i(t_a)] = \cap_i Pr[E_i(t_a)] = \Pi_i p_{ua}^i$ (assuming independence across data-centers).

Case 2:

Let,

$$t_a^i = min_j \ t_a^j \tag{3.3}$$

Then,

$$\forall j, \ t_a^j \geq t_a^i \tag{3.4}$$

Then, by definition of CDF function,

$$\forall j, \ f_j(t_a^i) \leq f_j(t_a^j) \tag{3.5}$$

By definition,

$$\forall j, \ (Pr[X_j \leq t_a^i] \leq Pr[X_j \leq t_a^j]) \tag{3.6}$$

$$\forall j, \ (Pr[X_j > t_a^i] \geq Pr[X_j > t_a^j]) \tag{3.7}$$

Multiplying all,

$$\Pi_j \ Pr[X_j > t_a^i] \geq \Pi_j \ Pr[X_j > t_a^j] \tag{3.8}$$

But this means,

$$p_{ua}^c(t_a^i) \geq \Pi_j \ p_{ua}^j \tag{3.9}$$

$$p_{ua}^c(min_j \ t_a^j) \geq \Pi_j \ p_{ua}^j \tag{3.10}$$

Similarly, let

$$t_a^k = max_j \ t_a^j \tag{3.11}$$

Then,

$$\forall j, \ t_a^k \geq t_a^j \tag{3.12}$$

$$\forall j, \ (Pr[X_j > t_a^j] \geq Pr[X_j > t_a^k]) \tag{3.13}$$

$$\Pi_j \ Pr[X_j > t_a^j] \geq \Pi_j \ Pr[X_j > t_a^k] \tag{3.14}$$

$$\Pi_j \ p_{ua}^j \geq p_{ua}^c(t_a^k) \tag{3.15}$$

$$\Pi_j \ p_{ua}^j \geq p_{ua}^c(max_j \ t_a^j) \tag{3.16}$$

Finally combining Equations 3.10, and 3.16, we get Equation 3.1.

The proof for composition rule `ALL` follows similarly. In this case, a latency deadline t is satisfied when all data-centers satisfy the deadline. So a deadline miss in the composed model means at-least one data-center misses the deadline. The derivation of the composition rules are similar and we invite the reader to work them out to arrive at the equations depicted in Table 3.1.

□

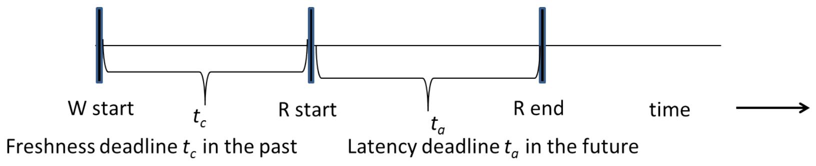
W start
t_c
R start
t_a
R end
time
Freshness deadline t_c in the past
Latency deadline t_a in the future

Figure 3.1: Symmetry of freshness and latency requirements.

3.3.2 Composing Consistency Models

t-latency (Definition 3) and t-freshness (Definitions 1) guarantees are time-symmetric (Figure 3.1). While t-lateness can be considered a deadline in the future, t-freshness can be considered a deadline in the past. This means that for a given read, t-freshness constrains how old a read value can be. So the composition rules remain the same for consistency and availability.

Thus the consistency composition rules can be obtained by substituting p_{ua} with p_{ic} and t_a with t_c in the latency composition rules (last 4 rows in Table 3.1).

This leads to the following theorem for consistency composition:

Theorem 4 *Let n data-centers store the replica for a key with consistency models $(t_c^1, p_{ic}^1), (t_c^2, p_{ic}^2), \ldots, (t_c^n, p_{ic}^n)$. Let $\mathcal{C}^A$ denote the composed system with consistency model (p_{ic}^c, t_c^c). Then for composition rule **`QUICKEST`** we have:*

$$\begin{aligned} p_{ic}^c(min_j\ t_c^j) \geq \Pi_j\ p_{ic}^j \geq p_{ic}^c(max_j\ t_c^j), \\ and\ min_j\ t_c^j \leq t_c^c \leq max_j\ t_c^j, \\ where j \in \{1, \cdots, n\}. \end{aligned} \tag{3.17}$$

*For composition rule **`ALL`**,*

$$p^c_{ic}(min_j\ t^j_c) \geq 1 - \Pi_j\ (1 - p^j_{ic}) \geq p^c_{ic}(max_j\ t^j_c), \tag{3.18}$$
$$and\ min_j\ t^j_c \leq t^c_c \leq max_j\ t^j_c,$$
$$where j \in \{1, \cdots, n\}.$$

3.3.3 Composing Consistency/Latency Model with a WAN Partition Model

All data-centers are connected to each other through a wide-area-network (WAN). We assume the WAN follows a partition model (t^G_p, α^G). This indicates that α^G fraction of messages passing through the WAN suffers a delay $> t^G_p$. Note that the WAN partition model is distinct from the per data-center partition model (Definition 5). Let X denote the latency in a remote data-center, and Y denote the WAN latency of a link connecting the local data-center to this remote data-center (with latency X). Then the total latency of the path to the remote data-center is $X + Y$.[1]

$$Pr[X + Y \geq t_a + t^G_p] \geq (Pr[X \geq t_a] \cdot Pr[Y \geq t^G_p]) = p_{ua} \cdot \alpha^G. \tag{3.19}$$

Here we assume the WAN latency, and data-center latency distributions are independent. Note that Equation 3.19 gives a lower bound of the probability. In practice we can estimate the probability by sampling both X and Y, and estimating the number of times $(X + Y)$ exceeds $(t_a + t^G_p)$.

[1]We ignore the latency of the local data-center in this rule, since the local data-center latency is used in the latency composition rule (Section 3.3.1).

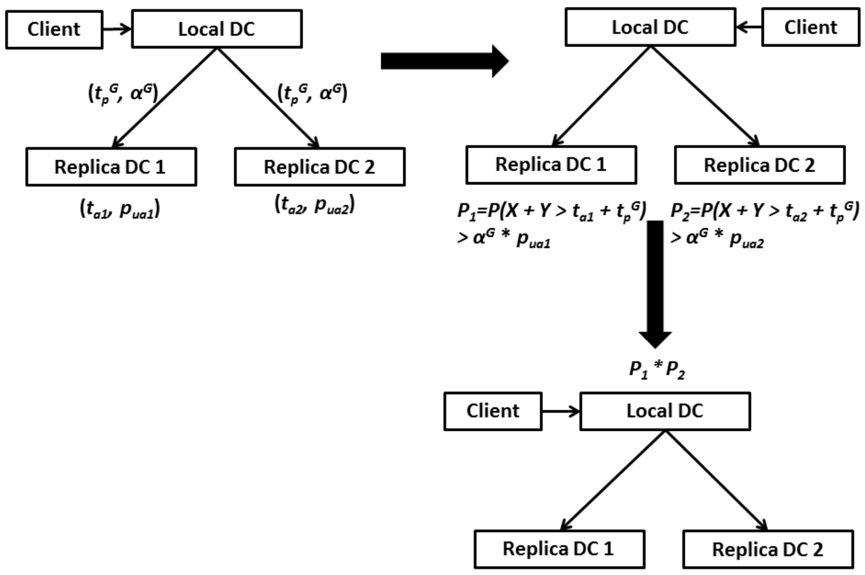

Figure 3.2: Example of composition rules in action.

3.3.4 Example

The example in Figure 3.2 shows the composition rules in action. In this example, there is one local data-center and 2 replica data-centers. Each data-center can hold multiple replicas of a data-item. First we compose each replica data-center latency model with the WAN partition model. Second we take the WAN-latency composed models for each data-center and compose them using the QUICKEST rule (Table 3.1, bottom part).

3.4 GeoPCAP Control Knob

We use a similar delay knob to meet the SLAs in a geo-distributed setting. We call this the *geo-delay* knob and denote it as Δ. The time delay Δ is the delay added at the local data-center to a read request received from a client before it is forwarded to the replica data-centers. Δ affects the consistency-latency trade-off in a manner similar to the read delay knob in a data-center (Section 2.3.1). Increasing the knob tightens the deadline at each replica data-center, thus increasing per data-center latency (p_{ua}). Similar to read delay (Figure 2.1), increasing the geo delay knob improves consistency, since it gives each data-center time to commit latest writes.

3.5 GeoPCAP Control Loop

Our GeoPCAP system uses a control loop depicted in Figure 3.3 for the Consistency SLA case using the `QUICKEST` composition rule. The control loops for the other three combinations (Consistency-`QUICKEST`, Latency-`ALL`, Latency-`QUICKEST`) are similar.

Initially, we opted to use the single data-center multiplicative control loop (Section 2.3.3) for GeoPCAP. However, the multiplicative approach led to increased oscillations for the composed consistency (p_{ic}) and latency (p_{ua}) metrics in a geo-distributed setting. The multiplicative approach sufficed for the single data-center PCAP system, since the oscillations were bounded in steady-state. However, the increased oscillations in a geo-distributed setting prompted us to use a control theoretic approach for GeoCAP.

As a result, we use a PID control theory approach [46] for the GeoPCAP controller. The controller runs an infinite loop, so that it can react to network delay changes and meet SLAs. There is a tunable sleep time at the end of each iteration (1 sec in Section 3.6 simulations). Initially the geo-delay Δ is set to zero. At each iteration of the loop, we use the composition rules to estimate $p^c_{ic}(t)$, where $t = t^{sla}_c + t^G_p - \Delta$. We also keep track of composed $p^c_{ua}()$ values. We then compute the error, as the difference between current composed p_{ic} and the SLA. Finally the geo-delay change is computed using

```
1: procedure CONTROL($\mathcal{SLA} =< p_{ic}^{sla}, t_c^{sla}, t_a^{sla} >$)
2:     Geo-delay $\Delta := 0$
3:     $E := 0$, $Error_{old} := 0$
4:     set $k_p$, $k_d$, $k_i$ for PID control (tuning)
5:     Let $(t_p^G, \alpha^G)$ be the WAN partition model
6:     while (true) do
7:         for each data-center $i$ do
8:             Let $F_i$ denote the random freshness interval at $i$
9:             Let $L_i$ denote the random operation latency at $i$
10:            Let $W_i$ denote the WAN latency of the link to $i$
11:            Estimate $p_{ic}^i := Pr[F_i + W_i > t_c^{sla} + t_p^G + \Delta]$ // WAN composition (Section 3.3.3)
12:            Estimate $p_{ua}^i := Pr[L_i + W_i > t_a + t_p^G - \Delta = t_a^{sla}]$
13:        end for
14:        $p_{ic}^c := \Pi_i p_{ic}^i$, $p_{ua}^c := \Pi_i p_{ua}^i$ // Consistency/Latency composition (Sections 3.3.1 3.3.2)
15:        $Error := p_{ic}^c - p_{ic}^{sla}$
16:        $dE := Error - Error_{old}$
17:        $E := E + Error$
18:        $u := k_p \cdot Error + k_d \cdot dE + k_i \cdot E$
19:        $\Delta := \Delta + u$;
20:    end while
21: end procedure
```

Figure 3.3: Adaptive Control Loop for GeoPCAP Consistency SLA (`QUICKEST` Composition).

the PID control law [46] as follows:

$$u = k_p \cdot Error(t) + k_d \cdot \frac{dError(t)}{dt} + k_i \cdot \int Error(t)dt \tag{3.20}$$

Here, k_p, k_d, k_i represent the proportional, differential, and integral gain factors for the PID controller respectively. There is a vast amount of literature on tuning these gain factors for different control systems [46]. Later in our experiments, we discuss how we set these factors to get SLA convergence. Finally at the end of the iteration, we increase Δ by u. Note that u could be negative, if the metric is less than the SLA.

Note that for the single data-center PCAP system, we used a multiplicative control loop (Section 2.3.3), which outperformed the unit step size policy. For GeoPCAP, we employ a PID control approach. PID is preferable to the multiplicative approach, since it guarantees fast convergence, and can reduce oscillation to arbitrarily small amounts. However PID's stability depends on proper tuning of the gain factors, which can result in high management overhead. On the other hand the multiplicative control loop has a single tuning factor (the multiplicative factor), so it is easier to manage. Later in Section 3.6 we experimentally compare the PID and multiplicative control approaches.

3.6 GeoPCAP Evaluation

We evaluate GeoPCAP with a Monte-Carlo simulation. In our setup, we have four data-centers, among which three are remote data-centers holding replicas of a key, and the fourth one is the local data-center. At each iteration, we estimate t-freshness per data-center using a variation of the well-known WARS model [50]. The WARS model is based on Dynamo style quorum systems [71], where data staleness is due to read and write message reordering. The model has four components. W represents the message delay from coordinator to replica. The acknowledgment from the replica back to the coordinator is modeled by a random variable A. The read message delay from coordinator to replica, and the acknowledgment back are represented by R, and S, respectively. A read will be stale if a read is acknowledged before a write reaches the replica, i. e. , $R+S < W+A$. In our simulation, we ignore the A component since we do not need to wait for a write to finish before a read starts. We use the LinkedIn SSD disk latency distribution [50], Table 3 for read/write operation latency values.

We model the WAN delay using a normal distribution $N(20\ ms, \sqrt{2}\ ms)$ based on results from [51]. Each simulation runs for 300 iterations. At each iteration, we run the PID control loop (Figure 3.3) to estimate a new value for geo-delay Δ, and sleep for 1 sec. All reads in the following iteration are delayed at the local data-center by Δ. At iteration 150, we inject a jump by increasing the mean and standard deviation of each WAN link delay normal distribution to 22 ms and $\sqrt{2.2}\ ms$, respectively. We show only results for consistency and latency SLA for the `ALL` composition. The `QUICKEST` composition results are similar and are omitted.

Figure 3.4 shows the timeline of SLA convergence for GeoPCAP Latency SLA ($p_{ua}^{sla} = 0.27, ta^{sla} = 25\ ms, tc^{sla} = 0.1\ ms$). It should be noted that a latency SLA ($p_{ua}^{sla} = 0.27, ta^{sla} = 25\ ms, tc^{sla} = 0.1\ ms$) for GeoPCAP means that when using the ALL composition rule (all individual data-center deployments must satisfy a latency deadline), each single data-center PCAP needs to provide an SLA specified as ($p_{ua}^{sla} = 0.1, ta^{sla} = 25\ ms, tc^{sla} = 0.1\ ms$) (using the composition rule in the third row of Figure 3.1). We observe that using the PID controller ($k_p = 1$, $k_d = 0.5$, $k_i = 0.5$), both the SLA and the

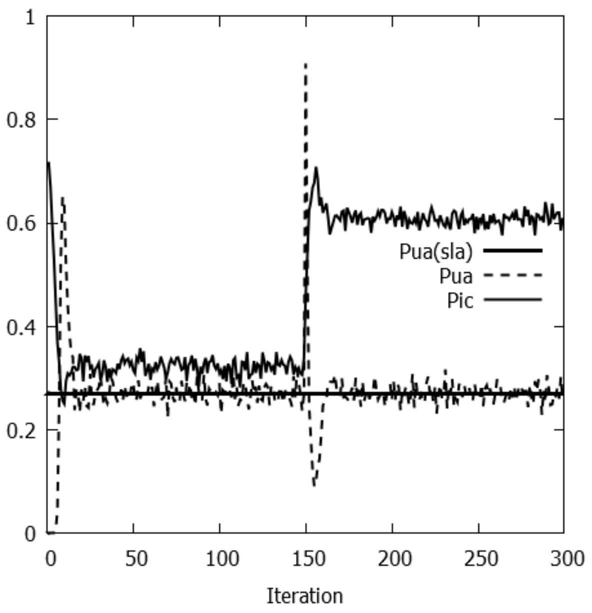

Figure 3.4: GeoPCAP SLA Timeline for L SLA (`ALL`).

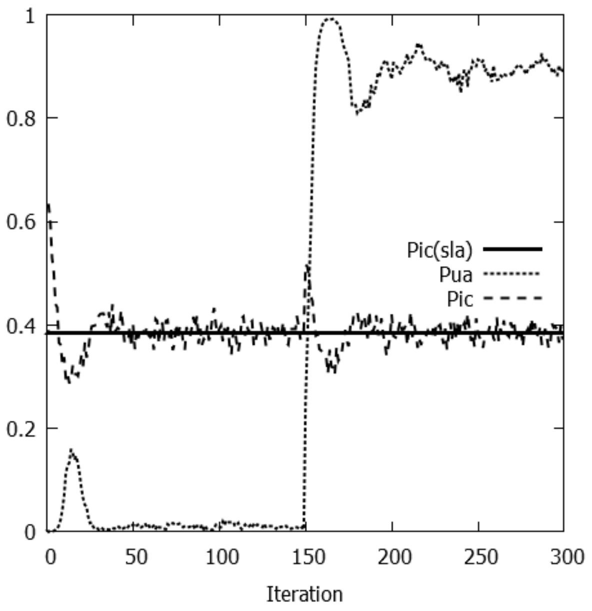

Figure 3.5: GeoPCAP SLA Timeline for C SLA (`ALL`).

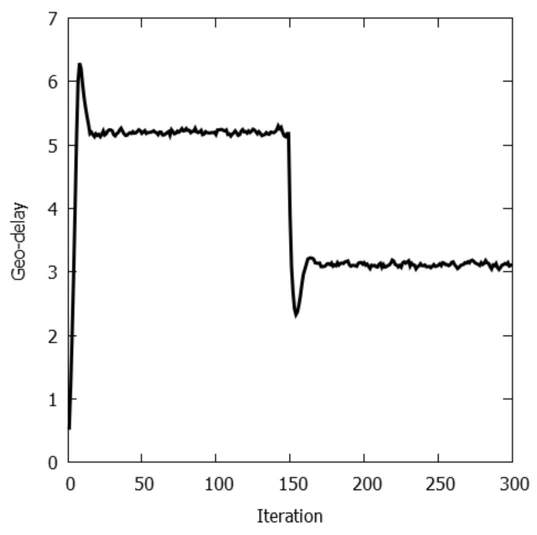

Figure 3.6: Geo-delay Timeline for L SLA (ALL) (Figure 3.4).

other metric converge within 5 iterations initially and also after the jump. Figure 3.6 shows the corresponding evolution of the geo-delay control knob. Before the jump, the read delay converges to around 5 ms. After the jump, the WAN delay increase forces the geo-delay to converge to a lower value (around 3 ms) in order to meet the latency SLA.

Figure 3.5 shows the consistency SLA ($p_{ic}^{sla} = 0.38, tc^{sla} = 1\ ms, ta^{sla} = 25\ ms$) time line. Here convergence takes 25 iterations, thanks to the PID controller (($k_p = 1$, $k_d = 0.8$, $k_i = 0.5$)). We needed a slightly higher value for the differential gain k_d to deal with increased oscillation for the consistency SLA experiment. Note that the p_{ic}^{sla} value of 0.38 forces a smaller per data-center p_{ic} convergence. The corresponding geo-delay evolution (Figure 3.7) initially converges to around 3 ms before the jump, and converges to around 5 ms after the jump, to enforce the consistency SLA after the delay increase.

We also repeated the Latency SLA experiment with the ALL composition (Figures 3.4, 3.6) using the multiplicative control approach (Section 2.3.3) instead of the PID control approach. Figure 3.8 shows the corresponding

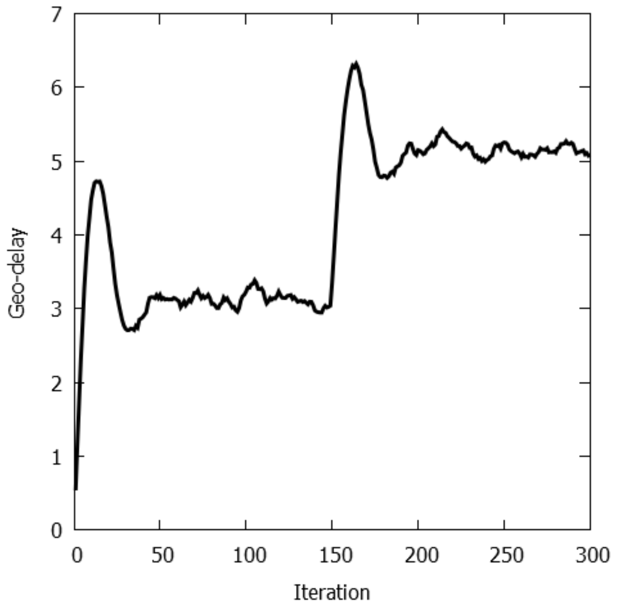

Figure 3.7: Geo-delay Timeline for C SLA (`ALL`) (Figure 3.5).

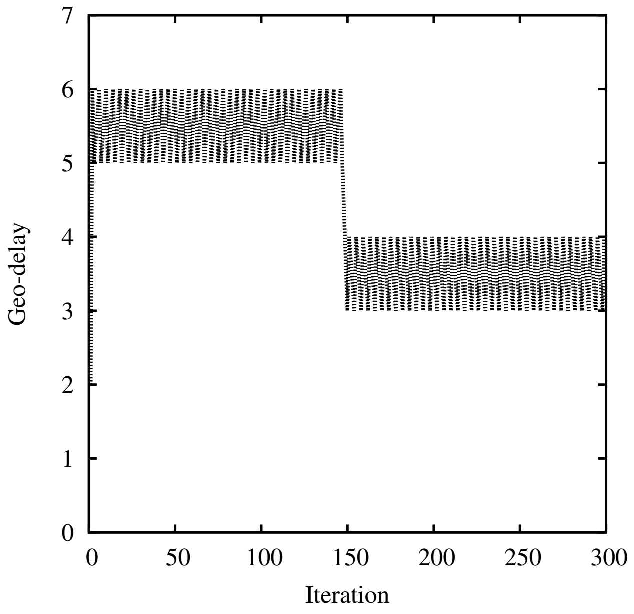

Figure 3.8: Geo-delay Timeline for A SLA (`ALL`) with Multiplicative Approach.

geo-delay trend compared to Figure 3.6. Comparing the two figures, we observe that although the multiplicative strategy converges as fast the PID approach both before and after the delay jump, the read delay value keeps oscillating around the optimal value. Such oscillations cannot be avoided in the multiplicative approach, since at steady state the control loop keeps changing direction with a unit step size. Compared to the multiplicative approach, the PID control approach is smoother and has less oscillations.

3.7 Related Work

In this section we discuss related work for our GeoPCAP system.

3.7.1 Composition

Composing local policies to form global policies is well studied in other domains, for example quality of service (QoS) composition in multimedia networks [103], software defined network (sdn) composition [115], and so on. Our composition techniques are aimed at consistency guarantees for geo-distributed systems.

3.7.2 Geo-distributed Systems

Recent geo-distributed systems include Google Spanner [68] which provides externally consistent strong transactions using gps clocks. Open source key value stores Cassandra and Riak can also be deployed in a geo-distributed manner. COPS/Eiger [105, 106] offer causal consistency across geo-distributed datacenters, whereas Gemini [102] provides a mixture of strong and eventual consistency by classifying operations as either RED (need strong consistency) and BLUE (eventual consistency suffices).

3.8 Summary

In this chapter we have presented our system GeoPCAP, which is a geo-distributed extension of PCAP from chapter 2. GeoPCAP has an adaptive control loop that tunes control knobs to meet SLAs under WAN delay variations. GeoPCAP also leverages a formal probabilistic framework for composing consistency-latency tradeoffs of individual data-center storage instances to characterize the global tradeoff. Realistic simulations show satisfactory SLA conformance for GeoPCAP under WAN delay variations.

Chapter 4

GCVM: Software-defined Consistency Group Abstractions for Virtual Machines

In this chapter we propose a practical scalable software-level mechanism for taking crash-consistent snapshots of a group of virtual machines. The group is dynamically defined at the software virtualization layer allowing us to move the consistency group abstraction from the hardware array layer into the hypervisor with very low overhead ($\sim$ 50 msecs VM freeze time). This low overhead allows us to take crash-consistent snapshots of large software-defined consistency groups at a reasonable frequency, guaranteeing low data loss for disaster recovery. By moving the consistency group abstraction from hardware to software, we incur a minor performance overhead, but we gain flexibility in managing the consistency group from the hypervisor software level. To demonstrate practicality, we use our mechanism to take crash-consistent snapshots of multi-disk virtual machines running two database applications: PostgreSQL, and Apache Cassandra. Deployment experiments confirm that our mechanism scales well with number of VMs, and snapshot times remain invariant of virtual disk size and usage.

4.1 Introduction

Virtualization service providers are gradually transitioning towards software defined storage architectures in their datacenters [27]. With prominent examples like VMware's virtual volumes (vVol) abstraction [30], and Openstack

Swift [20] the software control plane for storage operations can be clearly separated from the underlying hardware (e.g., storage arrays).

In traditional array based storage, a logical unit number (LUN), a unique identifier that maps to one or more hard disks, is used as the unit of storage resource management. Object storage allows virtual machine disks to become the unit of management instead. This results in flexible software level *policy* management of storage, while delegating snapshot and replication *mechanisms* transparently to hardware storage arrays.

For applications running across multiple VMs, storage arrays provide a *consistency group* abstraction for crash-consistent snapshots of all virtual disks attached to the VMs. The number of hardware consistency groups available for a storage array is typically limited (order of tens of groups) and administrators must manually map virtual disks to appropriate LUNs to ensure that they are snapshot or replicated as a group (see Figure 4.1). The number of VMs (and virtual disks) that can benefit from array-defined consistency groups are constrained by (1) the small fixed number of hardware/LUN-based consistency groups, and (2) the manual mapping of virtual disks to LUNs that administrators must (re-)do as VMs are provisioned and decommissioned.

We posit that the consistency group abstraction can be defined and managed in the hypervisor while leveraging the snapshot capabilities of an underlying storage array. We present a practical, scalable, mechanism to take crash-consistent snapshots of a group of virtual machines, each with multiple disks (devices) attached.

By carefully managing short ($\sim 50msec$), targeted, pauses of write I/O in hypervisors managing the virtual disks in a consistency group we provide a low-overhead, scalable and robust way to realize the consistency group

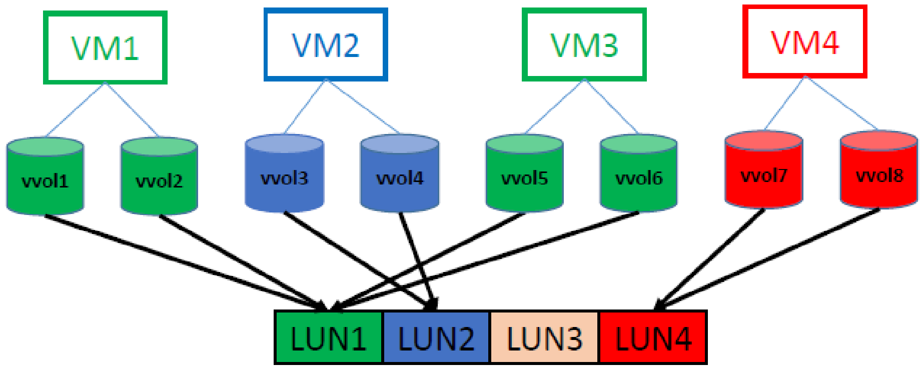

Figure 4.1: To manually configure a consistency group containing VM1 and VM3, the administrator has to ensure that their VMDKs are placed on storage backed by LUN1 in this example.

abstraction. Using our mechanism, we demonstrate the successful recovery of two non-trivial applications – PostgreSQL and Apache Cassandra. Detailed microbenchmarks and experiments on a hardware array confirm that our mechanism scales well with number of VMs, and the total snapshot time for a group remains invariant of virtual disk size and usage.

Thus our main contribution in this chapter is to move the consistency group (CG) abstraction from hardware to software. In hardware, reconfiguring (or managing) consistency group incurs high cost. But the impact of applications due to VM pause (availability performance) is less. For software defined consistency groups (our proposal), we lower the reconfiguration cost by managing groups at the hypervisor level. But we incur performance penalty due to VM pause overhead. So the tradeoff is between reconfiguration cost and application availability, and the two points in the tradeoff space are hardware consistency groups (existing solution) and software consistency groups (our solution).

4.2 Background

In this section we briefly discuss some background on disaster recovery mechanisms for virtual machines.

For disaster recovery purposes, replicating Virtual Machine data to a remote site is a common way to make VM state available. Many storage vendors, e.g., EMC, NetApp etc. usually provide replication as an additional data service.

Strategies for replication include *synchronous replication* – where each write operation must be completed at the remote target site before it is considered complete – and *asynchronous replication* (also known as periodic replication) – where a point-in-time snapshot is taken and then copied over to the remote target site periodically. The interval between two point-in-time snapshots is the *Recovery Point Objective* (RPO). Thus RPO refers to the acceptable amount of data that may be lost due to a disaster. EMC-Mirror View [11], NetApp SnapMirror [18] and Dell EqualLogic Replication [29] are all existing commercial systems that provide periodic replication schemes.

This work focuses on asynchronous replication since synchronous replication can have high overheads depending on the distance between the source and target remote site. Some storage arrays provide periodic replication functionality via a *replication consistency group*. A point-in-time snapshot of a consistency group is the union of the crash-consistent snapshots of all member volumes. The number of consistency groups available for a storage array is usually limited (order of tens of groups). As a result these are scarce resources.

4.3 Problem Formulation

Consider an application A running across n virtual machines (VM) $v_1, \ldots, v_n$. VM v_i has attached to it n_i virtual machine disks (VMDK) $d^i_1, \ldots, d^i_{n_i}$. The consistency group across all the VMs consist of $\sum_{i=1}^{n} n_i$ devices (objects). The application interacts with the VMs by issuing write operations to any VMDK in the consistency group. Our objective is to take a snapshot of the consistency group so that we can later recover the application state from VM crash failures by attaching the snapshotted VMDKs to a set of remote VMs.

Crash Consistency Defined: Let $w_1, w_2, \ldots, w_k$ be the ordered sequence of consecutive writes issued to a consistency group CG. Let $w \in W^{CG}$ denote that write w is persisted to a VMDK within CG, where W^{CG} denotes the set of all writes to CG. A snapshot S_{CG} of CG is said to be crash-consistent, if it captures a prefix $w_1, w_2, \ldots, w_p$ of the set of all writes $w_1, w_2, \ldots, w_k$, where $p \leq k$. Formally, S_{CG} is crash-consistent if $W^{S_{CG}}$ is a prefix of W^{CG}.

For correctness, we assume that the application follows the *dependent write principle* [13] where new writes are only issued after previous writes have been acknowledged as completed. This model of operation is common in systems with Write-Ahead-Logs (WAL) such as databases (e.g., PostgreSQL and Apache Cassandra) and journaling file systems (e.g., ext4).

Here, we make an important assumption about the application which is critical for the correctness of our system (Section 4.4.4). We assume that an application only issues new writes only after the previous write has been acknowledged back to the application. If a write is lost (no acknowledgment), then the application can retry by sending the same write again. An application that submits concurrent writes must go through a *write sequencer* before using our system for recovery. Many real world application follow such a *dependent write principle* principle [13], e.g., databases with write-ahead log (PostgreSQL, Apache Cassandra, SQLite), and journaling file systems (ext4).

4.3.1 Example

We use an example of a database application with write-ahead log to explain the crash-consistency criteria. Consider a write operation issued to the database. Internally the database issues a write ($w_{log-intent}$) to its write-ahead-log (WAL) to indicate the pending database update. After the write to the log completes then the actual write to the database (w_{data}) takes place followed by a write to the WAL ($w_{log-complete}$) to record that the update operation has completed. The application must wait for each write to complete, i.e., the writes are sequential: $W_{log-intent} \rightarrow W_{data} \rightarrow W_{log-complete}$. These are *dependent writes*: $W_{log-complete}$ depends on the completion and acknowledgment of W_{data}, which in turn depends on the completion and acknowledgment of $W_{log-intent}$.

For correctness, a crash-consistent snapshot of a device must preserve the write order of dependent writes. Further if W_{log-*} and W_{data} go to separate disks (i.e., a virtual machine running the database uses one disk for storing the database log and another disk for storing the actual tables/data) then a crash-consistent snapshot of the disks of the database VM must contain a prefix of the write-sequence: $W_{log-intent} \rightarrow W_{data} \rightarrow W_{log-complete}$.

Next we discuss the design of our mechanism for crash-consistent snapshots of a consistency group defined at the virtualization platform layer. Note that we only rely on the information available at the hypervisor (the coordinator) level to ensure crash-consistency. Enforcing stronger consistency guarantees (e.g., application level consistency [6]) would require visibility of application write or message dependencies and is outside the scope of this work.

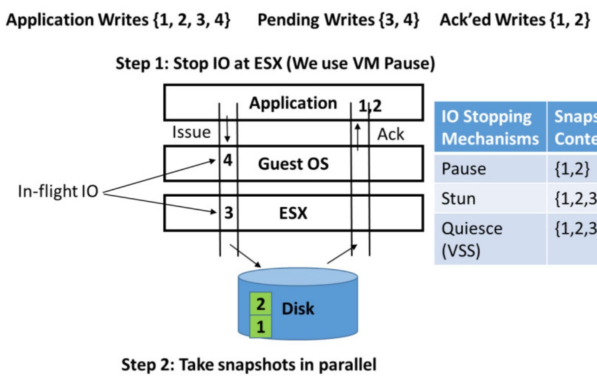
Application Writes {1, 2, 3, 4}
Pending Writes {3, 4}
Ack'ed Writes {1, 2}
Step 1: Stop IO at ESX (We use VM Pause)
Application
1,2
Issue
Ack
4
Guest OS
In-flight IO
3
ESX
2
1
Disk
Step 2: Take snapshots in parallel

IO Stopping Mechanisms	Snapshot Contents	Cost
Pause	{1,2}	Least (stops vCPU)
Stun	{1,2,3}	More (flushes vSCSI first)
Quiesce (VSS)	{1,2,3,4}	Most (requires VM tools to flush guest buffers)

Figure 4.2: Using the example of an application writing integers 1,2,3,4. Writes 1 and 2 have been written to disk and acknowledged. Writes 3 and 4 are in-flight at various levels of the stack – the vscsi layer and the guest buffer cache respectively. A crash-consistent snapshot is only required to contain writes 1 and 2. *Pause* stops the virtual CPUs (vCPUs), which prevents additional I/Os from being issued. *Stun* flushes any I/O that has made it to the vSCSI layer and waits for its completion. *VM Quiesce* (Volume Snapshot Service) informs the File System in the Guest Operating System, via VMware tools, about the pending VM freeze, allowing the file system to do any clean up, e.g., flushing buffered I/O that applications might have issued. As we go from Pause to Stun to Quiesce the amount of time it takes for the VM's activity to halt increases.

4.4 Design

Our VM hypervisor managed (software level) mechanism for consistency groups builds upon three primitives.

1. First, we require a mechanism for stopping (and later resuming) the I/O activity of a VM to its virtual disks (VMDKs).

2. Second, we need a mechanism for taking a snapshot of the current state of a VMDK.

3. Finally we need a mechanism for replicating that snapshot (or a delta from a previous anchor point) to a remote site.

4.4.1 IO Suspend/Resume Mechanism

The first primitive, the ability to stop (and later resume) the I/O activity of a VM, is the most critical. Many hypervisors (e.g., VMware ESXi, Xen, QEMU and Hyper-V) support this.

Figure 4.2 shows the mechanisms available on VMware's ESXi hypervisor – *pause, stun and quiesce*. The Xen, Hyper-V and QEMU hypervisors appear to support mechanisms similar to ESXi's stun and quiesce [16, 25, 35].

Standard virtualization platforms (e.g., vSphere, Xen, Hyper-V, QEMU) typically have three mechanisms for stopping a VM's I/O activity – *Pause*, *Stun* and *VM quiesce* [16, 25, 35]. *Pause* stops the virtual CPUs (vCPUs) of the VM preventing any further I/Os from being issued. Pause returns immediately. *Stun* flushes any I/O that has made it to the Virtual SCSI (vSCSI) layer. Stun waits for the I/O flushes to complete before returning. *VM Quiesce* causes VMware Tools to quiesce the file system in the virtual machine. Quiesce waits for I/Os buffered at the guest file system (and the layers below) to be flushed before returning. Thus in terms of time to complete, we have: *Quiesce* > *Stun* > *Pause*. Thus we use the relatively low-cost Pause mechanism in our work.

4.4.2 Snapshot Mechanism

Second, we need a mechanism for taking a snapshot of the current state of a VMDK. This mechanism is delegated to the storage backend. The efficacy of our approach – specifically the amount of time VMs need to remain stopped – strongly depends on the performance of the snapshot provider[1]. Snapshot

[1]Having VMs paused for too long may result in VM unavailability reports by monitoring systems. This concern also imposes an upper bound on the time spent coordinating a crash-consistent snapshot across groups of VMs that span ESXi hosts.

providers that employ technology that allows for efficient snapshots, e.g., constant-time snapshots [55, 116], light-weight diffs/deltas etc. allow us to significantly reduce the absolute time that a VM must remain paused.

Our work uses vVols, which means that the snapshot operation will be delegated to the backing array.

4.4.3 Replication Mechanism

The final mechanism we need is one for replicating crash-consistent snapshots to remote sites. For performance reasons snapshot replication needs to be asynchronous [34]. We rely on storage arrays to replicate to a remote site. In our experiments (in Section 4.5), we mount the snapshot of the consistency group to a different VM to test for correctness. In a production setting, the consistency group snapshot would be asynchronously replicated to a remote site (e.g., vCloud Air [33] cloud), instead of just a separate VM, for disaster recovery.

4.4.4 Model of Operation

Figure 4.3 shows how our system works. A centralized coordinator issues Pause directives to all the ESXi hosts where the VMs that are part of a consistency group are running. Note that pausing I/O for a specific VM is a precise operation, whereas the vCPUs of the target VM will stop, other VMs running on that ESXi host are unaffected. Once I/O has been paused for the target VMs, the coordinator issues snapshot directives to all the ESXi hosts in parallel. Once the snapshot completes, the coordinator issues UnPause directives to all the ESXi hosts. A two-phase commit (2PC) [124] protocol is used to robustly realize this interaction sequence.

The correctness of our approach depends on the *coordinated pause* across all the VMs that are part of a consistency group (possibly spread across multiple ESXi hosts) and the *Dependent Write Principle* [13].

The Dependent Write Principle simply says that write w_2 **depends** on a prior write w_1 if w_2 is only issued *after* w_1 is acknowledged. A real-world example of such a dependency is the ordering of writes to the write-ahead log (WAL) of a relational database and a write to a database table – the write to the database table, w_2, depends on (only happens after) the write to the log, w_1, completes [124] (Section 4.3).

For crash consistency if write w_1 happens before (completes before) w_2 (i.e., $w_1 \rightarrow w_2$) then if the snapshot contains w_2 then it *must* contain w_1. A crash-consistent snapshot is therefore *any prefix* of dependent writes[2].

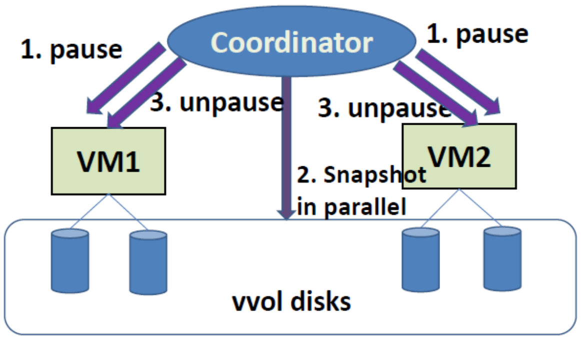

Figure 4.3: Our coordinator performs the steps of Pausing I/O of every VM what is part of a consistency group, issuing the directives to take snapshots and then issuing the directives to UnPause VM I/O.

4.5 Evaluation

Our evaluation consists of two stages: 1) micro-benchmarks, and 2) deployment experiments. The microbenchmark experiments demonstrate the cor-

[2]For $w_1 \rightarrow w_2 \rightarrow \cdots \rightarrow w_n$ a crash-consistent snapshot contains $w_1 \rightarrow \cdots \rightarrow w_k$ where $k \leq n$.

rectness of our proposed mechanism using a toy writer program which sequentially writes integers to disk using a sample vendor provider. The deployment experiments show that our crash-consistent snapshot mechanism can recover non-trivial applications, and that it scales well.

4.5.1 Experiment Setup

In our experiments we use as the virtualization platform an object build of ESXi 6.0 (vSphere 6.0) and a version of the CloudVM (a self-contained virtual appliance that contains Virtual Center – the application used to manage and configure VMware ESXi hypervisors). For correctness (but not performance testing) we use a sample *Vendor Provider* [32] – the sample Vendor Provider is a Linux appliance that behaves like a vVol-enabled array[3]. This allows us to configure it as a storage provider for the CloudVM and for ESXi and create VMDKs on it. Later for performance testing, we use a NetApp storage array as a real vendor provider.

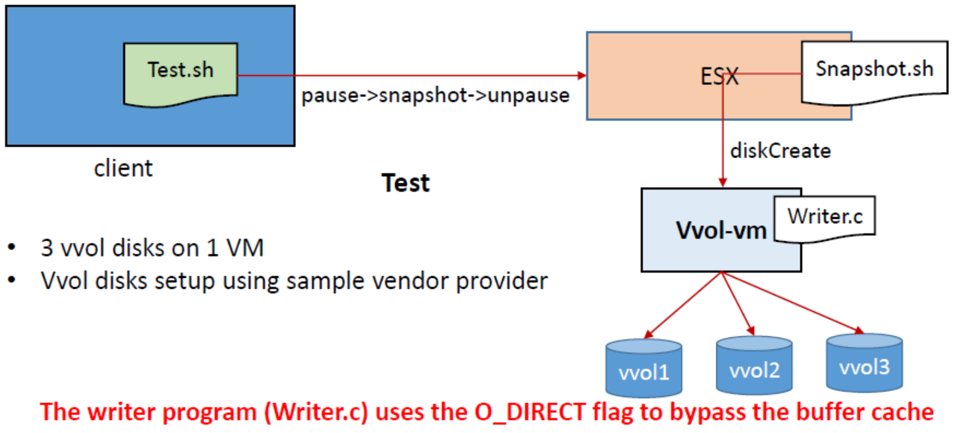
Test.sh
client
pause->snapshot->unpause
ESX
Snapshot.sh
diskCreate
Test
Vvol-vm
Writer.c
• 3 vvol disks on 1 VM
• Vvol disks setup using sample vendor provider
vvol1
vvol2
vvol3
The writer program (Writer.c) uses the O_DIRECT flag to bypass the buffer cache

Figure 4.4: Simple, single-VM, multi-vVol setup.

[3]A real Vendor Provider acts as the interface between Virtual Center and a specific array.

4.5.2 Microbenchmarks

Single VM Multiple Disk Consistency Groups

The first question we wish to answer is whether we can take a crash-consistent snapshot of a single VM with multiple (3) VMDKs stored on vVols. Figure 4.4 shows the setup. A small script initiates the calls to pause, snapshot and unpause. A short C-program (Writer.c) uses Direct I/O (the O_DIRECT flag) to write fixed-length records (512 bytes) containing integer data (see Listing 4.1) while bypassing the Operating System buffer cache to files stored on each VMDK/vVol. Figure 4.5 shows that our test program correctly stripes writes across the 3 vVols. To verify the contents of the snapshot we mount the snapshots of each vVol on a separate virtual machine and read back the records written to each data file. An epoch represents a round of writes across all (three) attached vVols.

Listing 4.1: 512 byte Record data structure of 4 byte integers

```
struct Record {
  int epoch;
  int data;
  int pad[126]; // 512 - 8 bytes
};
```

Multiple VM Multiple Disk Consistency Groups

The second question we wish to answer is whether we can take a crash-consistent snapshot across multiple VMs on multiple ESXi hosts, each with multiple vVols. This is shown in Figure 4.6. An extended writer program alternates writes across the vVols of VM1 (local) and VM2 (remote) – a write

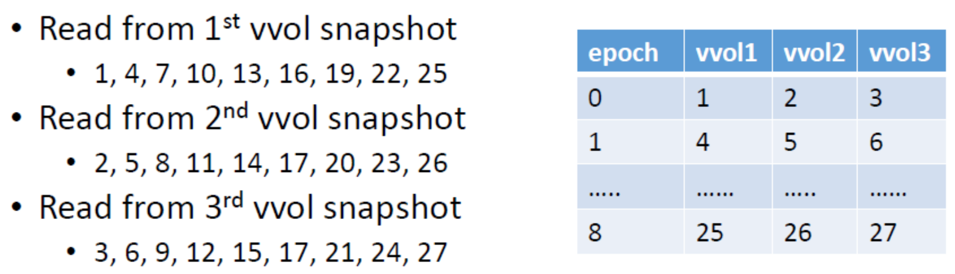

- Read from 1st vvol snapshot
  - 1, 4, 7, 10, 13, 16, 19, 22, 25
- Read from 2nd vvol snapshot
  - 2, 5, 8, 11, 14, 17, 20, 23, 26
- Read from 3rd vvol snapshot
  - 3, 6, 9, 12, 15, 17, 21, 24, 27

epoch	vvol1	vvol2	vvol3
0	1	2	3
1	4	5	6
.....	......	.....	......
8	25	26	27

Figure 4.5: Simple, single-VM, multi-vVol results. Our snapshot contains writes of integers striped across the 3 vVols.

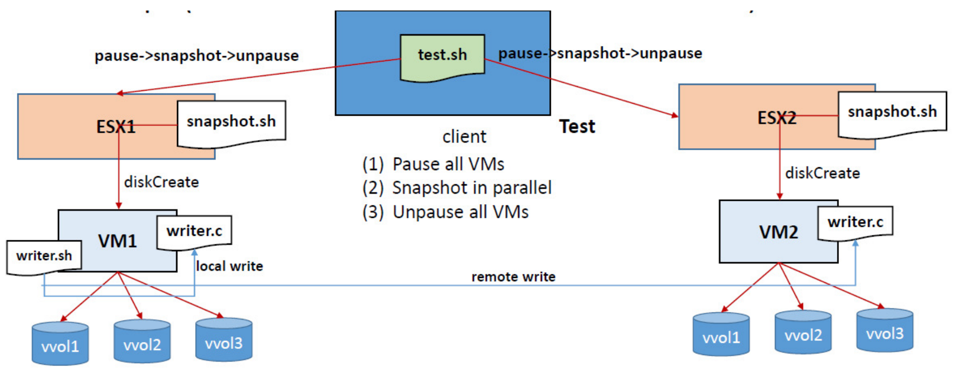

Figure 4.6: Multi-VM, multi-vVol, and multi-ESXi setup. In this setup our writer program alternates writing across "local" vVols and "remote" vVols.

to a vVol of VM1 is followed by a write to a vVol of VM2 before writing again to a vVol of VM1 etc. Each epoch represents a write across all the vVols for all the VMs. Figure 4.7 shows that a crash-consistent snapshot taken across the vVols of VM1 and VM2 contains a prefix of the writes.

Necessity of Coordinated Pause

The third question we wish to answer is whether the coordinated Pause is necessary. Using the multi-VM setup (Figure 4.6) we allow the writer program to run and first take a snapshot of one disk first, and then take snapshots (in parallel) of all the remaining disks. Figure 4.8 shows the "gaps" (missing writes) in the union of the snapshots of each vVol, i.e., the result does not capture a prefix of dependent writes and thus is *not* a crash-consistent

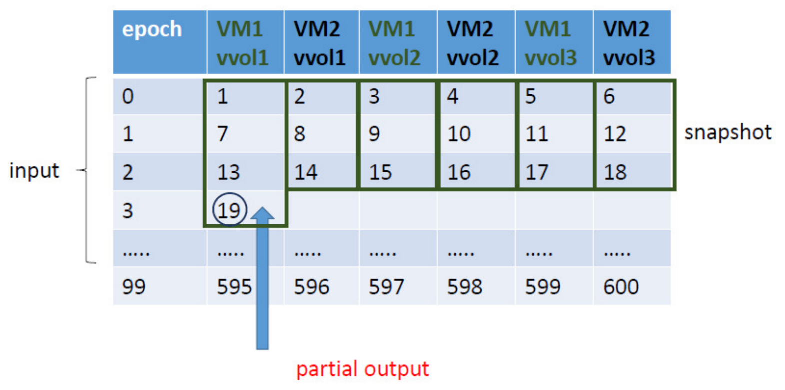

epoch	VM1 vvol1	VM2 vvol1	VM1 vvol2	VM2 vvol2	VM1 vvol3	VM2 vvol3
0	1	2	3	4	5	6
1	7	8	9	10	11	12
2	13	14	15	16	17	18
3	19					
.....	.....	.....	.....	.....	.....	.....
99	595	596	597	598	599	600

input
snapshot
partial output

Figure 4.7: Multi-VM, multi-vVol, and multi-ESXi results. Odd integers go to the vVols of VM1 (local) and even integers to the vVols of VM2 (remote). The highlighted portions represent the individual vVol snapshots that comprise the crash-consistent snapshot of the consistency group containing VM1 and VM2.

snapshot using our correctness criteria (Section 4.3). Thus all the disks in the consistency group must be simultaneously paused to ensure crash consistency.

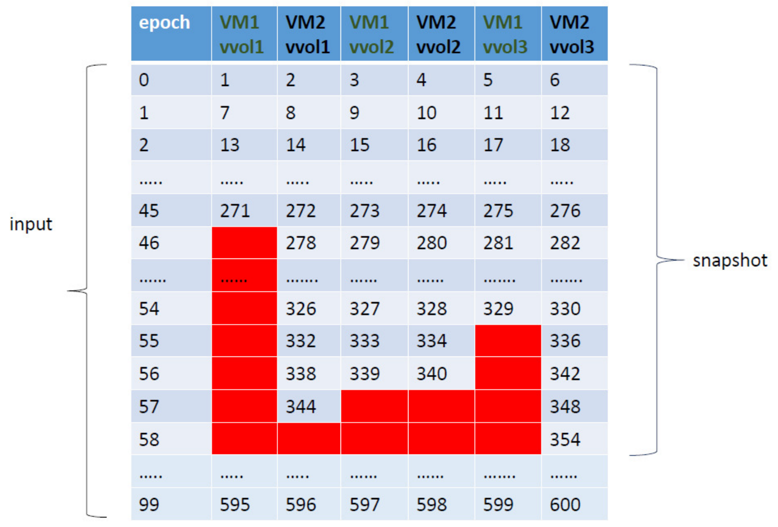

epoch	VM1 vvol1	VM2 vvol1	VM1 vvol2	VM2 vvol2	VM1 vvol3	VM2 vvol3
0	1	2	3	4	5	6
1	7	8	9	10	11	12
2	13	14	15	16	17	18
.....	.....	.....	.....	.....	.....	.....
45	271	272	273	274	275	276
46	🟥	278	279	280	281	282
......	🟥	....	......	......	....	....
54	🟥	326	327	328	329	330
55	🟥	332	333	334	🟥	336
56	🟥	338	339	340	🟥	342
57	🟥	344	🟥	🟥	🟥	348
58	🟥	🟥	🟥	🟥	🟥	354
.....	.....	.....	......	......	....	......
99	595	596	597	598	599	600

input
snapshot

Figure 4.8: Multi-VM, multi-vVol, and multi-ESXi results. Without pause, the union of snapshot contents contains gaps (missing preceding writes) and as a result the result is *not* a crash-consistent snapshot.

VMDK type	Size (GB)	Snapshot time time (msecs)
OS	20	49
Data1	1	56
Data2	10	40
Data3	100	41

Table 4.1: Time to create a snapshot on VMFS for different VMDK sizes.

Overhead of VM Pause

The fourth question we wish to answer is how long a VM needs to remain paused while we take a crash-consistent snapshot. We configure a VM with multiple VMDKs of different sizes – ranging from 1GB, 10GB, 100GB and measure the time taken to create the snapshot. For this experiment we use VMware Virtual Machine File System (VMFS) [136]. Table 4.1 shows that the time to take a snapshot is small (a few tens of milliseconds) and is independent of the size of the VMDK. In the case of VMFS, the time to create snapshots using redo logs depends on the number of changed sectors [31]. Later in Section 4.5.3, we also benchmark snapshot creation times for a NetApp storage array based vVol disk.

The ability to take snapshots in parallel within and across ESXi hosts and the relatively small snapshot creation time (depending on the snapshot provider's underlying technology) means that, with the appropriate snapshot creation technology, the total amount of time VMs need to be paused can be bounded and short.

4.5.3 Deployment Experiments

In this section we move towards reality in two aspects: (1) we replace the toy writer application with non-trivial applications, and (2) we replace the sample vendor provider with a real storage array (NetApp) and demonstrate the recovery of two non-trivial database applications: PostgreSQL [21] and Apache Cassandra [8], both of which use a write ahead log [114] for application level recovery.

First, we repeated our microbenchmarks on the NetApp storage array and verified that we can achieve crash consistency for the simple writer application described earlier. Next, we move on to the PostgreSQL and Apache Cassandra experiments.

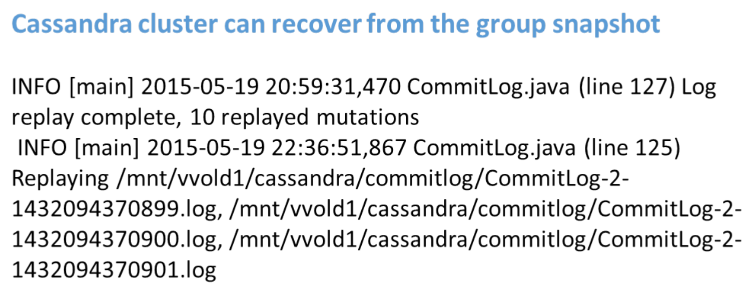
Cassandra cluster can recover from the group snapshot

```
INFO [main] 2015-05-19 20:59:31,470 CommitLog.java (line 127) Log
replay complete, 10 replayed mutations
 INFO [main] 2015-05-19 22:36:51,867 CommitLog.java (line 125)
Replaying /mnt/vvold1/cassandra/commitlog/CommitLog-2-
1432094370899.log, /mnt/vvold1/cassandra/commitlog/CommitLog-2-
1432094370900.log, /mnt/vvold1/cassandra/commitlog/CommitLog-2-
1432094370901.log
```

Figure 4.9: We show the 2 server Cassandra cluster log from a successful start from a crash-consistent snapshot (subset of log from one replica).

PostgreSQL Recovery

PostgreSQL [21] is a popular ACID compliant transactional database system that uses write-ahead logs for recovery [114]. We use the PostgreSQL database v9 (without replication) as the application writing data and pgbench [22] as a workload generator driving writes to the database. pgbench is similar to the TPC-B [28] workload that runs five select, update and insert commands per transaction. We configure PostgreSQL such that the directories concerned with the transaction log are all stored on one vVol while the directories associated with the actual database tables are stored on another [23] (Figure 4.10).

Figure 4.11 shows a successful restart from a crash-consistent snapshot

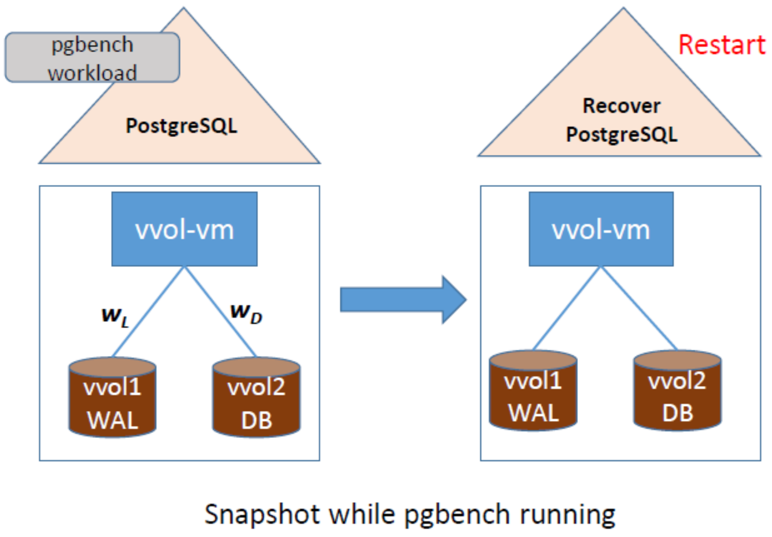

Figure 4.10: We configure PostgreSQL 9 such that the directories associated with its transaction log are stored on one vVol and the directories associated with actual database tables are stored on another vVol.

across the PostgreSQL vVols. PostgreSQL performs various integrity checks before starting the database, and the log indicates that the integrity checks of the snapshots were successful.

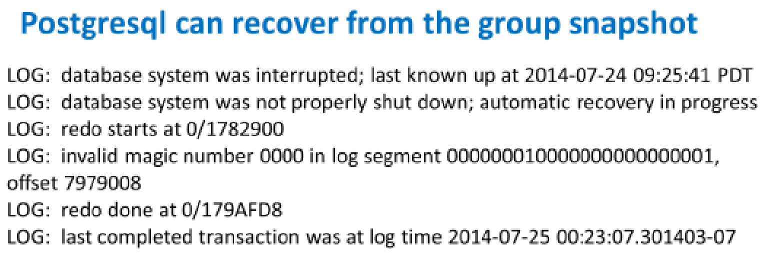
Postgresql can recover from the group snapshot

```
LOG:  database system was interrupted; last known up at 2014-07-24 09:25:41 PDT
LOG:  database system was not properly shut down; automatic recovery in progress
LOG:  redo starts at 0/1782900
LOG:  invalid magic number 0000 in log segment 000000010000000000000001,
offset 7979008
LOG:  redo done at 0/179AFD8
LOG:  last completed transaction was at log time 2014-07-25 00:23:07.301403-07
```

Figure 4.11: We show the PostgreSQL log from a successful start from a crash-consistent snapshot.

Apache Cassandra Recovery

Next we show we can use our mechanism to recover the state of a NoSQL database Apache Cassandra[8], running both in centralized and distributed modes.

We use YCSB v 0.1.4 [67, 36] to send operations to Apache Cassandra.

Each YCSB experiment consisted of a load phase, followed by a work phase. Unless otherwise specified, we use the following YCSB parameters: 1 YCSB client, 1GB data-set (1024 keys, 1 MB size values), and a write-heavy distribution (50% writes). The default key size was 10 B for Cassandra. The default throughput was 1000 ops/s. All operations use a consistency level of `ALL`.

We ran experiments in two modes: first we deploy Cassandra on a single VM, this setup is similar to the PostgreSQL setup shown in Figure 4.10. Second we deploy Cassandra over a cluster of 2 VMs, each VM located on a separate ESXi host. The experiment setup is shown in Figure 4.12. For cluster experiments, we setup 2 replicas for each key. We use YCSB to load Cassandra with 1024 keys during the load phase, and inject read/write operations during the work phase. Each YCSB run lasts for 60 seconds.

We configure Apache Cassandra such that the commit log directories (write-ahead logs) and data directories were located on separate vVols. Our Cassandra experiments involve vVols carved out of a 300GB NetApp storage array.

To verify that the snapshot of write operations actually is a prefix of all write operations, we instrument YCSB to log all operations. The *operation log* file is stored in the same disk as the commit log. Each entry in the operation log stores the key and the corresponding value for each write (put) operation. Thus when we take a group snapshot of all VMs, we also save as part of the snapshot, the operation log. For correctness, the snapshot operation log file should be a proper prefix of the full operation log file obtained at the end of the YCSB experiment.

During recovery, Apache Cassandra servers use the commit log to recover any missing data [9]. Similar to PostgreSQL, Cassandra writes follow the

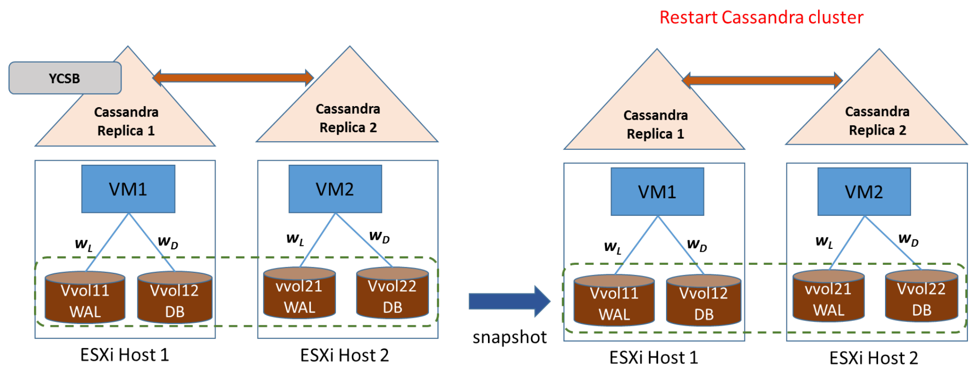

Figure 4.12: Apache Cassandra cluster setup and group snapshot experiment.

dependent write principle (writes to log precede writes to database tables) and we are able to correctly recover a single-node Cassandra instance. Due to space constraints we focus on the multi-node Cassandra setup.

In Figure 4.9, we show entries from the log file of one of the two replicas in the Cassandra cluster recovery experiment. Here the log entries indicate successful recovery.

The YCSB experiment for the Cassandra cluster was scheduled for 60 seconds. With one group snapshot across all vVols, the experiment completed in 61 seconds. This indicates a negligible overhead of 1.6% due to the coordinated VM pause/unpause phases in our mechanism.

We also verify crash consistency via a byte by byte comparison of the snapshot operation log file and the full operation log file. Concretely, we use the Unix `cmp` utility to confirm that the log as per the snapshot is a prefix of the full log.

Scalability Experiments

The intuition behind the scalability of our approach is that we snapshot each disk in a group in parallel. Thus the total snapshot time is only bounded by the worst-case snapshot time of any disk. We evaluate scalability in two dimensions: (1) disk size, and (2) number of VMs.

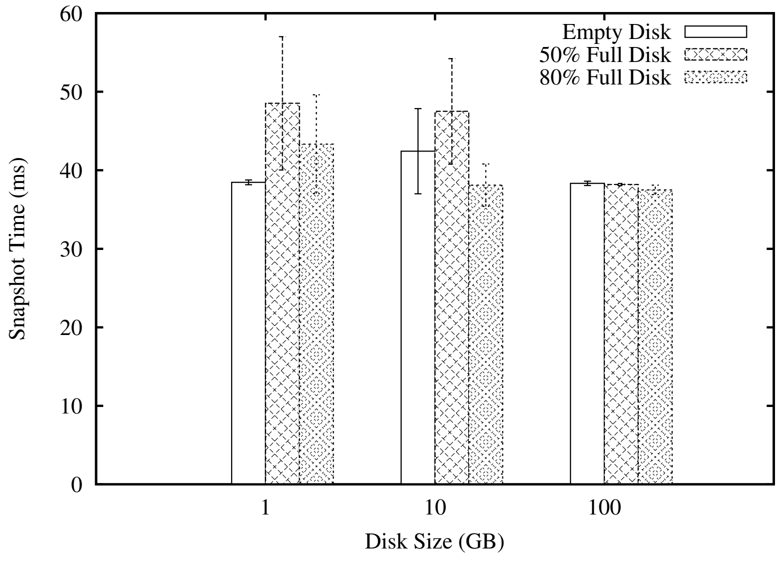

Figure 4.13: The average snapshot creation time on a NetApp storage array.

For our first experiment, we configure a VM with multiple vVol VMDKs of different sizes – ranging from 1GB, 10GB, 100GB, all carved out of a 300GB NetApp storage array. We measure the time taken to create the snapshot when the disk is empty, 50% full (half full), and 80% full (almost full). Figure 4.13 shows the average (with 95th percentile confidence intervals) snapshot times. We observe that on NetApp, the average vVol disk snapshot time is below 50 msecs irrespective of disk size and disk space, and thus the storage array snapshot technology only incurs minor overhead. For the 1GB disk, the snapshot time slightly increases as we move from an empty disk to a 50/80% full disk, due to more data to snapshot. For 100GB disks, we observe constant snapshot times irrespective of disk usage, thus is due to the efficient redirect-on-write (ROW) mechanism used by NetApp snapshots [91]. For 10GB disks, we observe a slight decrease in snapshot time as we move from 50% full to 80% disks. We attribute this to measurement noise.

Overall we have observed that snapshot creation times are small (about 50 msecs) and invariant with respect to the amount of data in a virtual disk (empty, half full, 80% full). This indicates we should be able to define the scalability constraint of a software-defined consistency group purely in terms of the number of VMs and not in units of the amount of data in the attached virtual disks.

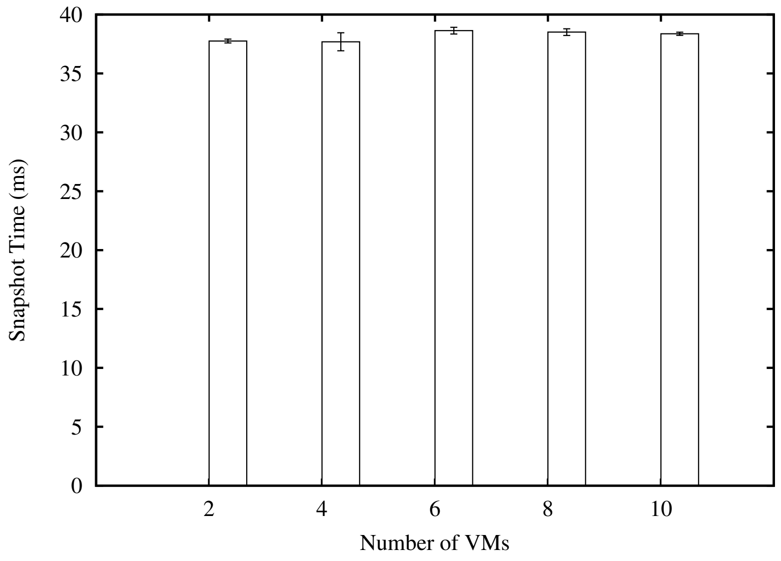

Figure 4.14: Snapshot time vs. number of VMs.

In the next experiment (Figure 4.14), we vary the number of VMs from 2 to 10, with increments of 2. Each VM had 3 disks attached to it, thus we run experiments with a maximum consistency group size of 30. With a distributed writer program alternatively writing consecutive integers to each disk in the consistency group, we take group snapshots using our mechanism. For each VM count, we measure the mean and 95th percentile confidence interval of snapshot time for each VM in the group. Since snapshots are done in parallel, and VM pause/unpause is instantaneous, these numbers quantify the overhead of taking group snapshots.

We observe that the worst case snapshot time for VMs in a consistency group stays below 40 ms as the number of VMs in a consistency group increases. This is mainly due to efficient redirect-on-write (ROW) snapshot mechanisms employed by the NetApp storage back-end. NetApp snapshots are based on the WAFL (Write Anywhere File Layout) [91]. The key idea in WAFL is to keep a set of pointers to blocks of data which enables the filesystem to make copies by just copying the pointers. Thus ROW snapshots redirect changes to new blocks, and creating a new snapshot only requires copying volume metadata (pointers) [19]. This indicates that our proposed crash-consistency mechanism scales well with increasing number of VMs in a consistency group. Overall, the two scalability experiments demonstrate that for our proposed mechanism, (1) disk size and disk space do not constrain scalability; (2) scalability can be defined purely in terms of number of VMs in a consistency group; and (3) worst case snapshot overhead remains bounded with increasing number of VMs in a consistency group. Thus we conclude that our proposed mechanism scales well.

Consecutive Snapshots and IO Bandwidth

Any realistic application will want to take consecutive snapshots at fixed intervals and push them to some reliable backup storage. The objective of this experiment is to measure the impact of multiple consecutive snapshots on application IO bandwidth. For this experiment we ran the IOzone [17] filesystem benchmark to measure IO bandwidth with and without snapshots issued from the hypervisor. We ran IOzone on a 10 GB disk to transfer a 256 MB file. First we ran the benchmark without any snapshots. Then we ran the benchmark again, but in conjunction with 5 disk snapshots with 1 minute sleep time in between snapshots. This resulted in about 30% drop in

IO bandwidth and a modest increase in the total time for the experiment.

The relatively high bandwidth reduction with consecutive snapshots indicate the possibility of optimizing consecutive snapshots. One approach could be to only take a full snapshot for the first time, and for each consecutive iteration, only take a delta snapshot (i.e., the follow-up snapshots only record the differences from the previous snapshot). Optimizing consecutive snapshots to minimize bandwidth overhead is left as future work.

4.6 Related Work

In this section we discuss related work for our GCVM system.

4.6.1 VM Replication

There has been much work on enabling consistent replication across multiple VMs. In host-based Replication (HBR) [34, 96], the host itself is responsible for replication, whereas our mechanism lets hardware storage arrays take care of replication. We extend on the HBR approach by adding coordination across multiple ESX hosts and provide implementation and experimental results to highlight the feasibility of our approach via an evaluation of the scalability constraints of ensuring crash consistency for multiple VMDKs that are spread across multiple ESX hosts.

HBR works via a HostAgent plugin that provides a way to manage and configure VM replication and a virtual SCSI (vSCSI) filter driver that (among other things) intercepts all VM I/O to disks and transfers replicated data to the remote site. Rather than coordinate group consistency at this lower level we do it in a higher layer.

It should be noted that crash-consistency is different from *application-level consistency* [6]. Given that a crash-consistent snapshot is the union of dependent writes it is possible that this collection of writes does not correspond directly to a previously observed application-level state.

4.6.2 Group Abstractions

Compared to the vast literature on checkpointing of distributed programs [73], here we look at checkpointing the state of a single application, which interacts with multiple virtual machines. Also these techniques checkpoint in-flight messages, whereas our mechanism ignores in-flight unacknowledged messages. Compared to hardware consistency group abstractions proposed by NetApp and EMC [12], we move the consistency group abstraction from hardware to software. Distributed process group abstractions were initially proposed in [62], and later incorporated in the ISIS virtual synchrony model [53]. In both cases, the objective is to support group multicast, whereas our goal is to checkpoint and recover a group of VMs for disaster recovery.

4.6.3 Checkpointing Distributed Applications

Many techniques have been proposed for checkpointing distributed applications. These techniques can be roughly categorized into application level (e. g. , ARIES write ahead log mechanism [114]), library level [61, 126], and OS level [120]. Our VM level group snapshot mechanism is closer to OS-level checkpointing mechanisms, but our focus is on taking snapshots, and not on migration which is complementary to our work. Application level checkpointing requires access and modification of application source code; our approach is application agnostic.

Note that our mechanism can take a crash consistent snapshot of a running distributed system, without resorting to complicated distributed snapshot algorithms (e. g. Chandy-Lamport algorithm [58]). We only use disk snapshots, and don't need to keep track of in-flight messages. In-flight messages are not acknowledged by an application adhering to the dependent writes principle, thus the application does not expect them to be part of the snapshot.

4.6.4 VM Snapshot Mechanisms

Virtualization provides a flexible solution to decouple application execution, and checkpoint/restart from the underlying physical infrastructure. ZapC [100] is a light-weight virtualization that provides checkpointing for a group of processes which form a process domain (pod). Compared to ZapC, we are check-pointing VM groups. Xen on InfiniBand [127] and VNsnap [95] both offer mechanisms to snapshot an entire virtual network environment. We are only concerned with checkpointing VM disks.

4.6.5 Consistency Models

Crash-consistency models were first proposed in modern file systems like EXT2, EXT3, and ZFS [55] for recovery purposes. The authors in [63] propose optimistic crash-consistency for better performance at the cost of only probabilistic guarantees for crash-consistency. However these systems are concerned with proper write ordering to a single disk, rather than across multiple disks spread across VMs, as we are.

4.7 Summary

In this chapter we proposed a practical scalable mechanism for taking crash-consistent snapshots of a group of virtual machines. This enabled us to move the consistency group abstraction from hardware to software with very low overhead ($\sim$ 50 msecs VM freeze time). This low overhead facilitated taking crash-consistent snapshots of large consistency groups at a reasonable frequency. Thus our mechanism can provide low RPO for disaster recovery. Experiments confirmed that in our mechanism, snapshot times are invariant of disk size and disk space, and that it scales well with increasing number of VMs.

There are a number of future research directions to pursue. First, in this chapter we have not focused on optimizing consecutive group snapshots. Since there is significant redundancy between consecutive snapshots, an important optimization problem is to find an optimal schedule for a sequence of group snapshots that meets certain data loss guarantees (RPO). Second, we rely on the dependent writes principle to ensure crash consistency. However not all applications might follow the dependent writes principle (e.g., a multi-threaded application with multiple writer threads). We can investigate relaxations of the dependent writes principle which could guarantee weaker consistency models (e.g., optimistic crash consistency [63]). Weaker models improve performance at the risk of data loss, but also require access to guest operating system resources (e.g, guest buffers).

Chapter 5

OPTiC: Opportunistic graph Processing in multi-Tenant Clusters

In this chapter, we present a system called OPTiC, or Opportunistic graph Processing in multi-Tenant Clusters. While existing clusters can process multiple graph computations, they do not take full advantage of the multi-tenant nature. We propose an opportunistic mechanism called PADP (Progress Aware Disk Prefetching) for creating additional replicas of the input graph of a job. The key idea is that the replica is placed at the servers that are currently running the maximum progress job. This is because the maximum progress job is most likely to complete before any other job, and free cluster resources for the next job. Thus prefetching the input of the next waiting job in the server(s) running the maximum progress job allows us to overlap the graph loading time of the next waiting job, with the computation of the current running jobs.

We utilize novel graph level metrics to identify which current running job has made maximum progress. Thus by trading the cost of an additional replica, we can opportunistically improve the run-time performance of jobs by reducing the time to fetch input data from a local disk (instead of remote disk) to memory. We have incorporated our technique into Apache Giraph [3], a popular graph processing system that can run on top of Apache YARN [4] cluster scheduler. Realistic experiments with Yahoo! and Facebook job traces indicate our technique improves median job turnaround time to up to 50%. To the best of our knowledge, we are the first to systematically explore and optimize multi-tenant graph processing systems.

5.1 Introduction

Distributed graph processing is a popular computational framework for processing large scale graphs with billions of vertices and trillions of edges. For example, Pregel [109], PowerGraph [84], GraphLab [107], and LFGraph [92] are prominent graph processing frameworks that achieve efficiency and scalability. The goal of these systems is to compute important metrics (e. g., pagerank, shortest path, centrality) on large-scale graphs (e. g., Facebook graph, the Web graph). These large-scale graphs typically have billions of vertices and trillions of edges [64]. Thus distributed graph processing systems are often deployed on large commodity clusters [110]. These frameworks usually organize a graph processing job into two phases: the graph preprocessing phase and the computational phase. The graph preprocessing phase loads the graph from disk, and partitions graph data into chunks, each of which is handled by a subset (usually one) of the computation unit. The computational phase runs the actual distributed graph algorithm, and is iterative in nature. Recent studies have shown that the graph pre-processing phase can take significant time [92].

Despite the widespread deployment of graph processing engines on commodity clusters, there exists a semantic gap between the graph processing layer and the cluster scheduling layer (Figure 5.1). For example, Apache Giraph is a popular graph processing engine that runs on top of Apache Hadoop. The Hadoop cluster scheduler (YARN) is only aware that it is processing a map-reduce job and is unaware that it is actually a graph processing job. Similarly the graph processing layer typically uses the entire cluster to run a

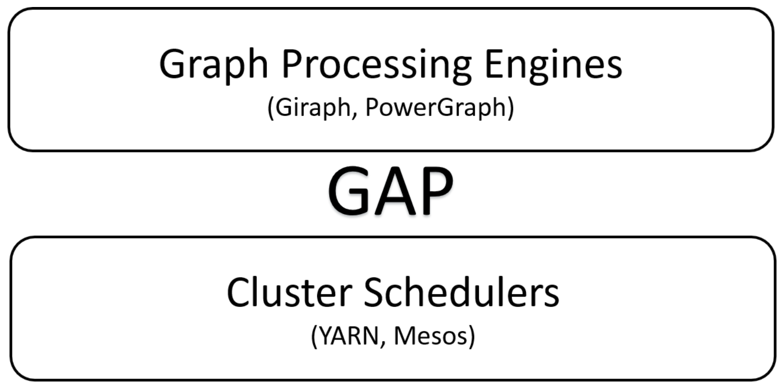

Figure 5.1: Semantic gap between graph processing and cluster scheduler layers. The graph processing layer does not take full advantage of multi-tenancy of underlying cluster scheduler. The cluster scheduler is not aware of the graph nature of jobs.

single job, and once a job finishes it starts another job that will again occupy the entire cluster. Thus both layers are unaware of any special structure or opportunities available in the other layer. As concrete examples of available opportunities, if the cluster layer knows that two consecutive graph processing jobs (e.g., PageRank followed by Shortest Path job on the Facebook Web Graph) share the same graph, then instead of freeing the task memory allocated for the graph partitions of the first job, the cluster manager can keep the graph partitions in memory for the next job. Thus the second job can avoid a costly graph loading and partitioning phase, and this can result in faster completion time for the second job.

In this chapter, we investigate for the first time the benefits of scheduling multi-tenant graph processing jobs on a shared and over-subscribed non-preemptive cluster. A multi-tenant cluster differs from a single-tenant cluster in that there can be multiple jobs running simultaneously on the cluster, thus fully utilizing the resources. The cluster scheduler serves to maximize the overall performance and resource utilization of the jobs. In our case, we assume that a given multi-tenant cluster is already fully occupied by currently running (graph processing) jobs. We also assume the scheduler uses a non-preemptive scheduling policy, and any upcoming jobs are placed into a FIFO waiting-queue.

We present a system called OPTiC for Opportunistically graph Processing on multi-Tenant Clusters. The key idea in our system is to opportunistically overlap the graph pre-processing phase of queued jobs with the graph computation phase of the current running job with maximum progress. Since the maximum progress job is most likely to complete first, our system optimizes run-time performance by prefetching the graph input of the next queued job onto the server(s) resources running the maximum progress job. As a concrete instantiation of this technique, we propose Progress Aware Disk Prefetching (PADP), where we prefetch the graph input of a waiting job (create one additional replica) into the disks of server(s) running the maximum progress job. This allows the new job to only incur a local fetch from disk to memory, instead of a remote network fetch. Such a remote fetch would be costly when disk bandwidth is much higher than network bandwidth, which is a realistic scenario for today's commodity clusters [39].

In order to decide which current running job is making maximum progress (and is most likely to complete before others), we propose a novel progress estimator for graph computation based on the percentage of active vertices in a graph processing system. This allows us to estimate progress in a profile-free and cluster agnostic manner. However our OPTiC system architecture is general enough to work with any suitable progress estimator.

Our deployment experiments with Apache Giraph [3] running on top of the Apache YARN [4] cluster scheduler show that we can reduce median job turn-around time for graph processing jobs up to 50% under realistic network and workload conditions, at the cost of one additional replica of the input graph stored in the distributed file system (DFS) associated with the cluster scheduler.

5.2 Graph Processing Background

In this section, we first give an overview of graph processing systems, and define some key terms that we use later.

A graph processing system performs computation on a graph loaded into the memory of a server or partitioned among a set of servers. In this chapter we mainly deal with graphs that can be loaded entirely within the memory of a single server. In general graph processing consists of two phases: (1) graph loading and partitioning, and (2) graph computation. The typical life-cycle of a graph processing job is shown in Figure 5.2.

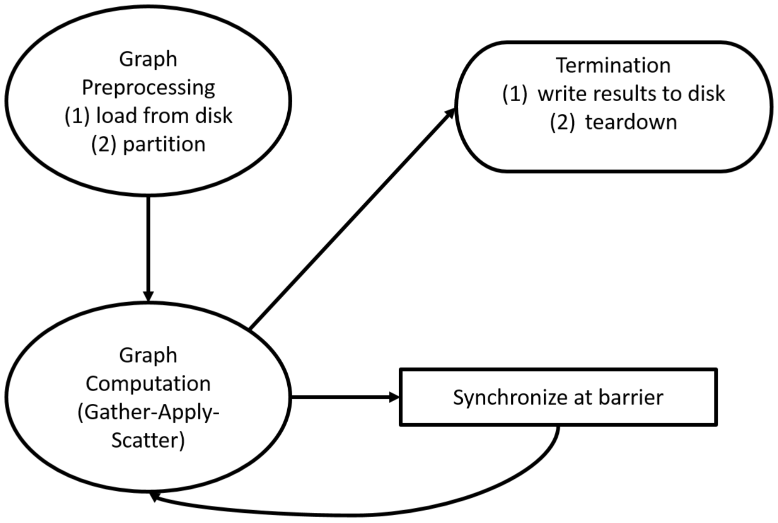

Figure 5.2: Anatomy of a graph processing job. Phase 1: Preprocessing (loading from disk and partitioning among distributed workers), Phase 2: Computation (Gather-Apply-Scatter by each vertex program), synchronize at barrier, Finally terminate when all vertices become inactive.

5.2.1 Loading and Partitioning

Typically in a distributed cluster, the graph input is stored in a fixed format in the distributed file system (DFS) associated with the cluster. For example production Facebook graph processing systems store the graphs either in HDFS or as Hive tables [64]. Before computation the graph must must be fetched from disk into the memory of a single server (if there is enough memory), or partitioned across the memory of multiple servers. Distributed graph partitioning can take various forms: simple hash partitioning [92], or edge based partitioning [60, 84, 125]. Both loading and partitioning the graph can be expensive [92].

5.2.2 Computation

The synchronous, vertex-centric Gather-Apply-Scatter (GAS) style of graph computation is the most common model, and is supported by most popular systems [64, 84, 92]. In this model, computation occurs in iterations or *supersteps*, wherein vertices gather values from neighbors, aggregate and apply the values to do local computation, and finally scatter the results to neighbors. Supersteps are separated by global synchronization barriers. A vertex can be in either of two states: active or inactive. At the beginning all vertices are generally active. At any time a vertex can voluntarily enter the inactive state or can be passively activated by an incoming message from a neighbor. When a vertex has no more pending messages in a superstep, it becomes inactive. The overall program terminates when all vertices become inactive.

5.3 Problem Statement

Consider n graph processing jobs running on a shared cluster. We assume a non-preemptive oversubscribed cluster, i.e., there are always jobs waiting to be scheduled, and current jobs are not preempted. The cluster is fully utilized by the current graph jobs. Now a new graph processing job J_{new} arrives in the system, and we need to decide where to schedule/place the new job. Our objective to place the resources for the job (graph input file) in a manner to improve overall job completion time performance.

5.4 Key Idea of OPTiC: Opportunistic Overlapping of Graph Preprocessing and Computation

The key idea in OPTiC is to *opportunistically overlap* the graph pre-processing phase of queued jobs with the graph computation phase of current jobs. Our system design is based on a few assumptions. First, we assume synchronous graph processing, where workers synchronize at a barrier at the end of each superstep, based on the bulk synchronous parallel [137] model of computation. Second, we assume the cluster is over-subscribed; thus there is always a job waiting to be scheduled. Third, we assume the cluster is non-preemptive; thus there is no priority among jobs, and a waiting job cannot preempt a running job. Finally, we assume all input graphs are stored somewhere in a distributed file system (DFS) associated with the cluster. For example, if the system uses the YARN cluster scheduler [4], then the input graphs could be all stored in HDFS [15]. The key idea of OPTiC is depicted in Figure 5.3.

Assuming we have a good estimation of the progress of currently running jobs (discussed later in Section 5.8), we want to exploit this information to increase the performance of jobs waiting to be scheduled. Each graph pro-

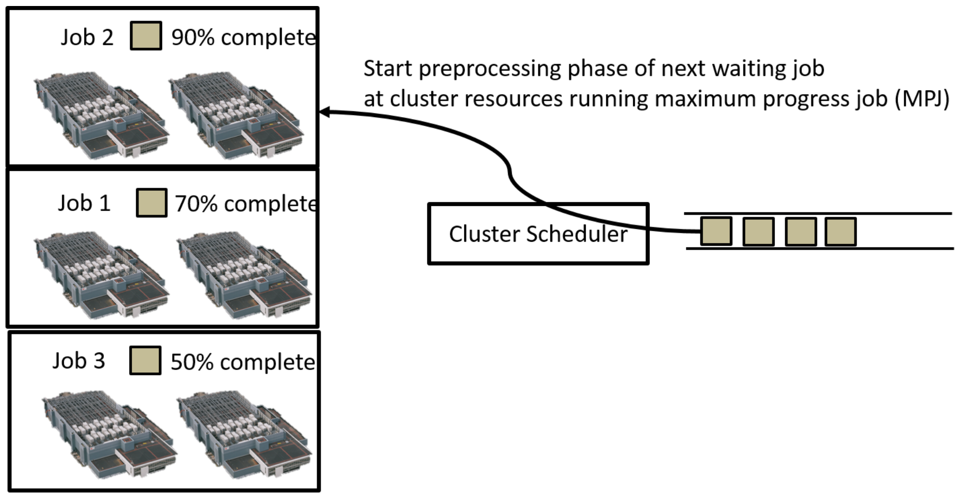
Job 2
90% complete
Job 1
70% complete
Job 3
50% complete
Start preprocessing phase of next waiting job
at cluster resources running maximum progress job (MPJ)
Cluster Scheduler

Figure 5.3: Key idea of OPTiC: overlap the graph preprocessing phase of the next waiting job with the graph computation phase of the maximum progress job.

cessing job consists of a graph loading (and partitioning) phase and a computational phase. By overlapping graph loading and preprocessing phase (including graph partitioning for multiple workers), with the actual computation phase of current jobs, we can improve the run-time performance of a sequence of graph processing jobs.

Our main technique is to utilize current progress metrics of the running jobs to prefetch the input graph data of a job waiting in the scheduler queue to an appropriate location in order to reduce the time to fetch the input data for computation. Since the cluster is work-conserving, if a job is waiting, there is no resource available to run the job. Thus instead of waiting in the queue, we can opportunistically try to move the input data of the waiting job closer to where the job will run next (the server(s) running the max progress job (MPJ)). We now describe the different design stages we went through for our system.

To implement this idea of overlapping graph pre-processing of waiting jobs with graph computation of current jobs, we first explored progress-aware memory prefetching techniques. The main idea was to start directly fetching (and if needed, partitioning) the graph input of the next job waiting in the queue, into the memory of the servers currently running the max progress job (MPJ). However the problem with this approach is that since the cluster is over-subscribed and non-preemptive, there is no free memory available to store the prefetched graph, since all of the cluster memory is used to store and do computation of the current running jobs.

Next we contemplated having a fixed percentage of memory in the cluster (e.g., 20% containers in YARN) just for prefetching new graphs in memory, while the remaining memory resources are used to run the current job. However as it turns out, this policy would have resulted in the same job schedule as the default FIFO policy used in schedulers like YARN.

5.5 PADP: Progress Aware Disk Prefetching

The key realization at this stage was that if we cannot utilize the memory of servers running the max progress job, we can at least try to utilize the disk resources of those servers by prefetching the graph to disk. Suppose based on our progress estimation, we know that J_{max} is the max progress job; that is, a future job J_{new} is most likely to run on the free resource of J_{max} once it finishes. We move the input data associated with J_{new} to be locally available at the cluster resources currently allocated to J_{max}, in order to reduce the remote fetching overhead once J_{new} starts. In other words, we pre-fetch J_{new}'s data into the disks of servers that J_{new} is going to be run on. Thus we create one additional replica for each chunk of the input graph for J_{new} at the servers running J_{max}. We call this technique as progress aware disk prefetching (PADP).

The PADP policy depends on one critical assumption. We assume disk bandwidth is higher than network bandwidth. For big data systems, disk locality has been a critical factor that has resulted in significant performance gains for many systems [43, 94]. Although there has been work [44] suggesting that the benefit of disk locality might disappear as data center bandwidths increase [86], follow up studies [39] have shown that the difference between disk and network bandwidth remain significant in reality. One difference with these systems and ours is that while existing systems move computation to disks holding input data, in our PADP policy, we move the input data near computation.

For example,the authors in [39] report (in Table II, page 3) that for a 20 server Amazon EC2 virtual cluster (public cloud), the mean disk bandwidth was 141.5MBps, while the mean network bandwidth was 73.2MBps. On the other hand, for a private cloud, the mean disk bandwidth was 157.8MBps, while network bandwidth mean was 117.7MBps. Thus our PADP assumption holds for both current public and private clouds. In our Emulab 9 server testbed cluster (Section 5.10), we observed that while network bandwidth was constrained to 1MBps (measured using the "iperf" tool), disk bandwidth was much higher (about 450 MBps, measured using "hdparm" tool). Thus the PADP assumption is also valid for our experimental cluster.

Thus we conclude that PADP can improve performance since it takes less time to fetch a graph dataset from a local server than a remote server from the network. Thus by identifying where a waiting job is most likely to run (the servers running the max progress job), we create additional replicas of the input at those servers. Thus when the current maximum progress job is complete, the new job can fetch data from a local disk (instead of a remote network fetch) and start computation faster.

It should be noted that OPTiC+PADP increases the input graph replication factor from the default (3) to default(3) + at most 1 opportunistically created replica. Although we incur increased storage and bandwidth cost to increased replication, in reality the actual increase in dollar cost is almost zero. This is because disk is much cheaper compared to main memory devices, and most disk resources are already under-utilized. Thus with a slight increase in replication storage cost, OPTiC+PADP policy can optimize job completion time. Thus OPTiC+PADP trades storage cost for improved runtime performance.

5.6 System Architecture

We now present the design of our system OPTiC for Opportunistically scheduling multi-Tenant graph processing jobs in a shared Cluster, using the PADP policy. The core idea of our system can be summarized in the following pseudo-code.

Algorithm 1 OPTiC-PADP Core Mechanism

```
function SCHEDULE(new job $G_n$)
    Step 1. Identify the current job $G_p$ that has made maximum progress (MPJ). Let $S$ denote the server(s) running $G_p$.
    Step 2. Prefetch input and schedule the new job $G_n$ to run on the disks of $S$
end function
```

Thus there are two main components of our system design in OPTiC. First is a component that tracks the progress of all currently running jobs and decides which job is the *maximum progress job (MPJ)*. We discuss the graph computation progress estimation later in section 5.8. In principle, different progress estimators can be plugged into the modular OPTiC architecture. Second, there is a component that prefetches resources for the next queued job onto the MPJ server(s).

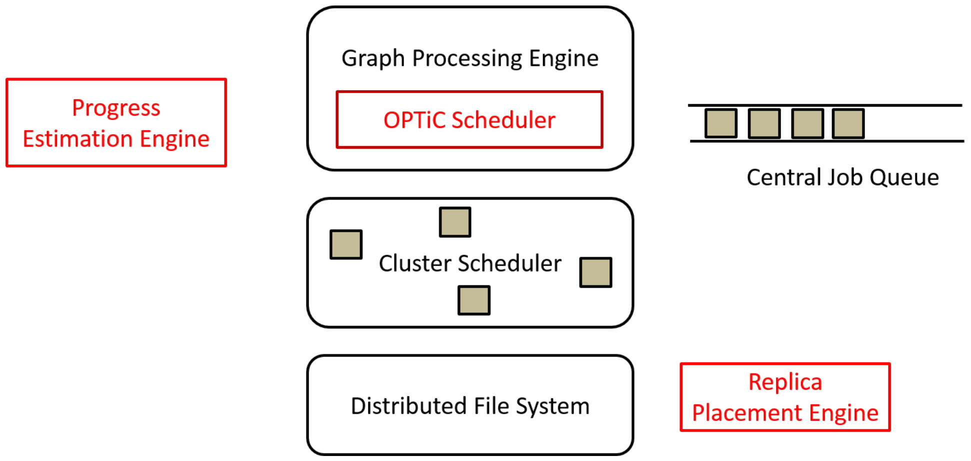

Figure 5.4: System Architecture.

Our overall system architecture is shown in Figure 5.4. There is a central job queue, where jobs are queued waiting to run on the cluster. When there are enough resources to run a new job, the graph processing engine fetches the job from the queue in FIFO order and submits it to the cluster scheduler. All input graphs for the jobs are already loaded in the distributed file system. The current running jobs in the cluster periodically send their progress metric values to the Progress Estimation Engine. For a new job fetched from the queue, if there are enough resources, generally they will be scheduled by the cluster scheduler on free resources (e.g., containers). The cluster scheduler by default will try to colocate new containers with the input data. When a job is waiting in the queue, the application coordinator for the job fetches the information about the servers running the maximum progress job. This data is then fed into the replication engine, which creates additional replicas for each chunk of the waiting jobs input graph at the specified locations. Finally when the next job in line is scheduled, it can load the graph (and possibly partition it) from a local disk instead of incurring remote network data transfer overheads. The OPTiC scheduling algorithm is depicted in Figure 5.5.

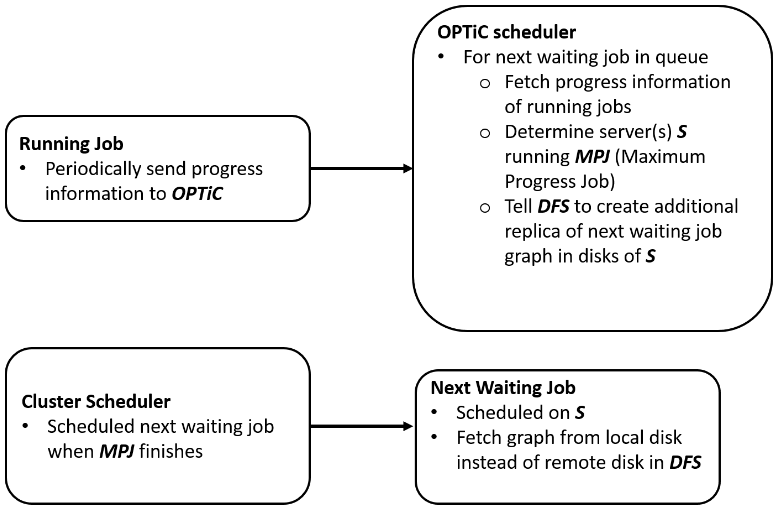

Running Job
• Periodically send progress information to OPTiC
OPTiC scheduler
• For next waiting job in queue
o Fetch progress information of running jobs
o Determine server(s) S running MPJ (Maximum Progress Job)
o Tell DFS to create additional replica of next waiting job graph in disks of S
Cluster Scheduler
• Scheduled next waiting job when MPJ finishes
Next Waiting Job
• Scheduled on S
• Fetch graph from local disk instead of remote disk in DFS

Figure 5.5: OPTiC Scheduling Algorithm. The OPTiC scheduler lives inside the graph processing run-time (Figure 5.4). Running jobs periodically report progress to the OPTiC scheduler. For a waiting job, the OPTiC scheduler fetches progress information of current jobs and uses Algorithm 2 (discussed later in Section 5.8) to decide the maximum progress job (MPJ). It then looks up the current server(s) resources S running the MPJ, and instructs the replica placement engine to place an additional replica of the waiting jobs graph input in S. The cluster scheduler independently schedules the next job on S, when the MPJ completes.

5.7 Progress-aware Scheduling

Our system proposes a progress-aware scheduling strategy. In this section we formalize this scheduling technique and state and prove a theorem about the optimality of progress-aware scheduling.

In progress aware scheduling, we keep track of the current progress of each running graph processing job. Assume the progress metrics for the n jobs $G_1, G_2, \ldots Gn$, are $p_1 \geq p_2 \geq \ldots \geq p_n$ without loss of generality. Higher values of p_i means the job is closer to completion. The progress metric indicates how much computation has been performed, and is an indicator of how long it will take for the job to finish. Then job G_1 with maximum progress p_1, is more likely to complete before any other job. Thus we can opportunistically schedule the new job G_{n+1} on the computation units (resources) currently holding the partitions for G_1. If G_1 takes $t_1(p_1)$ additional time to finish, then G_{n+1} needs to wait for $t_1(p_1)$ time to start. Estimating $t(p)$ for a job with progress percentage p requires profiling different graph processing jobs, and this has an overhead. We now present a theorem showing optimality of our approach.

Theorem 5 *Let $p_1 \geq p_2 \geq \ldots \geq p_n$ be the progress metric for a set of jobs running in a work conserving non-preemptive cluster such that $p_1 \geq p_2 \geq \ldots \geq p_n$. If the cluster has infinite bandwidth, then placing the graph dataset of the next queued job in the server(s) currently running job with progress p_1 minimizes job completion time for the next queued job.*

Proof: Let the next queued job be J_{next}, and the job with maximum progress p_1 be J_{max}. Let S_{max} denote the server(s) running the computation for J_{max}. Th total computation time for the new job running on S is $t^S_{total} = t^S_{load} + t_{compute}$. $t_{compute}$ is independent of where the graph input is fetched from. Let t^S_{load} denote the time the load the graph from server S. Since J_{next} will start on S_{max}, we have that $t^{S_{max}}_{load} < t^S_{load} \forall S$. Thus t^S_{total} is minimized for $S = S_{max}$. $\square$

This theorem makes a number of simplifying assumptions. First, we assume infinite bandwidth, thus making a copy of the input graph on a new server is instantaneous. Second, we assume that if S has more than one server, the time to partition the graph among servers in S is negligible. For finite bandwidth, the time to place a new replica at a destination server is not negligible. Thus a bandwidth-aware placement policy would be to find the maximum progress p job server(s) S such that the time to copy the graph to S is less than the time to run the remaining computation $(1 - p)$. The optimality of this strategy can be proved similarly, and is left as future work.

5.8 Graph Computation Progress Metric Estimation

We now discuss different ways of measuring progress of graph processing jobs.

The performance of progress-aware scheduling (PADP policy in OPTiC) depends heavily on the accuracy of graph job progress metrics, and estimating the remaining time. Such estimates allow us to decide which current job is making maximum progress. Doing this with high accuracy results in efficient scheduling results using OPTiC. Accurately estimating the progress metric can be challenging, since it depends on different factors, such as graph algorithm, the graph size, the active vertex count. Thus mathematically the remaining time estimate $t_i(p_i)$ of a graph processing job i with current progress p_i can be expressed approximately as a function of the graph algorithm, and the graph size. We describe three approaches to estimating the progress metric. We organize our discussion here by first discussing the approaches we initially proposed and found to be inadequate. Finally we present the design and algorithm that worked best for us. For each approach we discuss the pros and cons.

5.8.1 Profile-based Approach

One approach to estimate graph computation progress is to profile the job run-time characteristics of various graph algorithms on different input sizes and different cluster configurations. Then based on these profiles, we can estimate the progress of graph computation. For example at any given time t, we can calculate how much time the job has been running, and use the profiles to predict when it will complete. Machine learning techniques can be used for such predictions. The disadvantage of this approach is the huge profiling overhead. As a result we do not use such an approach in our system.

5.8.2 Utilizing Cluster Scheduler Metrics

A popular approach to graph processing is to map graph jobs to staged dataflow jobs. For example, Apache Giraph [3] (used by Facebook), and GraphX [85] deployed on Spark [144] (which is deployed on Mesos [90]), both map graph processing jobs to staged data-flows, which are then efficiently scheduled on a cluster scheduler like Mesos or YARN. GraphX maps Pregel [109] jobs to a sequence of join and group-by dataflow operators, whereas Giraph maps graph jobs to map-reduce stages.

Mature cluster schedulers like YARN have job progress estimators for each stage. For example for both YARN map and reduce stages, we can extract the current progress of mappers and reducers. So another approach to compare the progress of two arbitrary graph jobs G_1 and G_2, would be to check their current dataflow stage (map/reduce), and percentage complete within that stage. So for example, if G_1 is in map stage, and G_2 is in reduce stage, we say G_2 has closer to completion. If both G_1 and G_2 are in the same stage (e.g., reduce) then we could use the reducer percentage of the jobs to decide which job has made more progress.

This approach is attractive since it does not require profiling. This approach is also independent of graph algorithm type and graph size. A problem with this approach is that it depends on how a graph algorithm is implemented as a dataflow program. Also within a stage, progress does not always correspond to progress of a graph job. For example Giraph graph jobs are mapped to map-only map-reduce programs, and the map percentage reported by the scheduler is proportional to how much input data has been processed. This does not directly map to iterative graph algorithms. As a result, we do not use this approach in our system.

5.8.3 Profile-free Approach

Thus our goals are to avoid: (1) the overhead of profiling, and (2) the dependence on the underlying cluster scheduler metrics. If we can correlate job progress with a *graph processing level metric* that is independent of the platform, then we can track the evolution of such a metric to infer job progress. We choose the *active vertex count percentage (AVCP)* as such a metric. For a graph processing system, the active vertex count (AVC) is defined as the number of *active* vertices. A vertex is said to be active if it has some un-processed incoming message from the previous superstep (assuming synchronous graph processing). We define the active vertex count percentage (AVCP) as the ratio of active vertex count and total vertex count in the graph (n).

It should be noted that active vertex count is not an attribute of an abstract graph algorithm, rather it is a property of a distributed implementation of such an algorithm in a graph processing platform or framework. As long as a graph algorithm can be implemented in such a manner, we can use AVCP to track progress. Our objective in this *profile-free* approach is to estimate and compare graph computation progress without profiling and in a cluster-agnostic manner. We wish to see how far we can go in terms of estimating graph computation progress without any profiling. Our experiments in Section 5.10.7 demonstrate the accuracy limits of the profile-free approach.

Consider the evolution of AVCP of eight well known graph algorithms (Pagerank, Single Source Shortest Path (SSSP), K-core Decomposition, Connected Components, Undirected Triangle Count, Approximate Diameter, Graph Laplacian, and Graph Partitioning) running on a 100 million vertex graph using the PowerGraph [84] system, shown in Figures 5.6 - 5.12.

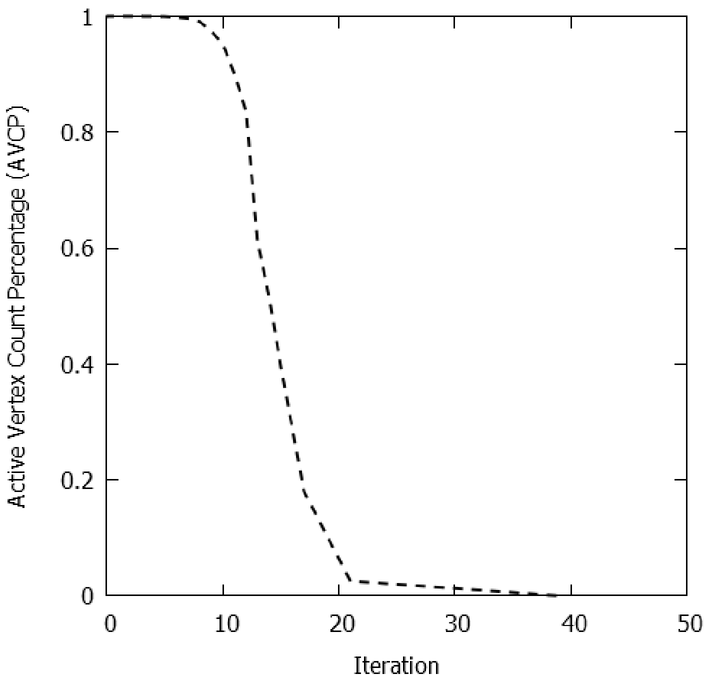

Figure 5.6: Active Vertex Count Percentage (AVCP) of a Pagerank job (using PowerGraph) on a 100 million vertex graph against superstep count.

In these plots, on the Y axis we plot the AVCP of a job running on a power-law graph with 100 million vertices. For Pagerank in Figure 5.6, we observe an initial phase where the AVCP stays at 1, and there is a second phase where the AVCP starts to decrease towards 0. For SSSP in Figure 5.7, we see an initial phase where AVCP is moving towards 1, and a second phase, where again as Pagerank, AVCP goes towards 0. In K-core decomposition [97], one repeatedly finds induced subgraphs where all subgraph vertices have degree atleast K. Such a decomposition can depict the hierarchical nature of large scale graphs (e.g., the Internet Graph). In Figure 5.8, we see that for K-core decomposition, the AVCP starts at the second phase where it is already moving towards 0. For connected components computation in Figure 5.9, we observe an initial non-decreasing phase where the AVCP stays near 1, and a second decreasing phase where it moves towards 0. Finally for the four remaining graph algorithms: undirected triangle count, approximate

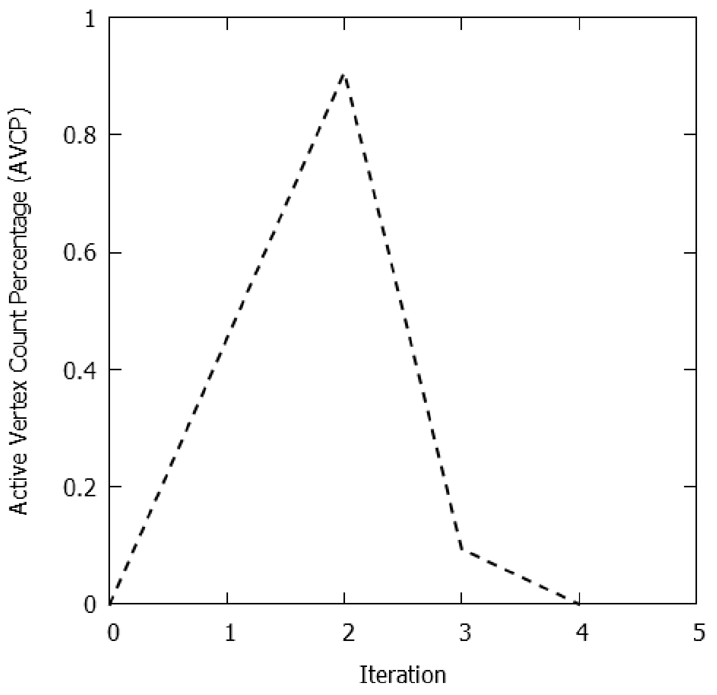

Figure 5.7: Active Vertex Count Percentage (AVCP) of an SSSP job (using PowerGraph) on a 100 million vertex graph against superstep count.

diameter, graph laplacian, and graph partitioning [84], we observe that the AVCP abruptly jumps from 1 to 0 in one lengthy superstep. Thus these four algorithms only have the second decreasing phase.

Based on these trends, we approximate the evolution of a graph computation running on a graph processing system (e.g., PowerGraph, Pregel, Giraph) with a sequence of two phases: (1) an initial optional non-decreasing phase (INC) where the AVCP is near or moves towards 100%, followed by (1) a decreasing phase (DEC) where the AVCP moves towards 0%.

We measure progress as the distance from the final state of AVCP=0%. This is infact the terminating condition of most graph processing systems. Intuitively AVCP is a measure of current work being done in the graph job. More active vertices indicate more work left to be done. For example, if a job has AVCP 100%, then all vertices are active and are working. Compared to that, if a job has AVCP=30%, then it has less work to finish.

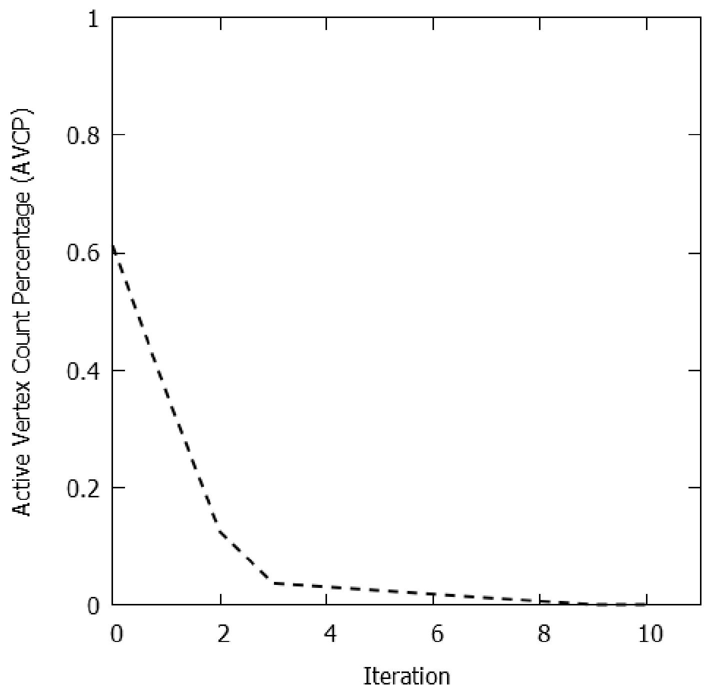

Figure 5.8: Active Vertex Count Percentage (AVCP) of a k-Core Decomposition job (using PowerGraph) on a 100 million vertex graph against superstep count.

We can now describe the algorithm to compare progress of two jobs. The basic idea is as follows. Consider two jobs J_1, J_2 with AVCP values a_1, a_2, $0 \leq a_1, a_2 \leq 1$. We have three cases:

1. Case 1: If J_1 is in the initial non-decreasing (INC) phase, and J_2 is in the second decreasing (DEC) phase, then we conclude J_2 is the maximum progress job (MPJ).

2. Case 2: If both J_1 and J_2 are in the INC phase [0%-100%], and $a_1 < a_2$, then J_2 is the MPJ.

3. Case 3: If both J_1 and J_2 are in the DEC phase[100%-0%], and $a_1 > a_2$, then J_2 is the MPJ.

Consider two jobs in the same phase (e.g. DEC phase) with AVCP values of 40% and 50%. Both these jobs have similar progress. Although, the job

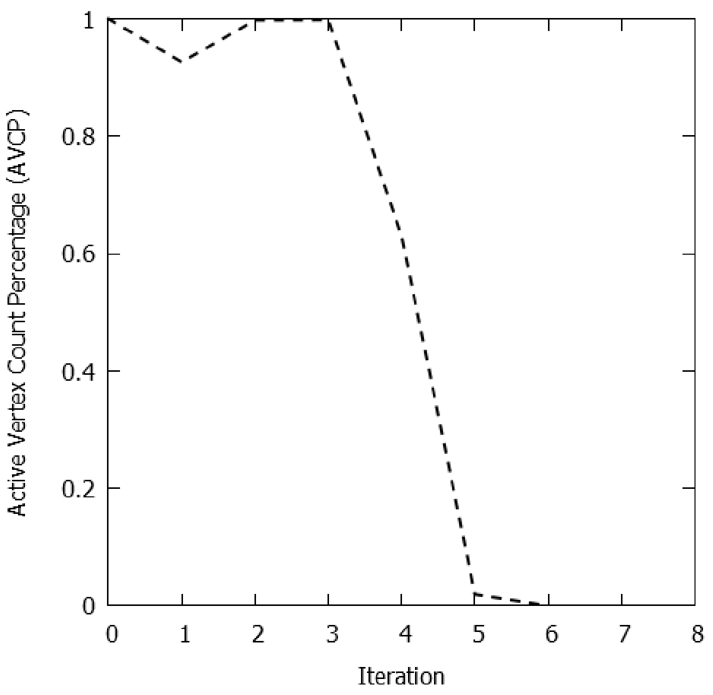

Figure 5.9: Active Vertex Count Percentage (AVCP) of an Connected Components job (using PowerGraph) on a 100 million vertex graph against superstep count.

with 40% AVCP is most likely to finish first, the rate of decrease of AVCP can vary, and the job with 50% could end up finishing slightly before the job with AVCP 40%. To account for this, we divide each phase into equal intervals. For example we can divide the DEC interval into three disjoint sub-intervals $H = [100\% - 67\%]$, $M = [67\% - 33\%]$,$L = [33\% - 0\%]$. We order the sub-intervals in terms of progress towards AVCP=0% (termination) as: $L > M > H$. Thus for two jobs in different intervals (job 1 in L, job 2 in M), we use this ordering to decide the maximum progress job (job 1). For two jobs in the same sub-interval (both in M), we toss a coin and randomly pick a job as the max progress job. This randomness allows us to deal with different rates of decrease of AVCP. The case where both jobs are in the INC phase is similarly handled.

The overall algorithm for comparing the progress of two graph processing

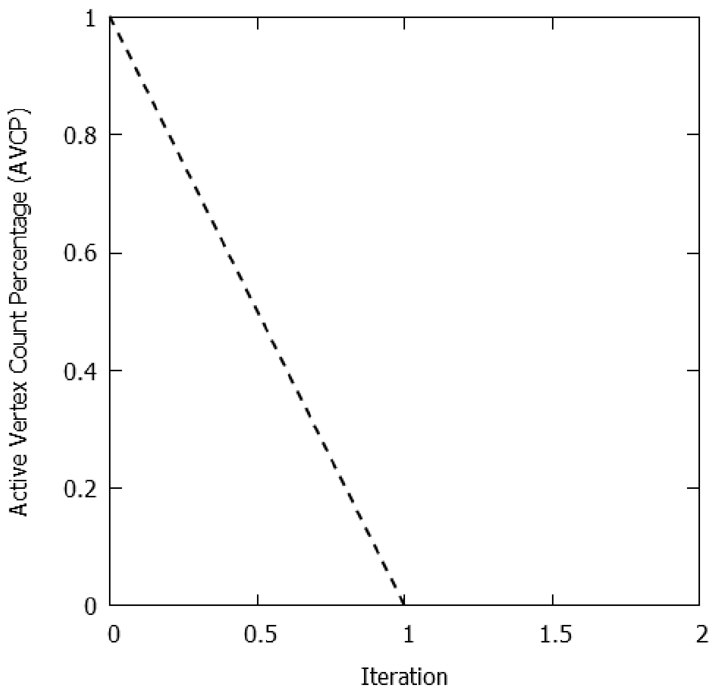

Figure 5.10: Active Vertex Count Percentage (AVCP) of an Undirected Triangle Count job (using PowerGraph) on a 100 million vertex graph against superstep count.

jobs at time t (usually the last superstep time) is shown in Algorithm 2.

The algorithm first checks whether the jobs are in INC or DEC phases (lines 5-14) by comparing AVCP at time t and $t-1$ (the last two recorded super-step times). If AVCP decreases by more than a threshold (e.g., $\epsilon =$ 10%), then the job is in DEC phase, otherwise it is in the initial INC phase. If they are in different phases, then the job in DEC phase wins and is the MPJ (lines 15-20). Otherwise, if both jobs are in the same INC phase (lines 21-31), then the interval is divided into I sub-intervals, and we check which sub-intervals contain $AVCP$ for each job. The job in the later sub-interval (based on the order) is returned as the MPJ. In case both jobs are in the same sub-interval, we randomly choose a job as the MPJ (lines). The case when both jobs are in DEC phase is similar (lines 32-42).

Algorithm 2 Heuristic to compare progress of two jobs.

```
function COMPARE(job $G_1$, job $G_2$, time $t$ , number of intervals $I$)
    Let $INC$ intervals be ordered as: $\mathcal{I}_1^{inc} = [0, \frac{1}{I}] < \cdots < \mathcal{I}_I^{inc} = [\frac{I-1}{I}, 1]$
    Let $DEC$ intervals be ordered as: $\mathcal{I}_1^{dec} = [1, \frac{I-1}{I}] < \cdots < \mathcal{I}_I^{dec} = [\frac{1}{I}, 0]$
    Let $a_1(t) \leftarrow AVCP(G_1)$ at time $t$, $a_2(t) \leftarrow AVCP(G_2)$ at time $t$
    if $a_1(t-1) > a_1(t) + \epsilon$ then
        $G_1 \in DEC$ phase
    else
        $G_1 \in INC$ phase
    end if
    if $a_2(t-1) > a_2(t) + \epsilon$ then
        $G_2 \in DEC$ phase
    else
        $G_2 \in INC$ phase
    end if
    if $G_1 \in INC$ and $G_2 \in DEC$ then
        Return $G_2$ as MPJ
    end if
    if $G_1 \in DEC$ and $G_2 \in INC$ then
        Return $G_1$ as MPJ
    end if
    if $G_1 \in INC$ and $G_2 \in INC$ then
        Find $\mathcal{I}_i^{inc}$ such that $a_1(t) \in \mathcal{I}_i^{inc}$
        Find $\mathcal{I}_j^{inc}$ such that $a_2(t) \in \mathcal{I}_j^{inc}$
        if $\mathcal{I}_i^{inc} < \mathcal{I}_j^{inc}$ then
            Return $G_2$ as MPJ
        else if $\mathcal{I}_i^{inc} > \mathcal{I}_j^{inc}$ then
            Return $G_1$ as MPJ
        else
            Randomly choose $G_1$ or $G_2$ to be MPJ
        end if
    end if
    if $G_1 \in DEC$ and $G_2 \in DEC$ then
        Find $\mathcal{I}_i^{dec}$,$\mathcal{I}_j^{dec}$ such that $a_1(t) \in \mathcal{I}_i^{dec}$, $a_2(t) \in \mathcal{I}_j^{dec}$
        if $\mathcal{I}_i^{dec} < \mathcal{I}_j^{dec}$ then
            Return $G_2$ as MPJ
        else if $\mathcal{I}_i^{dec} > \mathcal{I}_j^{dec}$ then
            Return $G_1$ as MPJ
        else
            Randomly choose $G_1$ or $G_2$ to be MPJ
        end if
    end if
end function
```

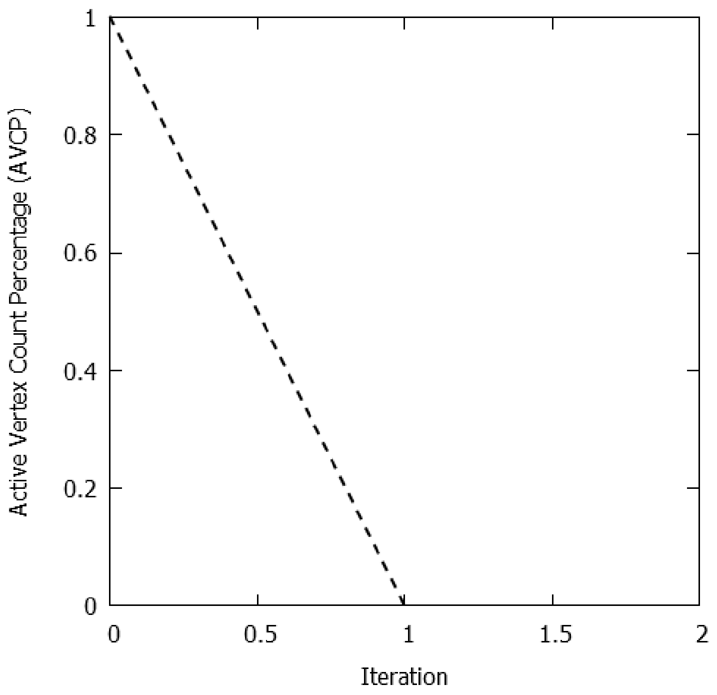

Figure 5.11: Active Vertex Count Percentage (AVCP) of an Approximate Diameter job (using PowerGraph) on a 100 million vertex graph against superstep count.

5.8.4 Variations of the Profile-free Approach

In the profile-free approach we estimate progress by tracking the evolution of AVCP. For two jobs, the job with AVCP closer to the terminal 0% is considered the max progress job. One variation is to estimate the actual job finish time, given current AVCP. We can use regression of curve-fitting to do this. The drawback of this approach is that different jobs can have different rates of change for AVCP. Thus a simple linear regression would not suffice, and might require profiling which we want to avoid.

Another variation is to keep track of first and second derivatives of AVCP (rate of change of AVCP or velocity, and acceleration). This would increase the overhead of tracking progress, and it is not guaranteed that the job with highest velocity and acceleration towards AVCP=0% will finish first.

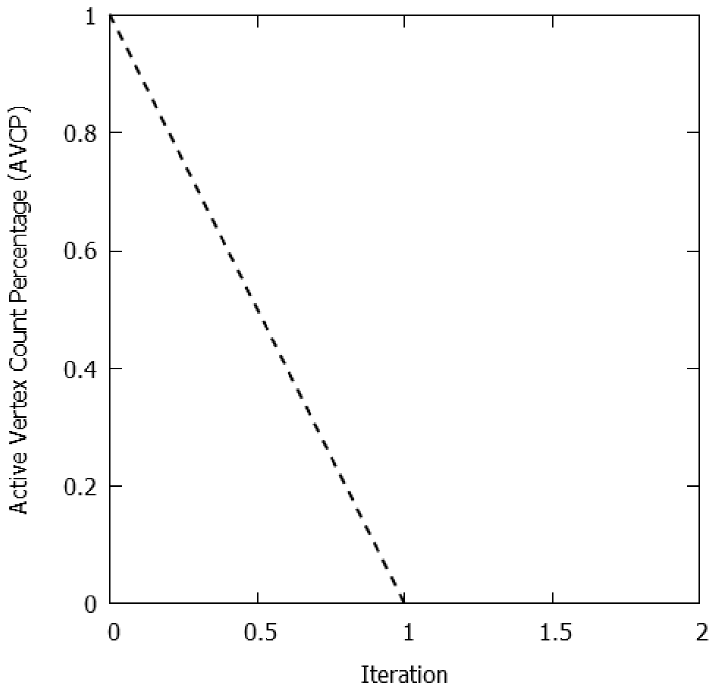

Figure 5.12: Active Vertex Count Percentage (AVCP) of a Graph Laplacian job (using PowerGraph) on a 100 million vertex graph against superstep count.

5.8.5 Generality of the Profile-free Approach

Our profile-free approach is motivated by the observed evolution of AVCP for four popular graph analytics algorithms shown in Figures. We believe the technique is general and applicable for a wider range of graph analytics algorithms including (1) triangle count (2) approximate diameter (3) group source shortest paths, (4) k-means clustering, and many more. The reason this is true is that all these algorithms have been implemented in graph processing frameworks like PowerGraph [84] and Giraph [3], where the job terminating condition is AVCP=0%. Thus our technique would work for these algorithms.

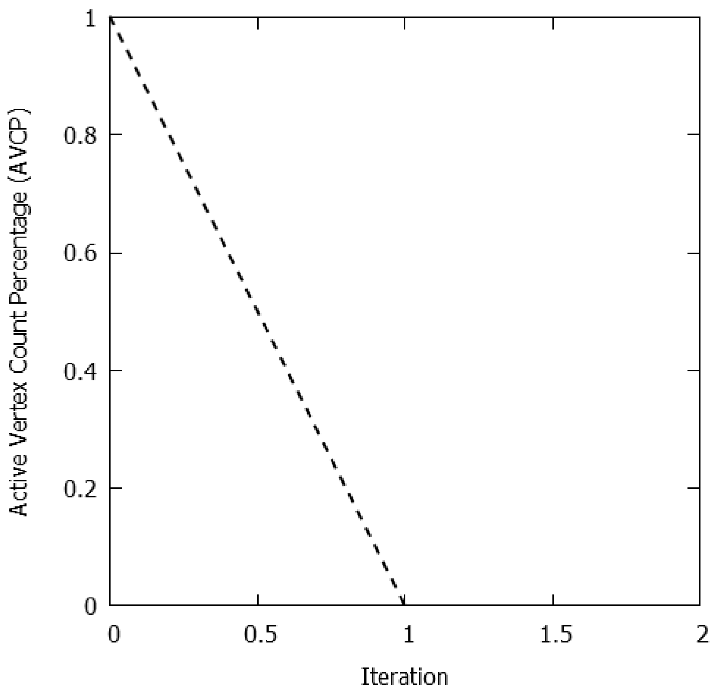

Figure 5.13: Active Vertex Count Percentage (AVCP) of a Graph Partitioning job (using PowerGraph) on a 100 million vertex graph against superstep count.

5.8.6 Accuracy of the Profile-free Approach

We now characterize workload conditions that lead to high accuracy for our profile-free approach. Our goal is to understand the limits of the profile-free approach.

The Algorithm works well for same type of graph jobs (e.g., SSSP) with different sizes. Consider two SSSP jobs on input graphs with 10K and 100K vertices respectively. Both jobs have the same amount of resource allocated to them. Since the maximum active vertex count of the 10K job is smaller, at any time, it will be closer to termination compared to the 100K job. Thus progress comparison algorithm works well in this case.

The Algorithm works well for different types of jobs with similar run-times. Consider comparing the progress of an SSSP job with a K-core job. If both jobs have similar run-times, then most likely during comparison, both jobs will be in the DEC phase. Thus the algorithm correctly predicts the MPJ in this case.

The Algorithm works poorly for different types of jobs with vastly different run-times. This tells us the limit of the profile free approach. Consider an SSSP job with estimated run-time T, and a K-core job with estimated run-time at-least $10 \times T$ Thus with equal resources allocated to both jobs, the SSSP job will always finish earlier than K-core. However SSSP has an INC phase before the DEC phase, whereas K-core starts at the DEC phase. Thus, if at the time of comparison, SSSP is in the first phase, then our algorithm mis-predicts K-core as the max progress job, even though SSSP always finishes first. This demonstrates that the profile-free approach starts to break down for different types of jobs with different run-time characteristics. We can remedy this by telling the system that k-core is always slower than SSSP, but that approach would no longer be profile-free.

5.9 Implementation

We have implemented a scheduler prototype that supports our PADP policy for the Apache Giraph [3] graph processing system on top of an Apache YARN [4] cluster.

5.9.1 Incorporating Multi-tenancy in Giraph

While Giraph can be deployed on top of YARN, it is not truly a multi-tenant graph processing system. To simultaneously schedule multiple graph processing jobs on YARN, we would need to run multiple separate Giraph instances, one for each job. We made modifications to Giraph such that multiple graph processing jobs can be scheduled using a single Giraph run-time. We use a Java thread-pool for this purpose. We implemented a console for submitting new jobs to the Giraph run-time. The console interface parses every job command and delivers it to the scheduling component. Each newly submitted job is handed of to a new thread in the thread-pool.

5.9.2 PADP Policy Implementation

Our PADP policy relies on two key pieces of information from the graph processing systems: active message count (which we normalize to get AVCP) and allocated containers for any currently running jobs. In Apache Giraph, these two information are available in the master node. The master node will aggregate active message count at each superstep, and for each job this aggregated value (Phase and Interval, Section 5.8.3) is propagated to a centralized log in the cluster. Also, in Giraph whenever a new container is allocated, we also propagate the information to a centralized log in the cluster. These values are therefore globally available in a centralized server so that the OPTiC scheduler can utilize them to schedule future jobs.

There are two approaches to disseminate AVCP and container information in the system: *push* and *pull*. In the push approach, the running jobs periodically send AVCP and container logs to the central master server. We use this *push* approach in our prototype implementation. In some scenarios, a *pull* method might fare well. In a pull method, whenever the scheduler needs AVCP and container logs, it requests such information from the master nodes, or from the ApplicationMaster of all currently jobs. One benefit of the *push* approach is that it reduces repeated communication overhead when there are a lot of incoming jobs. The downside of the *push* approach is that these logs must be aggregated and stored in a centralized manner and this creates a central point of failure. The centralized server can be made fault-tolerant using state machine replication [128] technique. We leave such fault tolerance techniques for future work.

5.9.3 HDFS Replication

To exploit the progress information of current jobs, we wish to pre-fetch the input data into the local disks of the maximum progress job. In our prototype, suppose we have an incoming job j with input graph data G and the maximum progress job j^* with associated machines M, we do the pre-fetching by creating a copy of G at each host in M, so that when j starts at the same machines of j^*, it can use the data that is already locally available.

Our prototype is built in Hadoop ecosystem and uses HDFS as the underlying distributed file system (DFS). To create the additional replica, we make an explicit copy (with replication factor 1) of G using HDFS's native file copy feature and place it in the disk of M. Thus we do not interfere with the default three replicas created by HDFS for every block of data. Thus our technique does not tamper with the default fault-tolerance level of HDFS.

5.9.4 Scheduler Implementation

Our PADP policy implementation proceeds as follows. Given a waiting job j, first it attempts to submit j to the YARN scheduler. We poll the YARN REST API to check whether the job is in RUNNING state in the cluster. If it is not in RUNNING state, we deduce that YARN currently does not have adequate resources to run j. It is for such jobs j that we wish to utilize the

PADP policy.

To implement PADP, the scheduler proceeds by first sending requests to YARN asking for a list of currently running jobs. For each job j_i, it retrieves the centralized progress log associated with j_i and extracts the phase (INC or DEC), and interval within the phase (Section 5.8.3). It then uses Algorithm 2 to determine the MPJ j^*. Next, it retrieves the list of allocated container(s) of j^*. It chooses one of the containers in the list, ssh'es into the container, and creates an HDFS file copy. This copy is created locally created at the server running that container. After the copy process is finished, the scheduler kills the original job j, and resubmits it but with the updated path of the copied input graph (the additional replica). The detailed algorithm is shown in Algorithm 3.

5.10 Evaluation

We performed our experiments on an Emulab [140] clusters with 9 quad-core servers, each with 64GB memory. We use delay emulation to mirror the network delays typically observed in a single data-center environment [52]. We implemented the PAPD policy and incorporated it into Apache Giraph graph processing framework (version 1.10) [3] running on top of the Hadoop YARN Cluster (version 2.7.0) [4].

We configure one server as the Master which runs the YARN resource manager (RM) and the HDFS name node (NN), while the remaining 8 servers act as slaves and contain node manager (NM), and data nodes (DN). Each slave has 1 8GB memory container, thus the total YARN cluster has 64GB memory for running jobs. We assume all input graph data are stored in the Hadoop Distributed File System (HDFS) [132], which is the default distributed stor-

Algorithm 3 Implementation of PADP Policy in Giraph+YARN

```
function PADP(J: newJob, yarnManager)
    G ← J.inputPath
    yarnManager.submit(J)
    status ← yarnManager.getStatus(J)
    if status = Queued then
        yarnManager.kill(J)
        K ← yarnManager.getCurrentJobs()
        maxProgress ←<>                                    ▷ Empty Tuple.
        maxProgressJob ← null
        for all k ∈ K do
            $progress =< phase, interval >$ ← readProgressLog(k)   ▷ Read
phase and interval (See Algorithm 2).
            if progress > maxProgress then
                maxProgress ← progress
                maxProgressJob ← k
            end if
        end for
        M ← readContainerLog(maxProgressJob)
        for all m ∈ M do
            ssh(m).HDFS-copy(G,concat(G,"copy"))
        end for
        J.inputPath ← concat(G,"copy")
        yarnManager.submit(J)
    end if
end function
```

age system used in conjunction with Apache YARN [4]. The average disk bandwidth of the cluster (measured using "'hdparm') is 450MBps, while the average network bandwidth (measured using "iperf") is 1MBps.

Our main performance metric is job turn-around time (TAT), defined as the difference between job finish time and job arrival time in the queue. Our cost metric is replication factor (RF) of the input graphs stored in DFS. We compare our OPTiC PADP policy (P) with the YARN baseline FIFO policy (B). The baseline policy cost is the default replication factor in DFS (3), whereas the cost of PADP is default(3) + at most 1 opportunistically created replica. We measure performance improvement of our PADP (P) policy over the baseline (B) as $\frac{B-P}{B} \times 100\%$.

We conduct five set of experiments. First, we vary the network delay conditions in the cluster using realistic delay distributions for a data-center network [52] and measure the performance of PAPD and baseline policies (Figure 5.14, Figure 5.15). For this experiment, we always use a fixed size graph input for all jobs and set a constant inter-arrival time between successive jobs. For the next set of experiments, we move towards reality by (1) generating job sizes that represent a realistic workload (Facebook Map-reduce cluster workload) [143] (Figure 5.18), and (2) setting the inter-arrival time between jobs to be exponentially distributed. For the third experiment, we use a larger production trace from Yahoo! with job size and arrival time values (Figure 5.19). Next, we define a metric called *graph commonality*, which measures how the different jobs share graph inputs. We vary this metric to evaluate PADP and baseline policies (Figure 5.20). In this experiment, we also vary the job sizes to evaluate the scalability of our system. For the final experiment, we test how our system works with a heterogeneous mix of different graph algorithms, and measure the limits of the profile-free approach (Figure 5.21, Figure 5.22).

5.10.1 Input Graphs

We conduct our experiments on large randomly generated undirected graphs. Uniform graphs are randomly generated in the way that the probability of an edge existing between any pair of vertices is the same. The uniform graph assumption does not impact our results, and we would get similar conclusions with Power-law graphs[74] of the same size. The reason is that our techniques are not targeted at or optimized for Power-law graphs. We expect them to work arbitrary graph inputs.

5.10.2 Test Graph Algorithm

We conduct most of our experiments on a distributed version of single source shortest path algorithm. Unless otherwise specified, this is the default graph processing job in our experiments. The pseudo-code of the algorithm is given in **Algorithm 2**, written in the semantics of Apache Giraph[3].

5.10.3 Impact of Realistic Network Delays

For this set of experiments, we use a lognormal distribution to emulate network delay conditions within a data-center network. In reality, a multi-tenant graph processing cluster is more likely to be deployed over a data-center network. Thus we make the network delays more practical in this setting. The network delays are set using a log-normal distribution, based on a recent measurement study of network characteristics in a single data-center [143]. We vary the lognormal distribution mean from 1ms to 4ms, and the standard deviation from 0.1ms to 0.4ms. This results in average network delay values

Algorithm 4 Algorithm for single source shortest path in Apache Giraph semantics

```
function VertexCompute(self,incomingMessages)
    if getSuperstep() = 0 then
        self.dist $\leftarrow$ 0
    end if
    if self = getSourceVertex() then
        minDist $\leftarrow$ 0
    else
        minDist $\leftarrow \infty$
    end if
    for all m $\in$ incomingMessages do
        minDist $\leftarrow$ min(m.getValue(), minDist)
    end for
    if minDist $<$ self.dist then
        self.dist $\leftarrow$ minDist
        for all e $\in$ self.getEdges() do
            d $\leftarrow$ e.getWeight() + minDist
            sendMessage(e.getTargetVertex(), d)
        end for
    end if
    voteToHalt()
end function
```

of 2.73ms, 7.61ms, 20.1ms, and 54.6ms, for lognormal means 1ms, 2ms, 3ms, 4ms, respectively.

We generate a synthetic workload of 10 shortest path jobs, with a constant inter-arrival time of 7s. We evaluate the PADP policy against baseline (default YARN FIFO policy) on two metrics. First, we measure the total completion time (TCT) = (finish time of last job) - (start time of first job). Second, we measure the average job turn around time (TAT). The results are shown in Figures 5.14 and 5.15, respectively.

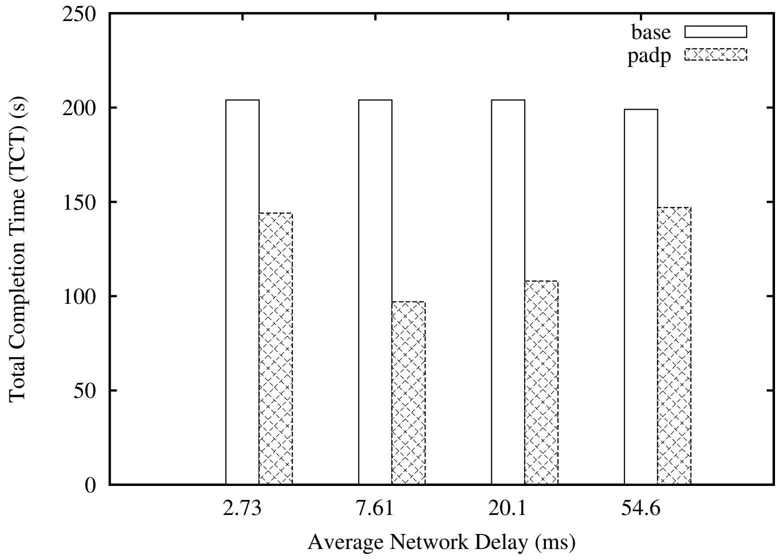

Figure 5.14: TCT comparison between policy and baseline for DC cluster.

First we observe that for the baseline policy, the TCT metric does not vary much in Figure 5.14. In general, Giraph jobs are mapped to map-only Hadoop jobs, thus without the shuffle phase, the network delay does not impact job completion time much. However the PADP policy shows improvement across all network variations. The improvement increases from 20% for 2.73ms average delay (lognormal with mean 1 ms) upto around 45% for 7.61ms (lognormal with mean 2ms) and 20.1ms (lognormal with mean 3ms) delays. The improvement starts to reduce as network delays start increasing

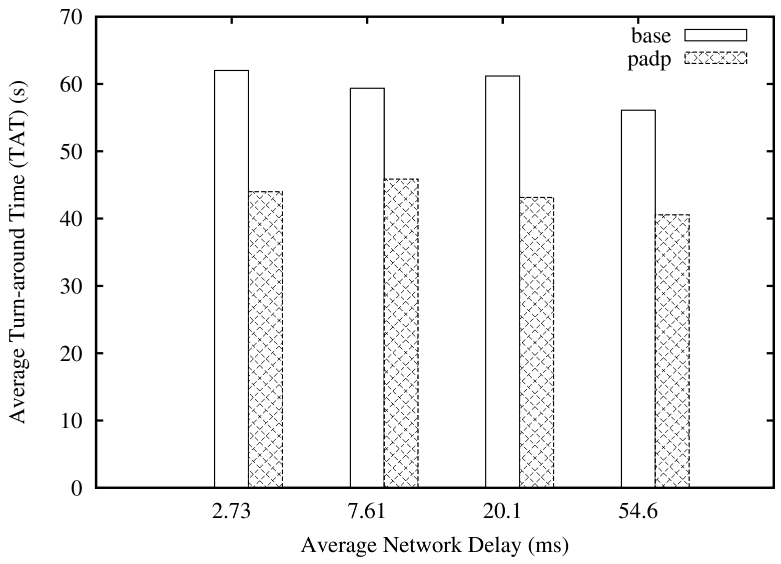

Figure 5.15: TAT comparison between policy and baseline for DC cluster.

beyond 20.1ms. The reason is that at 4 ms average delay, network conditions become too stringent, thus limiting the impact of the PADP policy. In general, for moderate delays, the PADP policy shows performance improvement by reducing the graph loading time. Since graphs are fetched from the local disk, at higher delays we avoid the cost of remote disk fetches. For TAT metric in Figure 5.15, we observe that under different network conditions, we always see improvement, but the amount of improvement does not vary much. Overall we conclude that network latency has less of an impact on the performance, compared to network bandwidth. Thus the performance improvements of PADP compared to baseline can be mainly attributed to higher disk bandwidth (450MBps) compared to network bandwidth (1MBps).

5.10.4 Realistic Job Size Distributions: Facebook Workload

In the previous experiments, we used a fixed graph input for all jobs, and constant job inter-arrival time. We now use a more realistic workload to evaluate the PADP policy. First we replace the constant inter-arrival time distribution with an exponential distribution with mean 7s. Next we, sample job sizes from a production Mapreduce cluster at Facebook [143].

We are not aware of any measurement studies or realistic workload analysis of multi-tenant graph processing clusters. We believe the Facebook workload trace is realistic for multiple reasons. First, specifically Giraph jobs are mapped to map-reduce jobs, thus a map-reduce workload job size distribution should closely match Giraph graph processing workloads. Second, and more generally, we conjecture that many Internet facing companies (especially social networking companies like Facebook, LinkedIn, Pinterest) running graph processing jobs on a multi-tenant cluster should observe a similar workload distribution, where most jobs are small, and only few large jobs exist.

For Facebook, running a massive Pagerank computation is atleast a daily necessity, since the Facebook graph is constantly evolving. This would be one large graph processing job that might take up most of cluster resources. However Facebook also need to do targeted advertising or recommendations to specific groups of people. This would require clustering the massive Facebook graph in to groups of people based on some common interest of pattern. A community detection [119] algorithm (another large job) could be used for this purpose. Or optionally, groups formed by members could serve as the required clustering of the graph. Once the graph is clustered into groups, Facebook needs to extract exponentially many subgraphs corresponding to these groups (many short jobs), and run targeted recommendation algorithms on each subgraphs (many short jobs). Thus we conclude that a workload with mostly short jobs, and few long jobs (not negligible) is a realistic workload for multi-tenant graph processing[1].

[1]We are not aware of any workload analysis studies of commercial graph processing systems.

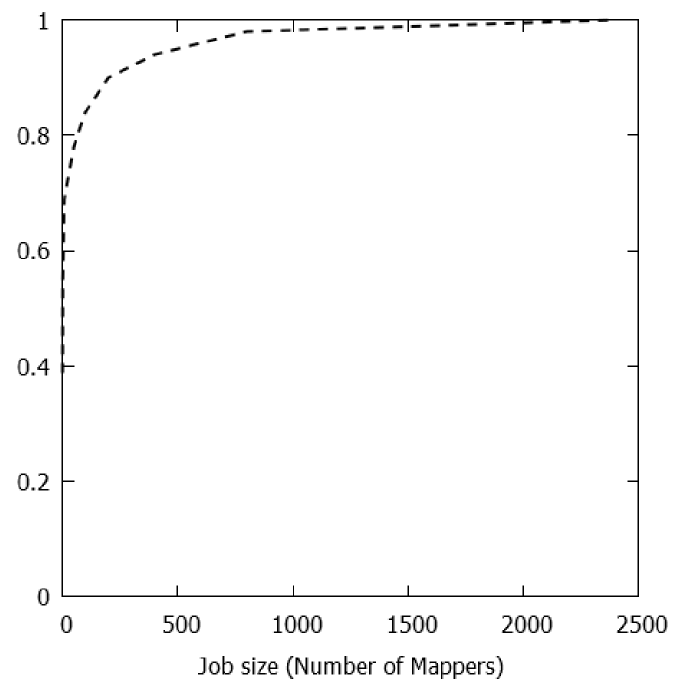

Figure 5.16: CDF of number of mappers for jobs in a production cluster at Facebook.

The Facebook cluster CDF is shown in Figure 5.16 [143]. We observe that the production cluster is dominated by short jobs which have few mappers. Many such jobs can be processed by containers within the same server. In fact a recent Facebook paper on Giraph mentions that the typical setting for a graph processing cluster is to allocate the entire memory of a server to a single container, and use it for a single job [64]. This makes our setting of 1 worker per job practical.

For our experiment, we sample job sizes from this distribution 100 times, once for each job in the trace. For each sample, we generate a graph with number of vertices proportional to the sampled value of number of mappers. The resulting sampled graph input size is shown in Figure 5.17. Inter-arrival times are sampled from an exponential distribution with mean 7s. The network delay is lognormally distributed with mean 3ms. The CDF of job completion time for the 100 jobs for PADP and baseline are shown in Fig-

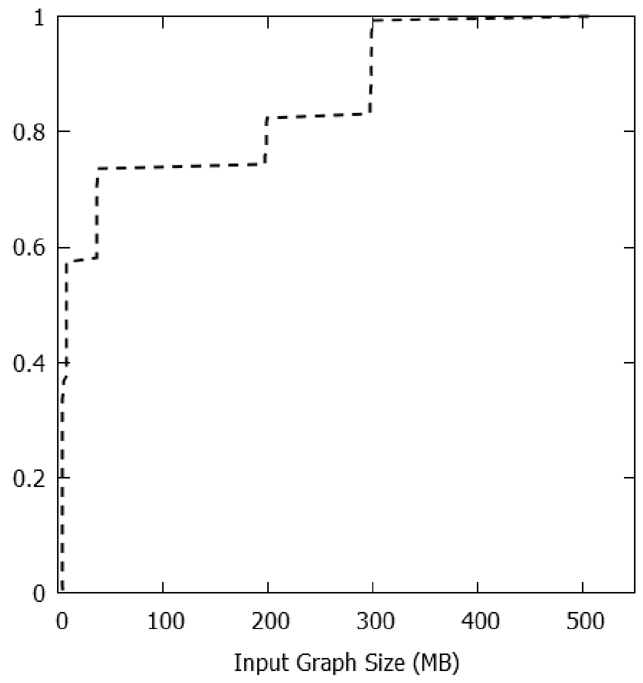

Figure 5.17: CDF of sampled graph input size (MB).

ure 5.18.

Figure 5.18 shows that for the baseline policy, the median job turn-around time is around 140s, and the quickest job takes about 50s. For PADP, the median job turn-around time is around 33sec, about 80% jobs complete within 60s, and the is less than 90s. Overall the median turn-around time improves by 73%, while the 95th percentile turn-around time improves by 54%.

5.10.5 Realistic Job Size and Job Arrival: Yahoo! Workload

While the previous experiment used realistic job size distributions, the arrival process was synthetic. Thus in this section we use a trace obtained from Yahoo!'s Production Hadoop clusters containing several hundreds of servers. We discuss the trace properties briefly without revealing any confidential information. The traces cover thousands of job submissions over several hours. They include job submission time, number of maps, and other information.

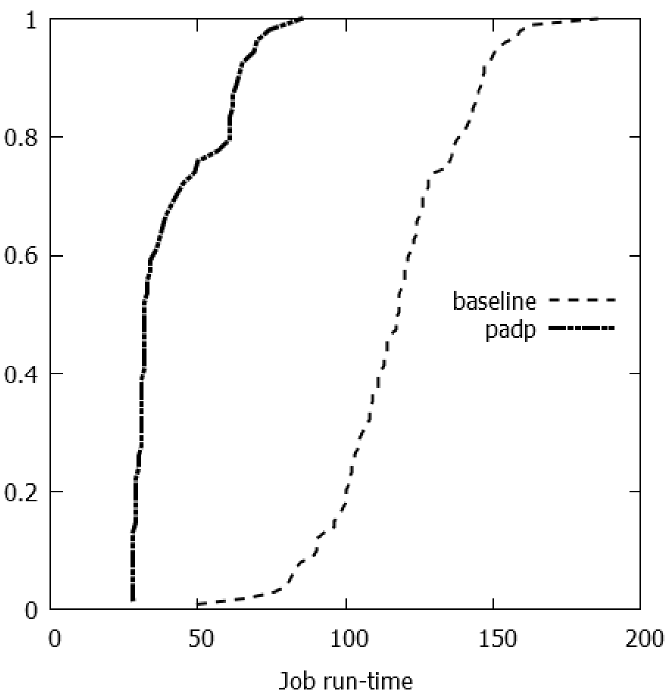

Figure 5.18: Job Completion Time (s) CDF for Facebook Trace (job-size) using Baseline and PADP Policy.

The jobs are of different sizes, the arrivals are bursty, and the load varies over time. Thus this trace captures realistic mix of conditions for a multi-tenant cluster.

We are not aware of any studies of graph processing jobs running on a shared cluster. Thus like the previous Facebook trace experiment, we set the graph size to be proportional to number of mappers in our experiment. We injected 1 hour of traces with 300 jobs into our 9-server test cluster configured with 8 containers (each server has 1 8GB container). The network delay is about 20ms between two servers, based on a log normal distribution of mean 3ms. Figure 5.19 shows the job run-time CDF for both baseline and PADP policies. We observe that for PADP, the median job completion time is around 27s, compared to the median of around 63s for baseline. The 95th percentile run-time for baseline is around 190s, whereas it is around 55s for

PADP. Thus PADP reduces median turn-around time for jobs by 47% and also reduces the 95th percentile turnaround time by 48%. It does so under realistic network and workload conditions.

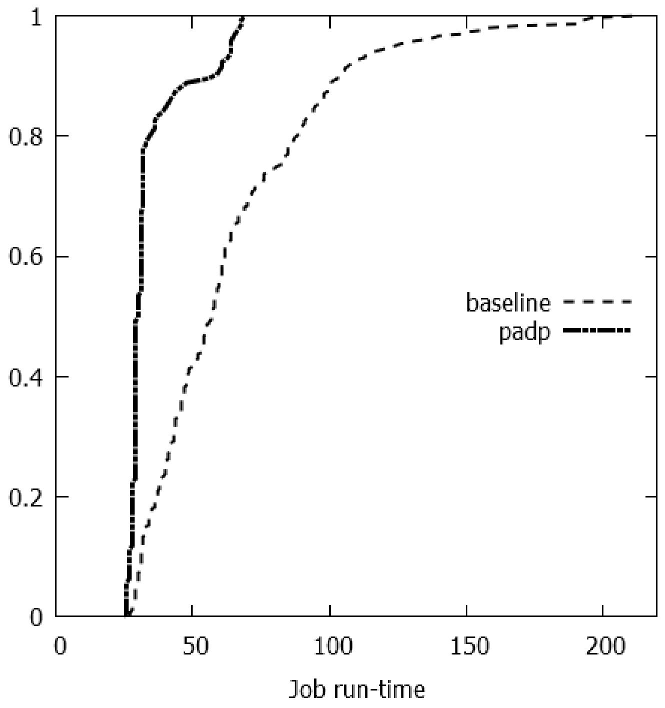

Figure 5.19: Job Completion Time (s) CDF for Yahoo Trace (job size and inter-arrival time) using Baseline and PADP Policy.

5.10.6 Scalability and Impact of Commonality of Graphs

In this section, we explore how our system scales with increased graph sizes, and increased sharing of graphs by different jobs. We first define a new metric called *graph commonality*, and denote it as g. g roughly captures the extent to which different jobs share the same graph. Thus, for example, $g = 100\%$ indicates that all the jobs share (do computation on) the same graph. $g = 50\%$ indicates half the jobs share one graph, the rest share another graph. $g = 0\%$ indicates no sharing, thus each job has its own input graph. In this next experiment, we vary g and evaluate the PADP policy against baseline. We use a trace of 50 jobs with a Poisson arrival process with mean 7s. Network delay is log-normal with mean 3ms. For $g = 100\%$ we use one graph of size 50K vertices. For $g = 50\%$ we use two graphs of size 50K and 25K vertices. For $g = 25\%$ we use four graphs of size 50K, 25K, 16K, and 12K vertices. Finally for $g = 0\%$, we use a separate graph for each job varying in size from 1K upto 50K vertices. The results are shown as a box plot in Figure 5.20.

The X axis shows commonality values for both PADP and baseline, and the Y axis shows job completion time (TAT). Each box represents the minimum, 1st quartile, median, 3rd quartile, and 95th percentile values for job completion time for the 50 job trace. We first observe that the job completion time scales linearly with increased commonality. At 100% g, job completion times are significantly high for the baseline. This is partly due to the larger job-sizes (each has 50K input). But the main reason for worse performance is that as more jobs share the same graph in disk (higher values for g), they simultaneously try to fetch the same graph into memory, which creates disk contention. The PADP policy avoids this contention by creating the additional replicas for jobs, and alleviates the single points of disk contention.

The average job size also increases from left to right in this plot. For $g = 0\%$, the average job size is $25K$, whereas for $g = 100\%$ it is $50K$. Thus the plot indicates that the PADP policy also scales much better with increased job size, compared to the baseline policy.

5.10.7 Impact of Job Heterogeneity

So far all our experiments were performed with a homogeneous trace of jobs of the same type. In this section, we see how PADP performs with a mixture

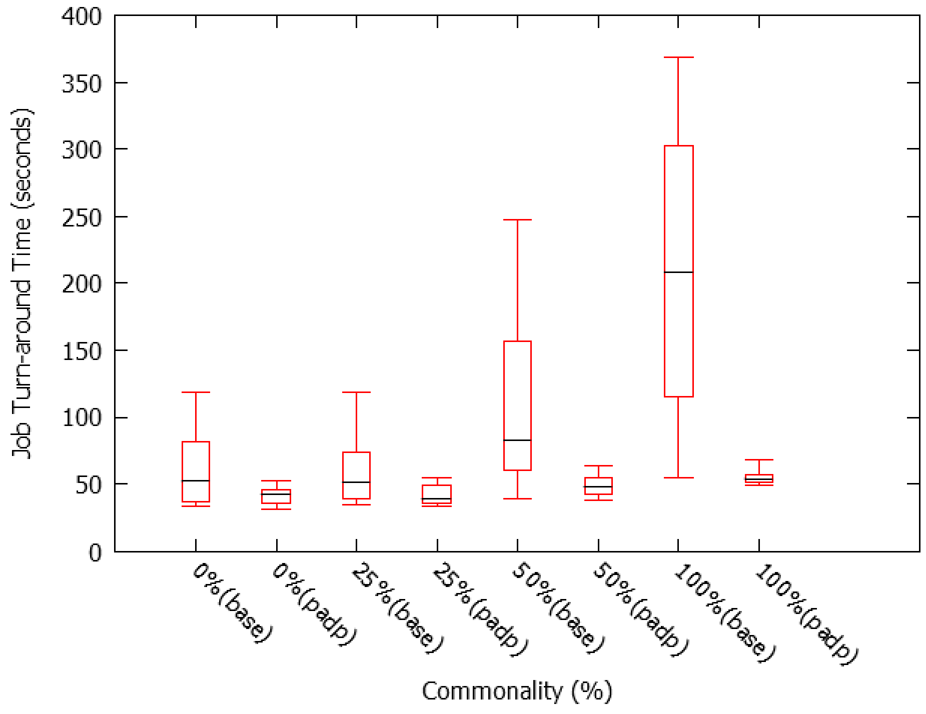

Figure 5.20: Job Completion Time (s) Box Plot (Minimum, First Quartile, Median, Third Quartile, 95th Percentile) against Graph Commonality (measure of how input graphs are distributed among jobs) for Baseline and PADP Policy.

of different types of jobs. We experiment with a trace of 20 jobs with 80% SSSP and 20% K-core jobs. The job inter-arrival time is Poisson with mean 7s, and network delay is lognormally distributed with mean 3ms. The job run-time CDF is shown in Figure 5.21. We observe that although PADP is competitive with baseline, there is not much performance improvement. The reason is that with vastly differing run-times, the progress comparison algorithm mis-predicts the max progress job.

Next we make the run-time of K-core comparable to SSSP, by using more distributed workers for K-core. The resulting job run-time CDF is shown in Figure 5.22. Now we see improved performance. Especially the median turn-around time for PADP improves by 82%, while the 95th percentile turn-around time improves by 70%. The reason for improvement is that with

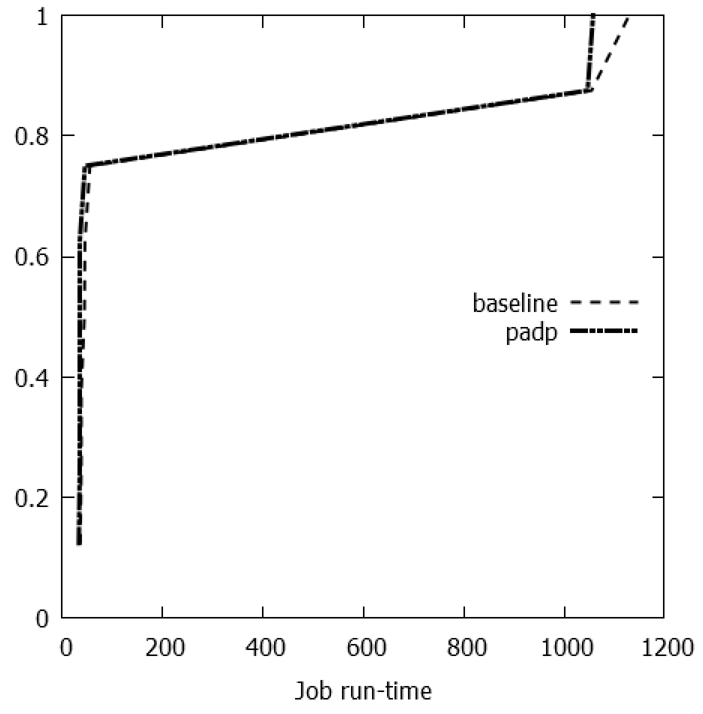

Figure 5.21: Job Completion Time (s) CDF for for Baseline and PADP Policy with 80% SSSP and 20% k-core jobs. Run-time of k-core at-least 10 times run-time of SSSP.

different job types but similar run-times, the progress comparison algorithm is more likely to correctly predict the max progress job. The similar run-times for SSSP and K-core mean that both jobs are more likely to be in the same DEC phase during comparision.

Thus this experiment confirms that for different types of job, the PADP policy works well when job run-times are similar, but starts to mis predict the max progress job when run-times start to vary significantly. This points towards an adaptive mechanism to remedy this drawback. We can continuously measure the standard deviation of job run-times. When the deviation is below a threshold, we use our profile-free approach. However when the threshold is exceeded we incorporate some profiling information in the system (e.g., K-core is always slower than SSSP). However, this adaptive

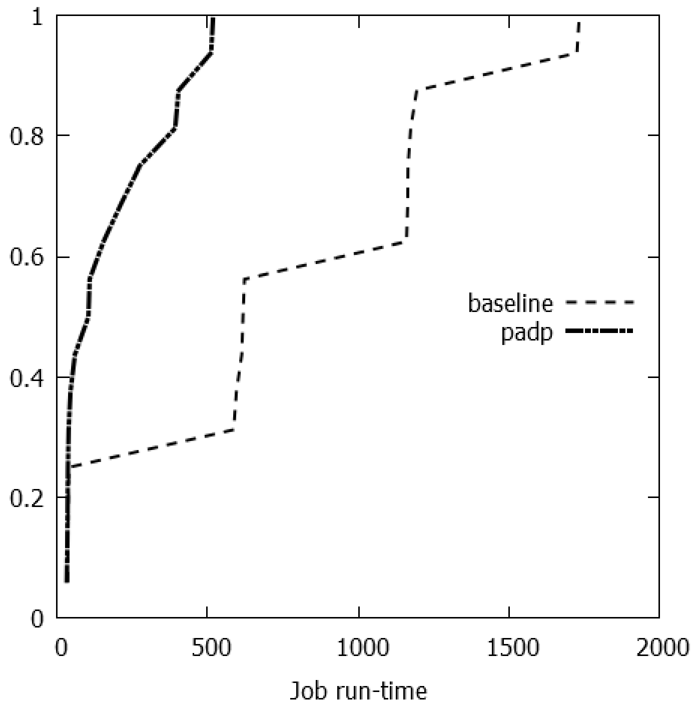

Figure 5.22: Job Completion Time (s) CDF for for Baseline and PADP Policy with 80% SSSP and 20% k-core jobs. Run-times of k-core and SSSP are similar.

approach will no longer be completely profile-free anymore.

5.11 Discussion

In this section we discuss variations and extensions of the OPTiC system.

5.11.1 Experiments with Larger Partitioned Graphs

In our current experiments, the graph input file sizes are bounded by 500MB, and can be run within 1 container. Our job sizes are motivated by a production cluster trace [143]. However in reality we might incur much larger graphs that will be partitioned across servers. To deal with larger graphs, we can extend the PADP policy. Instead of storing the entire new graph file replica at the single max progress server, we can use an existing partitioning algorithm to partition the new graph across the max progress servers. This would ensure that when the first waiting job is ready to run after the maximum progress job finishes, each server can fetch its assigned partition locally from its attached disk. This is left as future work.

5.11.2 OpTiC for Distributed Machine Learning

The OPTiC architecture can be applied to distributed machine learning jobs, provided we plug in a suitable progress estimator into the architecture. For example many machine learning jobs have mathematical convergence criteria, and we can check how far an algorithm is from convergence, and use such a distance metric to measure progress. On the other hand many machine learning algorithms (e.g., k-means clustering, Latent Dirichlet Allocation (LDA) [54], Alternating Least Squares (ALS) [93]) have already been implemented as distributed algorithms in graph processing frameworks like Giraph [64] and PowerGraph [84]. For such distributed implementations, our current OPTiC system with our PADP policy and profile-free progress estimator can be used without modification.

5.11.3 Theoretical Framework for OpTiC

If we have complete oracle knowledge of all jobs that will be submitted to the cluster, and we assume infinitely divisible computation resources (e.g., YARN containers can be of size infinitely small), then it is possible to mathematically formulate the OPTiC scheduling problem as a mathematical optimization problem (most likely a mixed integer linear program (MILP)). Such theoretical models could help us understand the the limits of our scheduling algorithm. We leave such mathematical modeling as interesting future work.

5.11.4 SLO-aware OPTiC

While we optimize run-time performance in OPTiC, we do not explicitly meet performance service level objectives (SLO). We can extend the design of OPTiC to make it SLO-aware. In the original OPTiC mechanism, we prefetch the next waiting job input graph onto the server(s) running the max progress job. While the server(s) running the max progress job are guaranteed to have at-least one unit of resource (e.g., one YARN container), that might not be enough to meet SLOs. We can use profiling to estimate how many containers are required for the new waiting job to meet the SLO. Using our progress estimation and comparison engine, we can already order the current running jobs in descending order or progress (p). For n current running jobs $J_1, J_2, \ldots, J_n$, let the ordered sequence be $p_1 > p_2 > \ldots > p_n$. For OPTiC, we always choose the servers running the job with progress p_1. For SLO-aware OPTiC, we need to choose the first job J_k with progress p_k such that the server(s) running J_k have enough resources (containers) to meet the SLO.

5.12 Related Work

In this section we discuss related work for our OPTiC system.

5.12.1 Graph Processing Systems

Google designed the first distributed graph processing system called Pregel [109] based on message passing. Subsequently, GraphLab [107] proposed shared memory style graph computation. PowerGraph [84] improved upon GraphLab by optimizing for Power-law graphs. In particular it proposed edge-based partitioning algorithms based on vertex-cuts to optimize the graph partitioning phase. LFGraph [92] improves performance using cheap hash-based partitioning and a publish-subscribe based message flow architecture. XStream [79] looks at edge centric processing for graphs. Systems have also explored disk optimizations for single host processing in GraphChi [99]. Presto [138] unifies graph computation and machine learning algorithms by expressing them in terms of matrix computations, and develop a distributed array implementation for doing matrix computations. Compared to all these systems, OPTiC, for the first time, improves performance for multi-tenant graph processing systems.

5.12.2 Multi-tenancy

Multi-tenancy has been explored in the context of cluster schedulers like YARN [4], Mesos [90]. Natjam [65] explores multi-level eviction policies to incorporate priorities and deadlines in a constrained map-reduce cluster. Like Natjam, we also assume a constrained over-subscribed cluster. Unlike Natjam, we assume no preemption. Compared to these three systems, we are the first to explore multi-tenancy for a cluster running graph processing jobs, instead of arbitrary dataflow (map-reduce) jobs. Pisces [131] explores multi-tenant storage systems. Compared to Pisces, we explore multi-tenancy for graph processing systems.

5.12.3 Progress Estimation for Jobs

There is a rich literature of progress estimators for map-reduce jobs and DAGs of map-reduce jobs [117, 118]. Compared to these progress estimators, we propose a novel progress metric for graph jobs utilizing graph level metrics which are independent of how such graph jobs are mapped to map-reduce jobs in many graph processing frameworks like Giraph [3], and GraphX [85]. Progress estimation for database queries has been a very fruitful area of research. Progress estimators like DNE (Driver Node Estimator), and TGN (Total Get Next) estimate progress by calculating the fraction of tuples output so far by operators in a query plan [59]. Similar to database query estimators, we estimate graph computation progress by measuring amount of work done in terms of the percentage of active vertices (working vertices) in a graph.

5.13 Summary

In our study, we explore the potential performance benefits to gain from opportunistically scheduling graph processing jobs on multi-tenant graph processing systems. We propose a profiling-overhead free and cluster-agnostic approach to estimate the progress of a graph processing job using a graph level metric (Active Vertex Count). Using this metric to compare the progress of multiple jobs, we propose a progress-aware scheduling policy (PADP) that schedules incoming jobs based on the progress of all currently running jobs on the cluster. For realistic workloads, we found that our progress-aware disk prefetching (PADP) policy can outperform baseline default scheduling in a multi-tenant cluster. Results indicate that the PADP policy in our system OPTiC reduces median and 95th percentile job turn-around time for realistic workload and network conditions. Our system also scales well with increased job sizes and increased sharing among graphs.

Chapter 6

Conclusion and Future Work

6.1 Summary

In this thesis, we have demonstrated adaptive and opportunistic mechanisms for navigating the cost-performance tradeoff space to meet desired tradeoffs for modern cloud systems, including distributed key-value storage systems, cloud-based disaster recovery systems, and multi-tenant graph processing systems. In doing so, we have presented the design, implementation, and evaluation of four systems.

Our first contribution, PCAP is an adaptive distributed storage system. The foundation of the PCAP system is a probabilistic variation of the classical CAP theorem, which quantifies the (un-)achievable envelope of probabilistic consistency and latency under different network conditions characterized by a probabilistic partition model. Our PCAP system proposes adaptive mechanisms for tuning control knobs to meet desired consistency-latency tradeoffs expressed in terms in service-level agreements.

Our second system, GeoPCAP is a geo-distributed extension of PCAP. In GeoPCAP, we propose generalized probabilistic composition rules for composing consistency-latency tradeoffs across geodistributed instances of distributed key-value stores, each running on separate datacenters. GeoPCAP also includes a geo-distributed adaptive control system that adapts new controls knobs to meet SLAs across geo-distributed data-centers.

Our third system, GCVM proposes a light-weight hypervisor-managed mechanism for taking crash consistent snapshots across VMs distributed over servers. This mechanism enables us to move the consistency group abstraction from hardware to software, and thus lowers reconfiguration cost while incurring modest VM pause times which impact application availability.

Finally, our fourth contribution is a new opportunistic graph processing system called OPTiC for efficiently scheduling multiple graph analytics jobs sharing a multi-tenant cluster. By opportunistically creating at most 1 additional replica in the distributed file system (thus incurring cost), we show up to 50% reduction in median job completion time for graph processing jobs under realistic network and workload conditions. Thus with a modest increase in storage and bandwidth cost in disk, we can reduce job completion time (improve performance).

6.2 Lessons Learned from Cost-Performance Tradeoffs for Cloud Systems

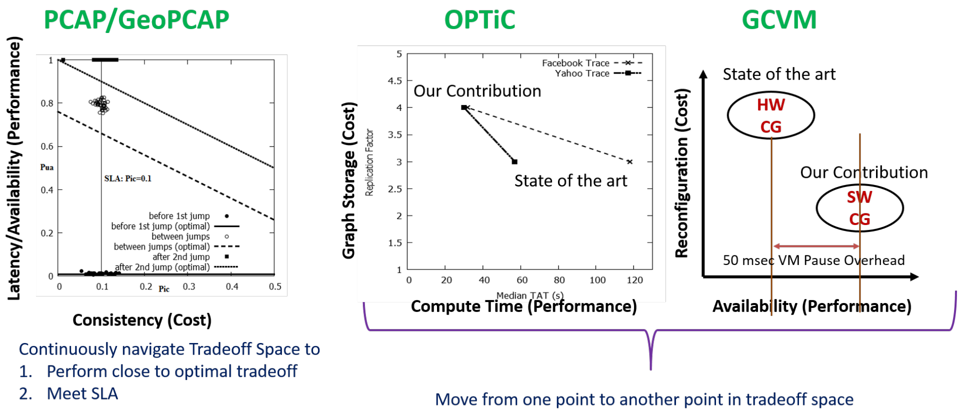

Figure 6.1: Cost Performance Tradeoffs in this Thesis.

A central tenet of this thesis is that cost-performance tradeoffs should be considered as first class citizens when designing cloud systems. In this section we discuss how explicitly thinking about and characterizing cost performance tradeoffs allows as to build better cloud systems.

The various cost performance tradeoffs considered in this thesis are depicted in Figure 6.1. For PCAP (Chapter 2) and GeoPCAP (Chapter 3), the tradeoff is between consistency (X axis) and latency/availability (Y axis) (left plot in Figure 6.1). The straight lines represent the optimal tradeoffs and the cluster of points represent the tradeoffs achieved by the PCAP system. For these storage systems, characterizing the optimal tradeoff allowed us to understand the limits of the storage system. This in turn allowed us to explicitly try to perform close to the optimal envelope, in addition to meeting SLAs. Thus an explicit characterization of the tradeoffs informed efficient navigation of the tradeoff space to perform close to the optimal envelope.

For GCVM (Chapter 4), the key abstraction is to checkpoint and replicate a group of virtual machines as a single unit. The state of the art hardware solution has high reconfiguration cost to change the membership of the group, whereas our proposed software solution reduces reconfiguration cost at the modest impact of application availability (right most plot in Figure 6.1). Explicitly mapping out the tradeoff space for this system allows us to consider future systems that lie in this tradeoff space. For example, can we build a hybrid software-hardware solution that has reconfiguration cost in between the pure hardware and pure software solutions, and with performance impact lower than the software solution? Only by explicitly thinking about the cost-performance tradeoff space, can we think of such systems in the future. It also allows us to conjecture performance characteristics of such new systems. For example, by looking at the explicit tradeoff space, we can conjecture that a hybrid hardware-software solution for group consistent snapshots for virtual machines can incur a performance penalty (VM pause time) somewhere around 20-30 msec.

For OPTiC (Chapter 5), the tradeoff is between the graph computation run-time and the storage replication cost (middle plot in Figure 6.1). Compared to existing systems, we improve run-time at a slight increase in storage cost. Like GCVM, this explicit tradeoff space allows us to think about other solution points in the tradeoff space. Unlike PCAP, where we know the optimal tradeoff, here we do not know what is the optimal solution with lowest storage cost and best run-time performance. Explicitly placing state of the art and our proposed solutions in the tradeoff space allows us to consider optimal tradeoffs (like PCAP optimal tradeoffs), and understand the implications of new system designs points with different cost-performance tradeoffs. For example the trend seems to indicate that by increasing replication factor beyond 4, we can get even lower performance. Thus the tradeoff space allows us to reason about optimal tradeoffs for these graph processing systems.

6.3 Future Work

We suggest several directions for future research related to this thesis.

6.3.1 Probabilistic Tradeoff Analysis for Distributed Transactional Systems

One theoretical research topic could be to explore probabilistic tradeoffs for transaction systems. This would include probabilistic isolation models for transactions that capture transactional semantics of different isolation models. PCAP characterizes and adapts the consistency-latency tradeoff space for distributed key-value storage systems through a probabilistic lens. Key-value stores have a simple data model. There is a value associated with a key. However many modern NewSQL [42, 141] storage systems have more structure, and support richer abstractions like distributed transactions. While this will not be a new transactional model, it could help us understand the space of models better, and understand the performance impact (throughput, fairness, contention) of various isolation levels better. Equipped with such probabilistic tradeoff analysis, we can explore adaptive mechanisms for meeting various performance and/or consistency requirements based on user SLA/SLO under workload and network variations.

6.3.2 Adaptive GCVM

It would be interesting to explore adaptive mechanisms that switch between crash consistency and application consistency based on application workload. In GCVM, we have proposed a software level consistency group abstraction. One direction to pursue would be to adaptively tune the consistency group semantics to meet different objectives. For example crash consistency might not be enough for some applications, and we might need stronger guarantees such as application consistency. However stronger guarantees are costly to maintain and impact application performance more (e.g., to ensure each snapshot is application consistent would require VMs to be paused longer than crash consistency requirements), thus increasing the duration between consecutive snapshots (RPO). For example when the application workload is light (low rate of writes), it could tolerate longer pauses and get application consistent snapshots. But when the write-rate increases, we should not pause for long, thus we need to switch back to cheaper crash consistency snapshots.

6.3.3 Extensions of OPTiC

OPTiC is concerned with efficient co-scheduling of multiple graph analytics jobs sharing a cluster. There are many avenues of future directions to consider, some of which have been mentioned already in the relevant chapter. Here we discuss a few more directions.

Data-aware Policies

The main mechanism in OPTiC is to place additional replicas for a queued graph job to reduce graph fetching time by utilizing progress metrics of current jobs. Such progress aware policies are not the only available opportunities in a distributed graph processing cluster. For example, we can also explore data aware strategies. If we know that a consecutive job will be running on a graph already in use by a current job, then we can save graph loading time by keeping that graph in memory for the subsequent job. This requires techniques to cache map-reduce containers, and we can utilize existing frameworks like Apache Tez [5] to investigate such mechanisms.

PADP for Arbitrary Dataflow Frameworks

We believe that the Progress Aware Disk Prefetching (PADP) can be applicable for computational frameworks beyond graph processing, for example, distributed machine learning jobs or generalized dataflow computations. The challenge is to develop general metrics for estimating progress of arbitrary jobs. This seems like a hard problem.

In the OPTiC graph progress estimator we use a graph level metric, active vertex count that helps us gauge current progress. Can we find such metrics for machine learning jobs? Many machine learning jobs have convergence criteria that define termination. We can utilize such criteria to decide which job will finish earlier. This also opens up the possibility of investigating various distance metrics that define the distance to termination. Some dataflow/-graph systems let applications specify a maximum number of iterations. This makes it easy to check progress.

Overall it seems like estimating progress is very much application specific, and a better architecture should separate the policy concern of application progress (applications can use call-back mechanisms to tell the run-time how to measure progress), whereas the actual mechanism for utilizing the progress data to tune the performance is confined withing the system.

Distributed Extensions of OPTiC

In OPTiC, we have mainly explored graph processing jobs with one worker. Thus the graph is not partitioned and distributed across workers. A distributed extension of OPTiC where each graph processing job is distributed across servers is an immediate extension worth exploring.

References

[1] Activo: “Why Low Latency Matters?”. http://www.activo.com/why-low-latency-does-matter-and-increases-online-sales/, last visited 2016-07-04.

[2] Amazon: milliseconds means money. http://www.uiandus.com/blog/2009/2/4/amazon-milliseconds-means-money.html, last visited 2016-07-04.

[3] Apache Giraph. http://giraph.apache.org/, last visited 2016-07-04.

[4] Apache Hadoop Yarn. http://hadoop.apache.org/docs/current/hadoop-yarn/hadoop-yarn-site/YARN.html, last visited 2016-07-04.

[5] Apache Tez. https://tez.apache.org/, last visited 2016-07-04.

[6] Application vs. crash consistency. http://www.n2ws.com/blog/ebs-snapshots-crash-consistent-vs-application-consistent.html, last visited 2016-07-04.

[7] Basho Riak. http://basho.com/riak/, last visited 2016-07-04.

[8] Cassandra. http://cassandra.apache.org/, last visited 2016-07-04.

[9] Cassandra commit log architecture. http://wiki.apache.org/cassandra/ArchitectureCommitLog, last visited 2016-07-04.

[10] Consistency in Amazon S3. http://shlomoswidler.com/2009/12/read-after-write-consistency-in-amazon.html, last visited 2016-07-04.

[11] Emc mirror view knowledgebook. http://goo.gl/8VjTRK, last visited 2016-07-04.

[12] EMC SRDF consistency groups. http://goo.gl/wBlgZQ, last visited 2016-07-04.

[13] Emc srdf/a multi-session consistency on z/os. http://goo.gl/81HuZe, last visited 2016-07-04.

[14] Facebook userbase. http://newsroom.fb.com/company-info/, last visited 2016-07-04.

[15] Hadoop distributed file system (hdfs). https://hadoop.apache.org/docs/r1.2.1/hdfs_design.html, last visited 2016-07-04.

[16] Hyper-V snapshots vs. VSS snapshots explained. http://goo.gl/5ia37H, last visited 2016-07-04.

[17] IOzone filesystem benchmark. http://www.iozone.org/, last visited 2016-07-04.

[18] Netapp snapmirror data replication. http://www.netapp.com/us/products/protection-software/snapmirror.aspx, last visited 2016-07-04.

[19] Netapp snapshots. http://community.netapp.com/t5/Technology/Are-All-Snapshots-Created-Equal/ba-p/83211, last visited 2016-07-04.

[20] Openstack Swift. http://docs.openstack.org/developer/swift/, last visited 2016-07-04.

[21] PostgreSQL. http://www.postgresql.org/, last visited 2016-07-04.

[22] PostgreSQL benchmarking tool. http://www.postgresql.org/docs/devel/static/pgbench.html, last visited 2016-07-04.

[23] PostgreSQL database physical storage. http://www.postgresql.org/docs/9.3/static/storage-file-layout.html, last visited 2016-07-04.

[24] Project Voldemort. http://www.project-voldemort.com/voldemort/, last visited 2016-07-04.

[25] QEMU features/snapshots. http://wiki.qemu.org/Features/Snapshots, last visited 2016-07-04.

[26] Real-time ad impression bids using DynamoDB. http://aws.amazon.com/blogs/aws/real-time-ad-impression-bids-using-dynamodb/, last visited 2016-07-04.

[27] The software-defined data center (sddc). http://www.vmware.com/software-defined-datacenter/, last visited 2016-07-04.

[28] Transaction processing performance council, TPC-B. http://www.tpc.org/tpcb/, last visited 2016-07-04.

[29] Understanding data replication between dell equallogic ps series groups. http://goo.gl/Ioxdv8, last visited 2016-07-04.

[30] Vmware , virtual volumes. http://www.vmware.com/products/virtual-volumes, last visited 2016-07-04.

[31] VMware Inc., disk chaining and redo logs. https://goo.gl/6dxM16, last visited 2016-07-04.

[32] VMware VASA. http://blogs.vmware.com/vsphere/2011/08/a-sneak-peek-at-how-vmwares-storage-partners-are-using-vasa.html, last visited 2016-07-04.

[33] VMware vCloud Air. http://vcloud.vmware.com/service-offering/disaster-recovery, last visited 2016-07-04.

[34] VMware vSphere Replication 6.0. https://www.vmware.com/files/pdf/vsphere/VMware-vSphere-Replication-Overview.pdf, last visited 2016-07-04.

[35] Xen snapshots halting I/O. http://discussions.citrix.com/topic/263681-xen-snapshots-halting-io/, last visited 2016-07-04.

[36] Yahoo! cloud serving benchmark (YCSB). https://github.com/brianfrankcooper/YCSB/wiki, last visited 2016-07-04.

[37] Yahoo! cloud serving benchmark (ycsb) workloads. https://github.com/brianfrankcooper/YCSB/wiki/Core-Workloads, last visited 2016-07-04.

[38] Cassandra multi data-center deployment, 2011. http://www.datastax.com/dev/blog/deploying-cassandra-across-multiple-data-centers, last visited 2016-07-04.

[39] Cristina L. Abad, Yi Lu, and Roy H. Campbell. Dare: Adaptive data replication for efficient cluster scheduling. In *Proc. IEEE Cluster Computing*, pages 159–168, 2011.

[40] Daniel Abadi. Consistency tradeoffs in modern distributed database system design: CAP is only part of the story. *IEEE Computer*, 45(2):37–42, 2012.

[41] Ittai Abraham and Dahlia Malkhi. Probabilistic quorums for dynamic systems. In *Distributed Computing*, volume 18, pages 113–124, 2005.

[42] Marcos K. Aguilera, Joshua B. Leners, and Michael Walfish. Yesquel: Scalable sql storage for web applications. In *Proc. ACM SOSP*, pages 245–262, 2015.

[43] Ganesh Ananthanarayanan, Sameer Agarwal, Srikanth Kandula, Albert Greenberg, Ion Stoica, Duke Harlan, and Ed Harris. Scarlett: Coping with skewed content popularity in mapreduce clusters. In *Proc. ACM Eurosys*, pages 287–300, 2011.

[44] Ganesh Ananthanarayanan, Ali Ghodsi, Scott Shenker, and Ion Stoica. Disk-locality in datacenter computing considered irrelevant. In *Proc. USENIX HotOS*, pages 12–12, 2011.

[45] Masoud Saeida Ardekani and Douglas B. Terry. A self-configurable geo-replicated cloud storage system. In *Proc. USENIX OSDI*, pages 367–381, 2014.

[46] K. J. Astrom and T. Hagglund. *PID Controllers: Theory, Design, and Tuning, 2nd Ed.* 1995.

[47] Hagit Attiya and Jennifer L. Welch. Sequential consistency versus linearizability. In *ACM Transactions on Computer Systems (TOCS)*, volume 12, pages 91–122, 1994.

[48] Peter Bailis and Ali Ghodsi. Eventual consistency today: Limitations, extensions, and beyond. In *ACM Queue*, volume 11, pages 20:20–20:32, 2013.

[49] Peter Bailis, Shivaram Venkataraman, Michael J. Franklin, Joseph M. Hellerstein, and Ion Stoica. Pbs at work: Advancing data management with consistency metrics. In *Proceedings of the 2013 ACM SIGMOD International Conference on Management of Data (SIGMOD)*, pages 1113–1116, New York, New York, USA, 2013.

[50] Peter Bailis, Shivaram Venkataraman, Michael J. Franklin, JosephM. Hellerstein, and Ion Stoica. Quantifying eventual consistency with pbs. In *The Very Large Data Bases (VLDB) Journal*, volume 23, pages 279–302, 2014.

[51] R. Baldoni, C. Marchetti, and A. Virgillito. Impact of wan channel behavior on end-to-end latency of replication protocols. In *Proc. EDCC*, pages 109–118, 2006.

[52] Theophilus Benson, Aditya Akella, and David A. Maltz. Network traffic characteristics of datacenters in the wild. In *Proc. ACM SIGCOMM IMC*, pages 267–280, 2010.

[53] Kenneth P. Birman. The process group approach to reliable distributed computing. *CACM*, 36(12):37–53, 1993.

[54] David M. Blei, Andrew Y. Ng, and Michael I. Jordan. Latent dirichlet allocation. *JMLR*, 3:993–1022, 2003.

[55] Jeff Bonwick, Matt Ahrens, Val Henson, Mark Maybee, and Mark Shellenbaum. The zettabyte file system. Technical report, Sun Microsystems, 2003.

[56] Eric Brewer. A certain freedom: Thoughts on the CAP theorem. In *Proc. ACM PODC*, pages 335–335, 2010.

[57] Eric A. Brewer. Towards robust distributed systems (Invited Talk). In *Proc. ACM PODC*, 2000.

[58] K. Mani Chandy and Leslie Lamport. Distributed snapshots: determining global states of distributed systems. *ACM TOCS*, 3(1):63–75, 1985.

[59] Surajit Chaudhuri, Vivek Narasayya, and Ravishankar Ramamurthy. Estimating progress of execution for sql queries. In *Proc. ACM SIGMOD*, pages 803–814, 2004.

[60] Rong Chen, Jiaxin Shi, Yanzhe Chen, and Haibo Chen. Powerlyra: Differentiated graph computation and partitioning on skewed graphs. In *Proc. ACM Eurosys*, pages 1:1–1:15, 2015.

[61] Y. Chen, K. Li, and J.S. Plank. Clip: a checkpointing tool for message passing parallel programs. In *Proc. ACM/IEEE SC*, pages 33–33, 1997.

[62] David R. Cheriton and Willy Zwaenepoel. Distributed process groups in the v kernel. *ACM TOCS*, 3(2):77–107, 1985.

[63] Vijay Chidambaram, Thanumalayan Sankaranarayana Pillai, Andrea C. Arpaci-Dusseau, and Remzi H. Arpaci-Dusseau. Optimistic crash consistency. In *Proc. ACM SOSP*, pages 228–243, 2013.

[64] Avery Ching, Sergey Edunov, Maja Kabiljo, Dionysios Logothetis, and Sambavi Muthukrishnan. One trillion edges: Graph processing at facebook-scale. *Proc VLDB Endowment*, pages 1804–1815, 2015.

[65] Brian Cho, Muntasir Rahman, Tej Chajed, Indranil Gupta, Cristina Abad, Nathan Roberts, and Philbert Lin. Natjam: Design and evaluation of eviction policies for supporting priorities and deadlines in mapreduce clusters. In *Proc. ACM SoCC*, pages 6:1–6:17, 2013.

[66] Adrian Cockcroft. Dystopia as a service (Invited Talk). In *Proc. ACM SoCC*, 2013.

[67] Brian F. Cooper, Adam Silberstein, Erwin Tam, Raghu Ramakrishnan, and Russell Sears. Benchmarking cloud serving systems with YCSB. In *Proc. ACM SoCC*, pages 143–154, 2010.

[68] James C. Corbett et al. Spanner: Google's globally-distributed database. In *Proc. USENIX OSDI*, pages 251–264, 2012.

[69] A Davidson, A Rubinstein, A Todi, P Bailis, and S. Venkataraman. Adaptive hybrid quorums in practical settings, 2013. http://goo.gl/LbRSW3.

[70] Jeff Dean. Design, Lessons and Advice from Building Large Distributed Systems, 2009.

[71] Giuseppe DeCandia, Deniz Hastorun, Madan Jampani, Gunavardhan Kakulapati, Avinash Lakshman, Alex Pilchin, Swaminathan Sivasubramanian, Peter Vosshall, and Werner Vogels. Dynamo: Amazon's highly available key-value store. In *Proc. ACM SOSP*, pages 205–220, 2007.

[72] Maria Eleftheriou and Marios Mavronicolas. Linearizability in the presence of drifting clocks and under different delay assumptions. In *Distributed Computing*, volume 1693, pages 327–341. 1999.

[73] E. N. (Mootaz) Elnozahy, Lorenzo Alvisi, Yi-Min Wang, and David B. Johnson. A survey of rollback-recovery protocols in message-passing systems. *ACM Computing Survey*, 34(3):375–408, 2002.

[74] Michalis Faloutsos, Petros Faloutsos, and Christos Faloutsos. On power-law relationships of the internet topology. *ACM SIGCOMM CCR*, 1999.

[75] Hua Fan, Aditya Ramaraju, Marlon McKenzie, Wojciech Golab, and Bernard Wong. Understanding the causes of consistency anomalies in apache cassandra. In *Proc. VLDB Endowment*, volume 8, pages 810–813, 2015.

[76] Armando Fox and Eric A. Brewer. Harvest, yield, and scalable tolerant systems. In *Proc. HotOS*, pages 174–178, 1999.

[77] Bugra Gedik., Scott Schneider, Martin Hirzel, and Kun-Lung Wu. Elastic scaling for data stream processing. In *IEEE TPDS*, volume 25, pages 1447–1463, 2014.

[78] Seth Gilbert and Nancy A. Lynch. Perspectives on the CAP theorem. *IEEE Computer*, 45(2):30–36, 2012.

[79] Lewis Girod, Yuan Mei, Ryan Newton, Stanislav Rost, Arvind Thiagarajan, Hari Balakrishnan, and Samuel Madden. Xstream: a signal-oriented data stream management system. *Proc. IEEE ICDE*, pages 1063–1189, 2008.

[80] Lisa Glendenning, Ivan Beschastnikh, Arvind Krishnamurthy, and Thomas Anderson. Scalable consistency in Scatter. In *Proc. ACM SOSP*, pages 15–28, 2011.

[81] Wojciech Golab, Xiaozhou Li, and Mehul A. Shah. Analyzing consistency properties for fun and profit. In *Proc. ACM PODC*, pages 197–206, 2011.

[82] Wojciech Golab, Muntasir Raihan Rahman, Alvin AuYoung, Kimberly Keeton, and Indranil Gupta. Client-centric benchmarking of eventual consistency for cloud storage systems. In *Proc. IEEE ICDCS*, pages 493–502, 2014.

[83] Wojciech Golab and John Johnson Wylie. Providing a measure representing an instantaneous data consistency level, January 2014. US Patent Application 20,140,032,504.

[84] Joseph E. Gonzalez, Yucheng Low, Haijie Gu, Danny Bickson, and Carlos Guestrin. Powergraph: Distributed graph-parallel computation on natural graphs. In *Proc. USENIX OSDI*, pages 17–30, 2012.

[85] Joseph E. Gonzalez, Reynold S. Xin, Ankur Dave, Daniel Crankshaw, Michael J. Franklin, and Ion Stoica. Graphx: Graph processing in a distributed dataflow framework. In *Proc. USENIX OSDI*, pages 599–613, 2014.

[86] Albert Greenberg, James R. Hamilton, Navendu Jain, Srikanth Kandula, Changhoon Kim, Parantap Lahiri, David A. Maltz, Parveen Patel, and Sudipta Sengupta. Vl2: A scalable and flexible data center network. In *Proc. ACM SIGCOMM*, pages 51–62, 2009.

[87] Joseph L. Hellerstein, Yixin Diao, Sujay Parekh, and Dawn M. Tilbury. *Feedback Control of Computing Systems*. John Wiley & Sons, 2004.

[88] Jiannong Cao Jian Lu Hengfeng Wei, Yu Huang. Almost strong consistency: "good enough" in distributed storage systems, 2015. `http://arxiv.org/abs/1507.01663`.

[89] Herodotos Herodotou, Fei Dong, and Shivnath Babu. No one (cluster) size fits all: Automatic cluster sizing for data-intensive analytics. In *Proc. ACM SoCC*, pages 18:1–18:14, 2011.

[90] Benjamin Hindman, Andy Konwinski, Matei Zaharia, Ali Ghodsi, Anthony D. Joseph, Randy Katz, Scott Shenker, and Ion Stoica. Mesos: A platform for fine-grained resource sharing in the data center. In *Proc. USENIX NSDI*, pages 295–308, 2011.

[91] Dave Hitz, James Lau, and Michael Malcolm. File system design for an nfs file server appliance. In *Proc. USENIX WTEC*, pages 19–19, 1994.

[92] Imranul Hoque and Indranil Gupta. Lfgraph: Simple and fast distributed graph analytics. In *Proc. ACM SIGOPS TRIOS*, pages 9:1–9:17, 2013.

[93] Yifan Hu, Yehuda Koren, and Chris Volinsky. Collaborative filtering for implicit feedback datasets. In *Proc. IEEE ICDM*, pages 263–272, 2008.

[94] Michael Isard, Vijayan Prabhakaran, Jon Currey, Udi Wieder, Kunal Talwar, and Andrew Goldberg. Quincy: Fair scheduling for distributed computing clusters. In *Proc. ACM SOSP*, pages 261–276, 2009.

[95] A. Kangarlou, P. Eugster, and Dongyan Xu. Vnsnap: Taking snapshots of virtual networked environments with minimal downtime. In *Proc. IEEE/IFIP DSN*, pages 524–533, 2009.

[96] C. Karamanolis, M.B. Amdur, and P.W.P. Dirks. Method and system for generating consistent snapshots for a group of data objects. `http://www.google.com/patents/US8607011`, dec 2013. US Patent 8,607,011.

[97] Wissam Khaouid, Marina Barsky, Venkatesh Srinivasan, and Alex Thomo. K-core decomposition of large networks on a single pc. In *Proc. VLDB Endowment*, volume 9, pages 13–23, 2015.

[98] Sudha Krishnamurthy, William H. Sanders, and Michel Cukier. An adaptive quality of service aware middleware for replicated services. *IEEE TPDS*, 14:1112–1125, 2003.

[99] Aapo Kyrola, Guy Blelloch, and Carlos Guestrin. Graphchi: Large-scale graph computation on just a pc. In *Proc. USENIX OSDI*, pages 31–46, 2012.

[100] O. Laadan, D. Phung, and J. Nieh. Transparent checkpoint-restart of distributed applications on commodity clusters. In *Proc. IEEE Cluster Computing*, pages 1–13, 2005.

[101] Hyunyoung Lee and Jennifer L. Welch. Applications of probabilistic quorums to iterative algorithms. In *Proc. IEEE ICDCS*, page 21, 2001.

[102] Cheng Li, Daniel Porto, Allen Clement, Johannes Gehrke, Nuno Preguiça, and Rodrigo Rodrigues. Making geo-replicated systems fast as possible, consistent when necessary. In *Proc. USENIX OSDI*, pages 265–278, 2012.

[103] Jin Liang and Klara Nahrstedt. Service composition for generic service graphs. *Multimedia Systems*, 11(6):568–581, 2006.

[104] Harold C. Lim, Shivnath Babu, and Jeffrey S. Chase. Automated control for elastic storage. In *Proc. IEEE ICAC*, pages 1–10, 2010.

[105] Wyatt Lloyd, Michael J. Freedman, Michael Kaminsky, and David G. Andersen. Don't settle for eventual: Scalable causal consistency for wide-area storage with COPS. In *Proc. ACM SOSP*, pages 401–416, 2011.

[106] Wyatt Lloyd, Michael J. Freedman, Michael Kaminsky, and David G. Andersen. Stronger semantics for low-latency geo-replicated storage. In *Proc. USENIX NSDI*, pages 313–328, 2013.

[107] Yucheng Low, Danny Bickson, Joseph Gonzalez, Carlos Guestrin, Aapo Kyrola, and Joseph M. Hellerstein. Distributed graphlab: A framework for machine learning and data mining in the cloud. *Proc. VLDB Endowment*, 5(8):716–727.

[108] Nancy Lynch and Seth Gilbert. Brewer's conjecture and the feasibility of consistent, available, partition-tolerant web services. *ACM SIGACT News*, 33(2):51–59, 2002.

[109] Grzegorz Malewicz, Matthew H. Austern, Aart J.C Bik, James C. Dehnert, Ilan Horn, Naty Leiser, and Grzegorz Czajkowski. Pregel: A system for large-scale graph processing. In *Proc. ACM SIGMOD*, pages 135–146, 2010.

[110] Grzegorz Malewicz, Matthew H Austern, Aart JC Bik, James C Dehnert, Ilan Horn, Naty Leiser, and Grzegorz Czajkowski. Pregel: a system for large-scale graph processing. In *Proc. ACM SIGMOD*, pages 135–146, 2010.

[111] Dahlia Malkhi, Michael Reiter, and Rebecca Wright. Probabilistic quorum systems. In *Proc. ACM PODC*, pages 267–273, 1997.

[112] Marios Mavronicolas and Dan Roth. Linearizable read/write objects. In *TCS*, volume 220, pages 267 – 319, 1999.

[113] Marlon McKenzie, Hua Fan, and Wojciech Golab. Fine-tuning the consistency-latency trade-off in quorum-replicated distributed storage systems. In *Proc. IEEE Big Data*, pages 1708–1717, 2015.

[114] C. Mohan, Don Haderle, Bruce Lindsay, Hamid Pirahesh, and Peter Schwarz. Aries: A transaction recovery method supporting fine-granularity locking and partial rollbacks using write-ahead logging. *ACM TODS*, 17(1):94–162, March 1992.

[115] Christopher Monsanto, Joshua Reich, Nate Foster, Jennifer Rexford, and David Walker. Composing software-defined networks. In *Proc. USENIX NSDI*, pages 1–14, 2013.

[116] Bill Moore. Zfs the last word in file systems. `http://goo.gl/a3p8hn`.

[117] K. Morton, A. Friesen, M. Balazinska, and D. Grossman. Estimating the progress of mapreduce pipelines. In *Proc. IEEE ICDE*, pages 681–684, 2010.

[118] Kristi Morton, Magdalena Balazinska, and Dan Grossman. Paratimer: A progress indicator for mapreduce dags. In *Proc. ACM SIGMOD*, pages 507–518, 2010.

[119] M E Newman. Modularity and community structure in networks. *PNAS*, 103(23):8577–8582, 2006.

[120] Steven Osman, Dinesh Subhraveti, Gong Su, and Jason Nieh. The design and implementation of zap: A system for migrating computing environments. *ACM SIGOPS OSR*, 36:361–376, 2002.

[121] Dorian Perkins, Nitin Agrawal, Akshat Aranya, Curtis Yu, Younghwan Go, Harsha V. Madhyastha, and Cristian Ungureanu. Simba: Tunable end-to-end data consistency for mobile apps. In *Proc. ACM EuroSys*, pages 7:1–7:16, Bordeaux, France, 2015.

[122] Muntasir Raihan Rahman, Lewis Tseng, Son Nguyen, Indranil Gupta, and Nitin Vaidya. Probabilistic cap and timely adaptive key-value stores. Technical Report http://hdl.handle.net/2142/50019, UIUC, July 2014.

[123] Muntasir Raihan Rahman, Lewis Tseng, Son Nguyen, Indranil Gupta, and Nitin H. Vaidya. Characterizing and adapting the consistency-latency tradeoff in distributed key-value stores. *CoRR*, abs/1509.02464, 2015.

[124] Raghu Ramakrishnan and Johannes Gehrke. *Database management systems*. McGraw-Hill, Inc., New York, NY, USA, 3 edition, 2003.

[125] Amitabha Roy, Laurent Bindschaedler, Jasmina Malicevic, and Willy Zwaenepoel. Chaos: Scale-out graph processing from secondary storage. In *Proc. ACM SOSP*, pages 410–424, 2015.

[126] Sriram Sankaran, Jeffrey M. Squyres, Brian Barrett, and Andrew Lumsdaine. The lam/mpi checkpoint/restart framework: System-initiated checkpointing. In *Proc. LACSI*, pages 479–493, 2003.

[127] D. P. Scarpazza, P. Mullaney, O. Villa, F. Petrini, V. Tipparaju, D. M. L. Brown, and J. Nieplocha. Transparent system-level migration of pgas applications using xen on infiniband. In *Proc. IEEE Cluster Computing*, pages 74–83, 2007.

[128] Fred B. Schneider. Implementing fault-tolerant services using the state machine approach: A tutorial. *ACM Computing Survey*, 22(4):299–319, 1990.

[129] Marc Shapiro. Structure and encapsulation in distributed systems: the Proxy Principle. In *Proc. IEEE ICDCS*, pages 198–204, 1986.

[130] Marc Shapiro, Nuno M. Preguiça, Carlos Baquero, and Marek Zawirski. Conflict-free replicated data types. In *Proc. SSS*, pages 386–400, 2011.

[131] David Shue, Michael J. Freedman, and Anees Shaikh. Performance isolation and fairness for multi-tenant cloud storage. In *Proc. USENIX OSDI*, pages 349–362, 2012.

[132] Konstantin Shvachko, Hairong Kuang, Sanjay Radia, and Robert Chansler. The hadoop distributed file system. In *Proc. IEEE MSST*, pages 1–10, 2010.

[133] K. C. Sivaramakrishnan, Gowtham Kaki, and Suresh Jagannathan. Declarative programming over eventually consistent data stores. In *Proc. ACM PLDI*, pages 413–424, 2015.

[134] Ion Stoica, Robert Morris, David Karger, M. Frans Kaashoek, and Hari Balakrishnan. Chord: A scalable peer-to-peer lookup service for internet applications. In *Proc. ACM SIGCOMM*, pages 149–160, 2001.

[135] Douglas B. Terry, Vijayan Prabhakaran, Ramakrishna Kotla, Mahesh Balakrishnan, Marcos K. Aguilera, and Hussam Abu-Libdeh. Consistency-based service level agreements for cloud storage. In *Proc. ACM SOSP*, pages 309–324, 2013.

[136] Satyam B. Vaghani. Virtual machine file system. *ACM SIGOPS OSR*, 44(4):57–70, 2010.

[137] Leslie G. Valiant. A bridging model for parallel computation. *CACM*, 33(8):103–111, 1990.

[138] Shivaram Venkataraman, Erik Bodzsar, Indrajit Roy, Alvin AuYoung, and Robert S. Schreiber. Presto: Distributed machine learning and graph processing with sparse matrices. In *Proc. ACM Eurosys*, pages 197–210, 2013.

[139] Werner Vogels. Eventually consistent. *CACM*, pages 40–44, 2009.

[140] Brian White, Jay Lepreau, Leigh Stoller, Robert Ricci, Shashi Guruprasad, Mac Newbold, Mike Hibler, Chad Barb, and Abhijeet Joglekar. An integrated experimental environment for distributed systems and networks. In *Proc. USENIX OSDI*, pages 255–270, 2002.

[141] Chao Xie, Chunzhi Su, Cody Littley, Lorenzo Alvisi, Manos Kapritsos, and Yang Wang. High-performance acid via modular concurrency control. In *Proc. ACM SOSP*, pages 279–294, 2015.

[142] Haifeng Yu and Amin Vahdat. Design and evaluation of a conit-based continuous consistency model for replicated services. *ACM TOCS*, pages 239–282, 2002.

[143] Matei Zaharia, Dhruba Borthakur, Joydeep Sen Sarma, Khaled Elmeleegy, Scott Shenker, and Ion Stoica. Delay scheduling: A simple technique for achieving locality and fairness in cluster scheduling. In *Proc. ACM EuroSys*, pages 265–278, 2010.

[144] Matei Zaharia, Mosharaf Chowdhury, Tathagata Das, Ankur Dave, Justin Ma, Murphy McCauley, Michael J. Franklin, Scott Shenker, and Ion Stoica. Resilient distributed datasets: A fault-tolerant abstraction for in-memory cluster computing. In *Proc. USENIX NSDI*, pages 2–2, 2012.

[145] Marek Zawirski, Nuno Preguiça, Sérgio Duarte, Annette Bieniusa, Valter Balegas, and Marc Shapiro. Write fast, read in the past: Causal consistency for client-side applications. In *Proc. Middleware*, pages 75–87, 2015.

[146] Chi Zhang and Zheng Zhang. Trading replication consistency for performance and availability: an adaptive approach. In *Proc. IEEE ICDCS*, pages 687–695, 2003.